

**Investigating diacylglycerol lipase-beta function in inflammation by activity-based
protein profiling (ABPP) and lipidomics**

Myungsun Shin

BS, Chemistry, Biology, Dickinson College, 2014

**A dissertation presented to the Graduate Faculty
Of the University of Virginia in Candidacy for the Degree of
Doctor of Philosophy**

Department of Chemistry

University of Virginia

May 2019

**©Copyright by
Myungsun Shin
All rights reserved.
May 2019**

ACKNOWLEDGEMENTS

First, I would like to thank my thesis advisor, Ku-Lung Hsu. Starting since 2014, he offered me an opportunity to be able to work in his lab and learn about the exciting field of chemical biology and a variety of different techniques. Under his supervision, I was taught how to identify and approach research questions in chemical biology. On a personal note, Ken demonstrated his hardworking passionate attitude in the lab that was an example of what it takes to be a passionate scientist. Besides my advisor, I would like to thank the rest of my dissertation committee members, especially David Cafiso and Thurl Harris for their input and guidance throughout my graduate school career.

I would like to thank my colleagues in the lab, especially Caroline Franks and Emmanuel Toroitich. I appreciate your friendship and support throughout the years. I wish you good luck in your future and hope to remain in touch.

I would also like to thank my undergraduate research advisor, Rebecca E. Connor. Since the day I joined her lab as a first-year undergraduate, she has supported my interests in science and taught me how to appreciate science. Her sheer excitement and passion for science have been instilled in me and have paved the road for my path to pursuing science ever since.

I also want to thank the Carrothers family for supporting me throughout my studies in the United States. Since arriving in the U.S., I was incredibly fortunate to be able to stay with the Carrothers starting with my high school years in Hawaii. They taught me great values and helped to shape me into the person I am today. I appreciate all the love and kindness that you have provided for me. Words can't describe the appreciation I have for you. Mr. Scott, Ms. Jan, Kasey, and Kyle-- Thank you.

I want to thank my parents for taking a chance on me and sending me to study abroad. I understand the difficulties and hesitation that you must have had for more than 13 years. I appreciate all the sacrifices that you've made to make it possible for me to explore studies that I enjoy. Mom and Dad, I love you.

Last but not least, I want to thank my partner Tatiana. You brought such a bright light into my life two years ago and I have never been so happy my entire life. I can only hope that I will be able to do the same for you. I hope to be there for you in the brightest of days and the darkest of nights. I can't wait to plan (well you do most of the planning), eat good food, and live life with you. Love you penguin.

Table of contents

Copyright page	ii
Table of contents	iv
List of figures	vii
Abbreviation	ix
Chapter 1: GENERAL INTRODUCTION	1
1.1.1 Role of lipid signaling in inflammation.....	1
1.1.2 Efficacy of NSAIDs in neuropathic pain, cyclooxygenases (COXs)	4
1.1.3 Pathogenic pain models (inflammatory, and neuropathic pain models)	5
1.1.4 DAGL β as a promising target for pain signaling.....	7
1.1.5 Introduction to diacylglycerol lipase-beta (DAGL β)	12
1.1.6 DAGL lipid metabolism and signaling.....	14
1.1.7 DAGL β regulates macrophage and microglia inflammatory signaling.....	16
1.1.8 Current DAGL inhibitors.....	19
1.1.9 cPLA2 α regulation of arachidonic acid in inflammation.....	20
1.1.10 Functional cross-talk of cPLA2 α and DAGL β signaling pathways.....	20
1.1.11 Dissertation Summary.....	21
1.1.12 References.....	23
Chapter 2: SELECTIVE DELIVERY OF DIACYLGLYCEROL LIPASE-BETA INHIBITORS USING LIPOSOMAL ENCAPSULATION FOR IMPROVED EFFICACY AND SELECTIVITY <i>IN VIVO</i>	
2.1 Overview	33
2.2 Introduction	34
2.3 Materials and Methods	37
2.4 Results	45
2.4.1 Encapsulation of KT109 in Liposomes.....	45
2.4.2 Characterization of Liposomal KT109.....	48
2.4.3 Chemical Proteomic Analysis of Liposomal KT109.....	55
2.4.4 Liposomal KT109 exhibits high potency in reversing LPS-induced mechanical allodynia.....	56
2.5 Discussion	59

2.6 Acknowledgements.....	61
2.7 References.....	62
Chapter 3: DIACYLGLYCEROL LIPASE-BETA IS REQUIRED FOR TNF-ALPHA RESPONSE BUT NOT CD8+ T CELL PRIMING CAPACITY OF DENDRITIC CELLS	
3.1 Overview.....	66
3.2 Introduction.....	67
3.3 Materials and methods.....	68
3.4 Results.....	76
3.4.1 Chemoproteomic discovery of DAGL β activity in primary dendritic cells....	76
3.4.2 DAGL β regulates endocannabinoid and arachidonic acid metabolism in BMDCs.....	79
3.4.3 DAGL β regulates LPS-stimulated TNF- α release of BMDCs.....	79
3.4.4 DAGL β inactivation does not affect DC-mediated T cell priming <i>in vivo</i>	83
3.5 Discussion.....	87
3.6 Significance.....	88
3.7 Acknowledgements.....	89
3.8 References.....	90
CHAPTER 4: INVESTIGATION OF DIACYLGLYCEROL LIPASE-BETA FUNCTION IN INFLAMMATION BY ACTIVITY-BASED PROTEIN PROFILING (ABPP) AND LIPIDOMICS	
4.1 Overview.....	94
4.2 Introduction.....	95
4.3 Materials and Methods.....	97
4.4 Results.....	103
4.4.1 ABPP analysis of BMDM shows enriched activity of DAGL β but not DAGL α	103
4.4.2 DAGL β disruption does not result in PKC hyperactivation.....	105
4.4.3 Untargeted lipidomics analysis of BMDMs shows selective accumulation of triacylglycerols composed of PUFAs.....	109
4.4.4 Biochemical validation that DAGL β functions as a PUFA-specific TAG lipase	115

4.4.5 ABPP discovery of FASN regulation by DAGL β using SILAC BMDMs.....	119
4.4.6 Chemical or genetic disruption of DAGL β activates AMP-activated protein kinase (AMPK)	121
4.4.7 Chronic DAGL β blockade does not result in steatosis in mouse liver.....	129
4.5 Discussion.....	132
4.6 References.....	139
Chapter 5: CONCLUSIONS AND FUTURE DIRECTIONS.....	146
5.1 Summary.....	146
5.2 Conclusions and significance.....	147
5.3 Limitations and Future direction.....	150

List of Figures

Chapter 1

1.1 Currently available pharmacological treatment for pain conditions and its side effects	3
1.2 Predictive lipid flux from DAGL-beta inhibition based on current understanding of DAGLβ	11
1.3 Schematic of lipid signaling pathways that lead to prostaglandins biosynthesis	15
1.4 Tissue expression and activity of 2-AG biosynthetic and hydrolytic serine hydrolases that regulate endocannabinoid metabolism and signaling	17
1.5 Distribution of 2-AG biosynthetic/hydrolytic serine hydrolases across cell types in brain.	18

Chapter 2

2.1 DAGLβ hydrolyzes DAGs to regulate lipid precursors important for inflammation....	35
2.2. LC-MS analyses to measure KT109 concentrations in liposomes.....	42
2.3 Characterization of liposomal KT109 by DLS, NTA, and LC-MS.....	47
2.4 Chemical proteomic evaluation of liposomal KT109 potency and selectivity <i>in vivo</i>	50
2.4.1 Gel-based activity-based protein profiling (ABPP) of kidney proteomes from mice treated with ghost liposomes or liposomal KT109.....	51
2.4.2 Gel-based activity-based protein profiling (ABPP) of heart from mice treated with liposomes.....	52
2.4.3 Gel-based activity-based protein profiling (ABPP) of brain from mice treated with liposomes.	53
2.4.4 Gel-based activity-based protein profiling (ABPP) of liver from mice treated with liposomes.	54
2.5 Efficacy and selectivity of liposomal KT109 in the LPS inflammatory pain model....	58

Chapter 3

3.1 Gating strategy for flow cytometry analysis of dendritic cells.....	71
3. 2 Gating strategy for flow cytometry analysis of OVA-specific CD8+ T cells from spleens of mice vaccinated with BMDCs.....	72
3.3 Chemical proteomic and metabolomic analysis of BMDCs	78

3.4 DAGL β regulates TNF- α response of LPS-stimulated BMDCs.....	82
3.5 DAGL inactivation does not impair BMDC activation/maturation.....	85
3.6 DAGL inactivation does not affect BMDC priming of antigen-specific CD8+ T cells <i>in vivo</i>	86

Chapter 4

4.1 Activity-Based Protein Profiling of DAGLs in mouse brain and bone marrow derived macrophages	104
4.2 Phosphorylated PKC substrate changes in BMDMs with DAGL β disruption and untargeted lipidomics analysis.....	106
4.2.1 Western blot analysis of phosphorylated PKC substrates on soluble fractions from BMDMs generated from DAGL $\beta^{+/+}$ and DAGL $\beta^{-/-}$ mice.....	107
4.2.2 Western blot analysis of phosphorylated PKC substrates on membrane fractions from BMDMs generated from DAGL $\beta^{+/+}$ and DAGL $\beta^{-/-}$ mice.....	108
4.3 Activity-Based Protein Profiling analysis of the BMDMs with in-situ compound treatment for dose dependent inhibition of DAGL β	112
4.4 Untargeted lipidomics analysis of the DAGL $\beta^{+/+}$ BMDMs treated with KT109 (200 nM) or KT195 (200 nM) at for 4 hours.....	113-114
4.5 Biochemical substrate assay of DAGL β using triacylglycerols.....	116
4.6 Quantitative chemoproteomics analysis of serine hydrolases in BMDMs	123
4.6.1 Western blot analysis of total AMPK levels in soluble fraction of BMDMs generated from DAGL $\beta^{+/+}$ and DAGL $\beta^{-/-}$ mice.....	124
4.6.2 Western blot analysis with p-AMPK (Thr172) levels in soluble fraction of BMDMs generated from DAGL $\beta^{+/+}$ and DAGL $\beta^{-/-}$ mice.....	125
4.6.3 Western blot analysis of p-AMPK (Ser485/Ser491) levels in soluble fraction of BMDMs generated from DAGL $\beta^{+/+}$ and DAGL $\beta^{-/-}$ mice.....	126
4.6.4 Western blot analysis of DAGL β levels in membrane fraction from BMDMs generated from DAGL $\beta^{+/+}$ and DAGL $\beta^{-/-}$ mice.....	127
4.6.5 Flow cytometry analysis of SILAC BMDMs.....	128
4.7 Hepatic steatosis and TG accumulation in DAGL $\beta^{+/+}$ and DAGL $\beta^{-/-}$ mice.....	131
4.8 Untargeted lipidomics analysis of BMDM lipidomes.....	138

Abbreviation

ABPP-	activity based protein profiling
DAGLβ-	diacylglycerol lipase-beta
DAGLα-	diacylglycerol lipase-alpha
AA-	arachidonic acid
COX-	cyclooxygenase
DAG-	diacylglycerol
GPCR-	G-protein-coupled receptor
LPS-	lipopolysaccharide
FP-Rh-	fluorophosphate-rhodamine
DOPE-	1,2-dioleoyl-<i>sn</i>-glycero-3-phosphoethanolamine
DSPC-	1,2-distearoyl-<i>sn</i>-glycero-3-phosphocholine
PEG2000PE-	1,2-dioleoyl-<i>sn</i>-glycero-3-phosphoethanolamine-<i>N</i>- [methoxy(polyethylene glycol)-2000]
i.p.-	intraperitoneal
DLS-	dynamic light scattering
NTA-	nanoparticle tracking analysis
FTLA-	finite track length adjustment
MRM-	multiple-reaction monitoring

LC-MS-	liquid chromatography-mass spectrometry
NSAIDs-	nonsteroidal anti-inflammatory drugs
TNF-α-	tumor necrosis factor-alpha
PGE2-	prostaglandin E2
PLGA-	poly(lactide-co-glycolide)
PLA/PEO-	poly(lactic acid)-poly(ethylene oxide)
DC-	Dendritic cells
2-AG	2-arachidonyl glycerol
FBS-	Fetal Bovine Serum
SH-	Serine Hydrolases
MHC-	Major histochemistry complex
TLR-	Toll like receptor
AMPK-	AMP-activated protein kinase
ACC-	Acetyl-Coa carboxylase
SAG-	1-steroyl 2-arachidonly glycerol
CIPN-	Chemotherapy induced peripheral neuropathy
CCI-	Chronic constriction injury
NSAIDs-	Non-steroidal anti-inflammatory drugs

BMDMs-	Bone marrow derived macrophages
ABP-	Activity based probe
PUFA-	Polyunsaturated fatty acid
PKA-	Protein kinase C
RBC-	Red blood cell
PEI-	Polyethyleneimine
H&E-	Hematoxylin eosin
TAG-	Triacylglycerol
PE-	Phosphatidylethanolamine
PS-	Phosphatidylserine
PC-	Phosphatidylcholine
FASN-	Fatty acid synthase
SS-	Side scatter
FS-	Forward scatter
HSL-	Hormone sensitive lipase
ATGL-	Adipose triacylglycerol lipase
HFD-	High fat diet

Chapter. 1 General Introduction

1.1.1 Role of lipid signaling in inflammation

Inflammation is a natural defense mechanism that is defined by a number of responses against foreign pathogens or caused by internal cellular responses from cells being damaged^{1, 2}. This process is necessary to maintain homeostasis and tissue repair processes. However, unregulated inflammatory responses can lead to pathological conditions that can result in pathological conditions such as arthritis, diabetes, and cardiovascular diseases^{1, 2}. Disease conditions derived from inflammation could be largely divided into two major causes. First, the inflammatory response elicited by adaptive and innate immunity often results in concomitant damage to tissue^{3, 4}. Second, damage could also come from inflammation that is mediated by malfunctioning adaptive immune responses, which results in unrecognized self-antigens. In these cases, adaptive immune components, such as antibodies, and immune cell-mediated functions damage tissues. This results in auto-inflammatory diseases such as rheumatoid arthritis⁵ and multiple sclerosis (MS)⁶. Therefore, understanding the biological systems involved in the development of inflammation as well as ways to reduce elicited tissue damage is of great interest for basic and translational research.

The significance of lipids in biological systems have been emerging as uniquely central to cellular functions, not only as structural components or energy sources, but also as transmitters in cell. The function of lipids can vary greatly depending on its class , which include phospholipids (Phosphatidyl Choline (PC), phosphatidyl serine (PS), phosphatidylethanolamine (PE), and phosphatidic acid

(PA)), glycerol lipids (triacylglycerol, diacylglycerol, and monoacylglycerol), fatty acids, prostaglandins, and sterols⁷. These lipids play an important role in regulating a variety of cellular processes including structure, metabolism, and immune function^{7, 8}. As lipids are closely associated with cellular functions, they also play an important role in the development of pathobiology if there are imbalance/excess of certain lipid components. The resulting imbalance could lead to disruption in basic metabolic responses as well as the development of chronic inflammation⁹⁻¹¹.

There have been a number of pharmacological interventions that have been developed to treat inflammation. Non-steroidal anti-inflammatory drugs (NSAIDs), selective serotonin reuptake inhibitors (SSRIs)^{12, 13}, corticosteroids^{14, 15}, and opioids^{16, 17} are being used as a treatment for inflammation. Although these drugs are effective in addressing acute symptoms of inflammation, it has been demonstrated that chronic treatment with these agents result in severe side-effects (**Figure 1.1**). For instance, NSAIDs targets enzymes called cyclooxygenases (COX)¹⁸, which produce prostaglandins from a ω -6 polyunsaturated fatty acid (PUFA) called arachidonic acid. These prostaglandins are involved in many physiological processes including vasodilation, pain sensation, and ovulation^{19, 20}. But most notably, prostaglandins are known to be involved in elicitation of inflammation²⁰. The utilization of pharmacological inhibitors such as aspirin and ibuprofen have shown a compelling case for targeting lipid signaling to media inflammatory signaling²¹. Therefore, it shows the potential to target lipid signaling in treatment of inflammation.

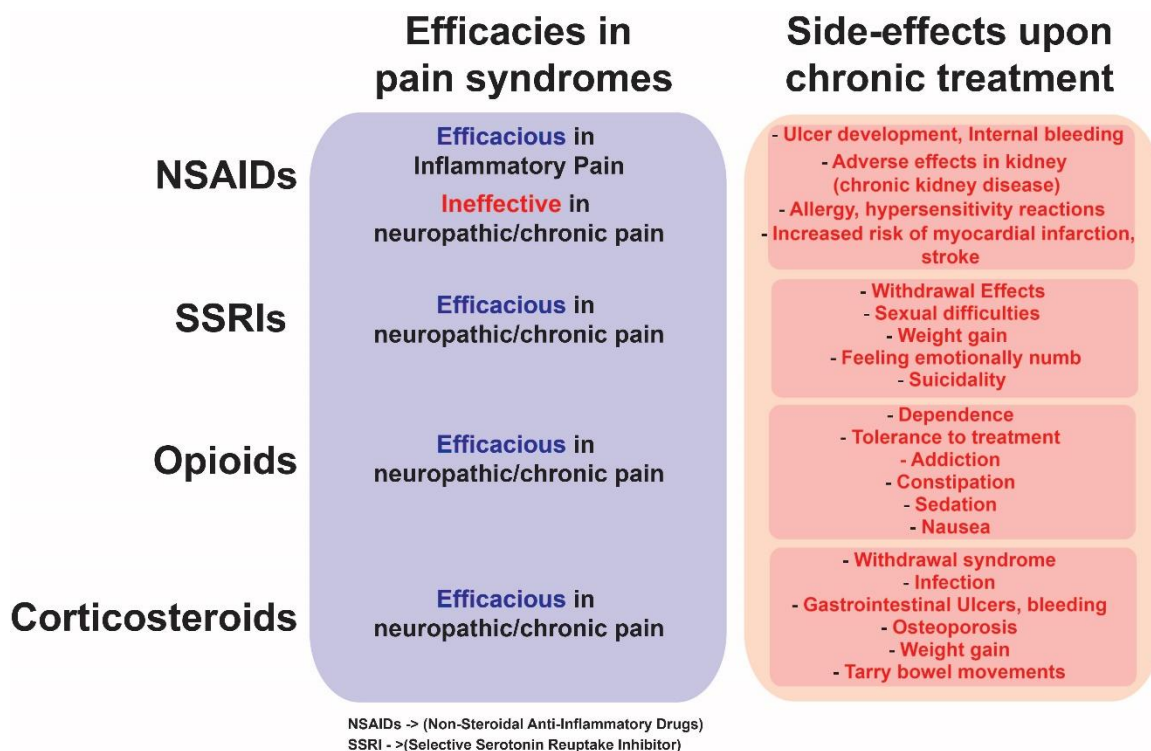


Figure 1.1 Currently available pharmacological treatment for pain conditions and its side effects Pharmacological treatments that are currently available for treating pain sensation is summarized with their efficacy and side effects. Currently available drug class includes non-steroidal anti-inflammatory drugs (NSAIDs), selective serotonin reuptake inhibitors (SSRIs), opioids, and corticosteroids. These drugs can be administered to attenuate chronic pain except for NSAIDs. However, long-term treatment with current drugs can result in severe side-effects.

1.1.2 Efficacy of NSAIDs in neuropathic pain, cyclooxygenases (COXs)

The current understanding of how DAGL β inhibition leads to anti-inflammatory effects is centered around the class of lipid molecules called prostaglandins. To this date, the most effective way to inhibit prostaglandin production is through the inhibition of enzymes called cyclooxygenases (COXs)¹⁸⁻²⁰. Nonsteroidal anti-inflammatory drugs (NSAIDs) are one of the most widely used drugs to treat inflammation. NSAIDs reduce inflammation by inhibiting enzymes called cyclooxygenases (COX). There are two isoforms of COX enzymes, COX-1, and COX-2²². COX-1 is a constitutively expressed form of the enzyme, whereas COX-2 is inducible. COX synthesizes prostaglandins from a fatty acid called arachidonic acid (20:4). Prostaglandins are one of the most important initiators of inflammation. Aside from the initiation of the inflammatory signaling process, prostaglandins are essential for maintaining physiological homeostasis (i.e. vasodilation, blood clotting, platelet regulation, and gastrointestinal functions...etc)^{19, 20}. Widely used COX inhibitors such as ibuprofen inhibit both COX-1 and COX-2. Although the utility of COX inhibitors has been demonstrated in a number of inflammatory conditions, it is well accepted that chronic treatment of COX inhibitors leads to severe side effects including internal hemorrhaging, kidney-failure, hypertension^{23, 24}. Therefore, chronic treatment using COX inhibitors is not suitable for chronic conditions such as neuropathic pain syndromes.

Although chronic COX inhibition results in various forms of side effects, the efficacy of acute treatment for inflammation has been shown to be effective. The currently available NSAIDs have a number of favorable chemical properties,

including bioavailability and their capacity to be able to readily cross the blood-brain barrier (BBB)^{25, 26}. In addition, there has been a large body of work showing NSAIDs to be effective in attenuating pain associated with acute inflammation²¹. For instance, an array of NSAIDs were tested in an inflammatory pain model with mice that had been sensitized with CFA (Complete Freund's Adjuvant)²⁷, which causes allodynia, a condition where non-noxious stimuli trigger a pain response. The oral administration of NSAIDs had a dose-dependent positive effect in relieving allodynia developed by CFA. The recovery rate varied depending on the NSAID tested; however, NSAIDs were not able to completely abolish the pain response²⁷.

1.1.3 Pathogenic pain models (inflammatory and neuropathic pain models)

The mechanism of how pain sensitization is developed in response to prostaglandins have been studied in various contexts²⁸⁻³⁰. Neurons that have been exposed to prostaglandins such as PGE2 showed a lowered excitation threshold, leading to hyperactivation of the neuronal firing rate, ultimately causing hypersensitivity to applied stimuli. In terms of pain sensation, such hypersensitivity leads to allodynia³¹. In studies that focused on prostaglandins in pain response, prostaglandin production was measured across different tissues after neuropathic pain was elicited in mice via sciatic nerve neuropathic pain induction³². The results showed a significant increase in prostaglandin production in sciatic nerve and dorsal root ganglia (DRG) tissues compared to the sham experimental group. In this study, NSAID treatment resulted in a reduction of prostaglandins after neuropathic pain was induced. Interestingly, there was no significant improvement

in allodynia from these mice that had been treated with NSAID in the mechanical allodynia model³².

Even though the dual COX inhibitors did not show significant improvement in neuropathic pain models, there has been a significant effort in developing COX-2 specific inhibitors^{33, 34}. The side effects that are caused by chronic COX inhibition are proposed to be from the inhibition of constitutive COX-1³⁵. Therefore, a number of inhibitors targeting the inducible form of COX-2 have been developed and tested to show efficacy in treating inflammatory conditions. The inducible form of COX that is expressed upon induction of inflammation, infection, and cancer could provide selective targeting of the pharmacological endpoint in order to effectively target inflammation³⁵. The development and testing of selective COX-2 inhibitors such as celecoxib showed attenuated pain response when tested with the thermal hyperalgesia model but was not effective against the mechanical hypersensitivity test^{35, 27}. In addition, chronic treatment of rofecoxib in the nerve injury model has shown no effect in preventing or alleviating allodynia developed by the experimental model³⁶.

Interestingly, further exploration of COX-2 inhibitors showed results that weren't observed in other COX inhibitors. The efficacy of the COX-2 specific inhibitor GW406381 was tested in neuropathic pain in addition to conventional COX-1/2 and other COX-2 inhibitors. Sprague-Dawley rats were subjected to the chronic constriction injury (CCI) and orally dosed with respective compounds for 5 days³⁷. After five days of the compound treatment, rats were evaluated in two different pain sensitization measurement methods (Von Frey and Randall-Sellitto

test)³⁷. Ibuprofen showed no improvement in reversing pain sensitization in both Von Frey and Randall-Sellitto tests as was reported in previous literature. However, the Randall-Sellitto test showed that GW406381 resulted in significant recovery from the pain sensitization whereas Rofecoxib (brand name Vioxx, COX-2 selective inhibitor) showed no improvements in anti-nociceptive effects³⁷.

The CCI model is unique to the inflammatory pain model in that systematic allodynia develops over time after surgery. Fourteen days after surgery, contralateral paws (paws from the legs that were not subjected to surgery) were also subjected to pain measurements after the 5 additional days of drug dosing. The results show that there is a decrease in the paw withdrawal threshold (PWT) in both vehicle and Rofecoxib treated animals³⁷. Intriguingly, GW406381 treated animals showed no decrease in pain threshold, which suggests that further development of the pain sensitization could be prevented by chronic treatment with GW406381³⁷. However, GW406381 was not effective when evaluated by Von Frey experiment.

1.1.4 DAGL β as a promising target for pain signaling

As it is demonstrated in a case from an example of cyclooxygenases, lipid signaling pathways are tightly associated with biological functions. Other than the structural contribution in cellular environments, lipids can be highly potent signaling molecules that could be induced with associated enzymes that are dedicated to performing specific biological functions. As lipid molecules are central to metabolism and initiating cascades of signaling pathways, it is difficult to pinpoint the function of the given enzyme without exhaustive studies^{38, 39}. The background

on DAGL β will be discussed further in the following chapter. In this short section, the motivation and biological importance of studying DAGL β will be briefly discussed.

Arachidonic acid is significant in bioactive lipid biology as it can be converted to potent signaling lipids called prostaglandins by cyclooxygenases. In generating the arachidonic acid available for cyclooxygenase activity, cPLA2 has been known as the primary enzyme for providing arachidonic acid⁴⁰. The alternative pathway in generating arachidonic acid was proposed in 2011⁴¹, involving diacylglycerol lipases (DAGLs) and monoacylglycerol lipase (MAGL). The specific diacylglycerol species denoted in this pathway is 1-stearoyl 2-arachidonoyl glycerol (SAG)⁴². SAG is further cleaved at the sn-1 position by DAGL β and produces 2-arachidonoyl-glycerol (2-AG), which is sequentially processed by MAGL to release arachidonic acid that is ultimately used for prostaglandin biosynthesis.

The discovery of a distinct pathway that allows regulation of arachidonic acid involving DAGL β was further investigated by Hsu et. al⁴². Along with the development of an activity-based protein profiling (ABPP) chemical probe tailored for the DAGL β activity, Hsu et al demonstrated that the inflammatory function of peritoneal macrophages could be reduced by inhibiting DAGL β . Further lipid analysis showed that there was a reduction in prostaglandins (PGE2) as well as a reduction in arachidonic acid and 2-AG⁴². The significance of this finding is that the discovery of cellular sources of arachidonic acid outside of the well known cPLA2 pathway.

The utility of targeting DAGL β for inflammation was investigated in works published by Wilkerson et al. from Aron Lichtman's lab at VCU⁴³. This work tested the efficacy of DAGL β disruption and inhibition in a variety of pain models. The study showed that DAGL β disruption reversed inflammatory pain. In addition, DAGL β specific inhibitor KT109 was capable of allodynia in a dose-dependent manner⁴³. Several key findings emerged from these studies including discovery of complete recovery from nociception developed by chronic constriction injury (sciatic nerve pain model) as well as chemotherapy-induced peripheral neuropathy (CIPN)⁴³.

In understanding the anti-nociceptive results from DAGL β inhibition, our lab investigated signaling pathways that are regulated with DAGL β . The first anti-inflammatory effect could be due to reductions in arachidonic acid, which leads to a decrease in prostaglandins (**Figure 1.2**). However, reduced endocannabinoid 2-AG suggests that cannabinoid receptor activation via 2-AG, which produces anti-nociception, is not present in a system and does not contribute to the anti-inflammatory pathway. Lastly, the most notable function of DAGL β is to process diacylglycerols⁴⁴. Thus, the concentration of diacylglycerols would be upregulated by inhibiting DAGL β activity (**Figure 1.2**). Therefore, the current understanding of the signaling pathways regulated by DAGL β shows that the primary anti-inflammatory function would be mediated through a reduction in prostaglandins.

However, the contribution of the arachidonic acid reduction does not explain the efficacy of DAGL β inhibition in a variety of pain models. If the reduction in prostaglandins is the only mode of action, the anti-nociceptive effects would not be

as high as NSAIDs, especially if DAGL β inhibition does not result in complete reduction of prostaglandins⁴². On the contrary, DAGL β inhibition shows a reversal of allodynia not only in inflammatory pain models but also in neuropathic models (chronic constriction injury (CCI) and chemotherapy-induced peripheral neuropathy (CIPN)⁴³). In conclusion, the mechanism of the action for DAGL β is not clearly defined in its capacity to be able to mediate pain signaling. The understanding of molecular pathways that could mediate chronic pain are ill-defined. Therefore, we decided to investigate the mechanism of how DAGL β regulates the lipid environment with a focus on its potential as a therapeutic target for chronic inflammation.

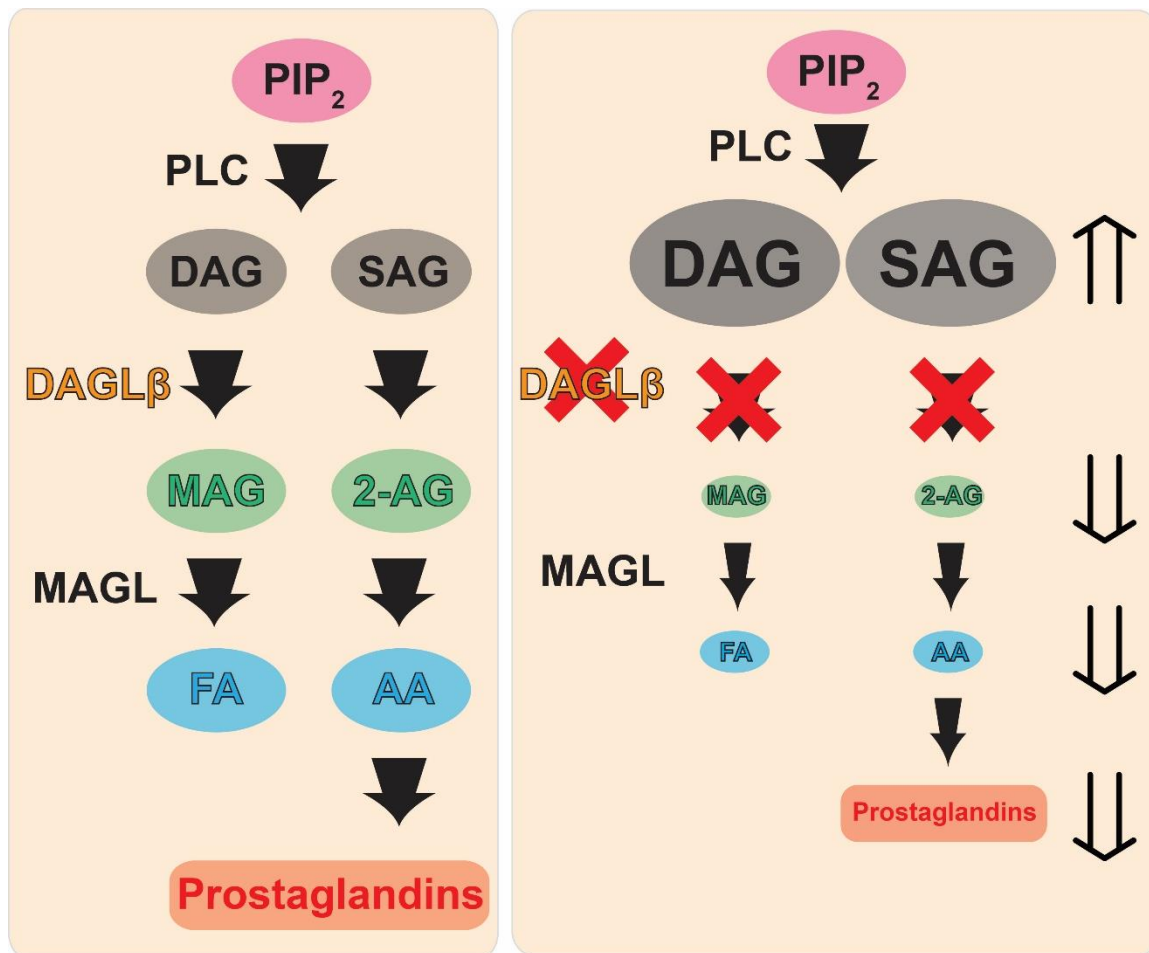


Figure 1.2 Predictive lipid flux from DAGL-beta inhibition based on current understanding of DAGL-beta The lipid flux of the biological system during DAGL-beta inhibition based on current understanding of the DAGL-beta enzyme function is described. The diacylglycerol lipase-beta is known to process diacylglycerols to generate a fatty acid and a monoacylglycerol. The inhibition of DAGL-beta would result in accumulation of diacylglycerols, reduction in monoacylglycerol, and fatty acids including arachidonic acid).

1.1.5 Introduction to diacylglycerol lipase-beta (DAGL β)

Diacylglycerol lipase-alpha and -beta (DAGL α and DAGL β) are ~120 and ~70 kDa, respectively, serine hydrolases that hydrolyze AA (arachidonic acid)-esterified diacylglycerols (DAGs) to produce 2-AG^{45, 46}. *In vitro*, DAGLs preferentially hydrolyze DAGs at the sn-1 position, can be stimulated with calcium, and have negligible activity against other lipids including monoacylglycerols and phospholipids⁴⁵. DAGLs show high conservation between humans and mice (97% and 79% identity for alpha and beta, respectively⁴⁵) but surprisingly low homology between isoforms within a given species (~20% sequence identity for human and mouse DAGLs, <https://www.uniprot.org>). Mammalian DAGLs are expressed as transmembrane proteins composed of a 4-transmembrane domain region at the N-terminus followed by a canonical α/β hydrolase domain (containing the nucleophilic serine residue). The C-terminal tail largely differentiates DAGL α and DAGL β with the former isoform showing a more pronounced domain region. Activated calcium/calmodulin-dependent protein kinase II (CaMKII) has been shown to phosphorylate the C-terminal domain of DAGL α (serine 782 and 808 of mouse DAGL α) to inhibit DAGL α activity in regulation of 2-AG metabolism and signaling *in vivo*⁴⁷ (**Figure 1.3**).

In contrast, post-translational regulation of DAGL β has not been well studied. Several reports have identified cysteine palmitoylation of DAGL β , which may serve as a novel post-translational modification (PTM) to regulate function⁴⁸.⁴⁹ Future studies aimed at studying the post-translational regulation of DAGL activity

in vivo will be important to understand the cross-talk between lipid and protein signaling pathways.

1.1.6 DAGL lipid metabolism and signaling

In addition to differences in domains and PTMs, DAGL function is segregated by tissue- and cell type-specific expression. DAGL α is expressed predominantly in central tissues (brain, spinal cord) and pancreas while DAGL β expression is enriched in the liver and immune cells, including macrophages and microglia⁵⁰⁻⁵³ (**Figure 1.5**). Consistent with gene expression profiles, lipid analyses of *Dagla*^{-/-} mice showed 80–90% reductions in brain 2-AG as well as the downstream product arachidonic acid (AA)^{50, 51, 54}. *Daglb*^{-/-} mice showed 90% reductions in liver 2-AG and negligible effects on brain 2-AG and AA, although one report demonstrated modest changes in brain 2-AG⁵⁰.

DAGL activity is further regulated by expression and activity within individual cell types of the brain⁵⁴ (**Figure 1.5**). Lipid profiles of neurons, astrocytes, and microglia revealed substantial reductions in 2-AG and AA (60–90%) in *Dagla*^{-/-} neurons and astrocytes with negligible changes in these lipids measured in microglia. In contrast, lipid profiles of *Daglb*^{-/-} neurons were not impacted. *Daglb*^{-/-} microglia showed ~50% reductions in 2-AG, AA, and prostaglandins (PGE2 and PGD2) compared with wild-type counterparts⁵⁴. Astrocytes showed a mixed lipid profile with significant reductions in 2-AG, AA, and PGE2/D2 in *Dagla*^{-/-} cells. Disruption of DAGL β resulted in a modest (~20%) but significant reduction in astrocyte 2-AG. Taken together, these metabolomic findings illustrate

the importance of DAGL expression and activity across tissues and individual cell-types of tissues to fine-tune 2-AG metabolism and signaling⁵⁴.

In the context of 2-AG signaling, disruption of DAGL α results in functional antagonism of CB1 through depletion of 2-AG available for CB1 signaling. Consistent with this hypothesis, *Dagla*^{-/-} mice recapitulate many of the metabolic (lean, hypophagic, improved glycemic control in obesity) and behavioral phenotypes (anxiety, depression) observed in CB1 knockout mice^{55, 56}. In addition, reductions in adult neurogenesis were observed in *Dagla*^{-/-} mice^{50, 57}. Localization of DAGL α at the postsynaptic density⁵⁸, potentially through protein-protein interactions of its C-terminal tail with postsynaptic Homer adaptor proteins⁵⁹ and CaMKII⁴⁷, positions this lipase for regulation of synaptic plasticity (e.g. DSI and DSE) via retrograde signaling at presynaptic CB1^{50, 51}. In summary, the comparable phenotypes of knockout mice and complementary localization of DAGL α and CB1 supports a key role for DAGL α in regulating 2-AG signaling in the CNS^{50, 57}.

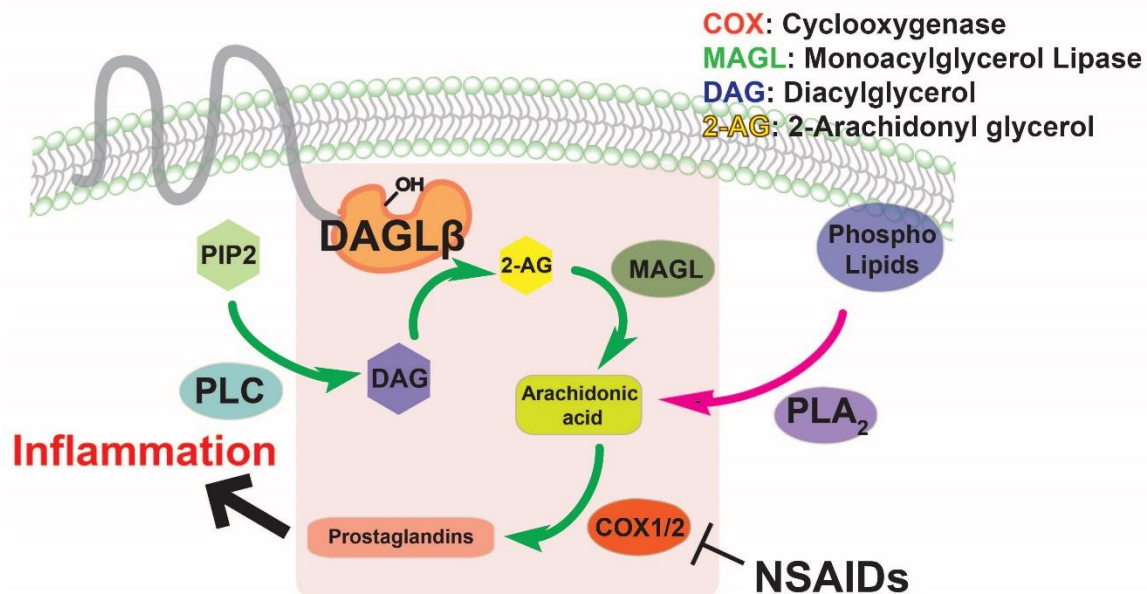


Figure 1.3 The schematics of the lipid signaling pathway that leads to prostaglandins productions Prostaglandins are generated by cyclooxygenases 1/2 (COX1/2) that converts arachidonic acid (AA) into potent bioactive lipids. Arachidonic acid is primarily generated by cPLA₂ that releases AA at sn-2 position. Additional source was discovered to be contributed by 2-arachidonyl glycerol, which is generated by DAGLs processing diacylglycerols with AA.

1.1.7 DAGL β regulates macrophage and microglia inflammatory signaling

DAGL β disruption does not result in the same metabolic and behavioral phenotypes observed in *Dagla*^{-/-} mice^{50, 51, 55}. Chemoproteomic studies have shown enrichment of DAGL β activity in macrophages and microglia (brain macrophage subset) immune cells^{52, 54} (**Figure 1.4**). Consistent with its activity profile, disruption of DAGL β results in accumulation of AA-esterified DAGs (specifically the C18:0/C20:4 DAG species) and depletion of 2-AG, AA, and prostaglandins (PGE2 and PGD2) in macrophages⁵² and microglia⁵⁴. Regulation of both 2-AG and AA by DAGL β revealed important cross-talk between endocannabinoid and eicosanoid signaling in macrophages (**Figure 1.4**). Disruption of DAGL β in macrophages and microglia also attenuated proinflammatory cytokine (TNF- α) signaling in response to lipopolysaccharide stimulation^{52, 54}. Thus, DAGL β is a complementary pathway to classical cPLA2 α pathways⁶⁰ for regulation of AA pools.

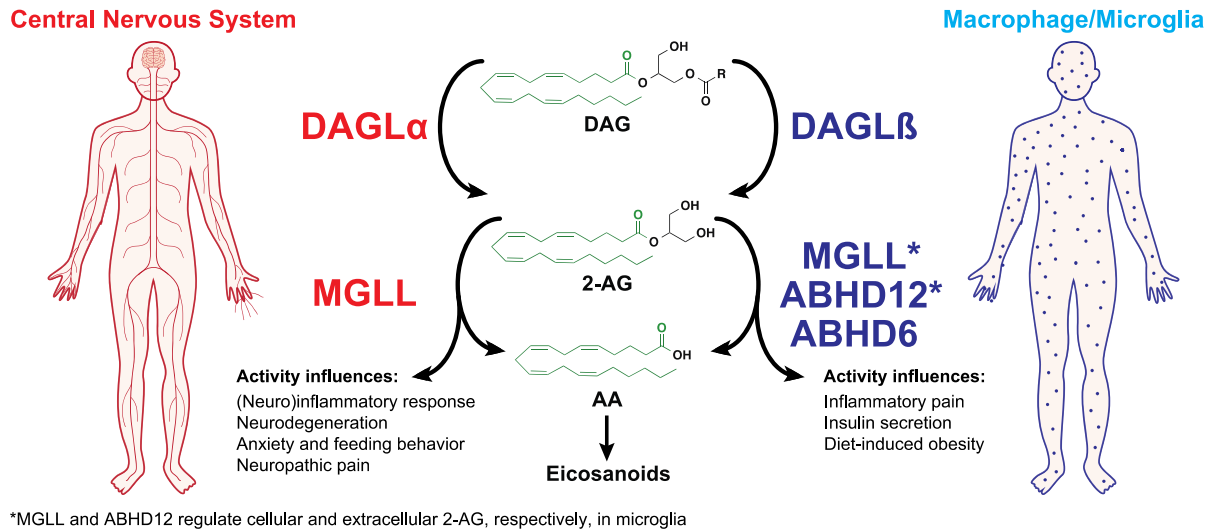


Figure 1.4 Tissue expression and activity of 2-AG biosynthetic and hydrolytic serine hydrolases that regulate endocannabinoid metabolism and signaling
Schematic depicting 2-AG (2-arachidonoylglycerol) biosynthetic and degradation pathways and their respective tissue expression that is important for regulation of endocannabinoid signaling. DAGLs (DAGL α and DAGL β) preferentially hydrolyze sn-1 fatty acids from diacylglycerols (DAG) that contain arachidonic acid (AA) esterified at the sn-2 position to biosynthesize 2-AG. DAGL α expression and activity is enriched in the central nervous system while DAGL β is found largely in macrophages and microglia. MGLL is the principal 2-AG hydrolase in the central nervous system. In microglia and macrophages, DAGL β produces 2-AG pools that are metabolized by downstream 2-AG hydrolases to release arachidonic acid (AA) utilized for production of proinflammatory lipids including eicosanoids. In microglia, MGLL, ABHD12, and ABHD6 have been shown to function as 2-AG hydrolases.

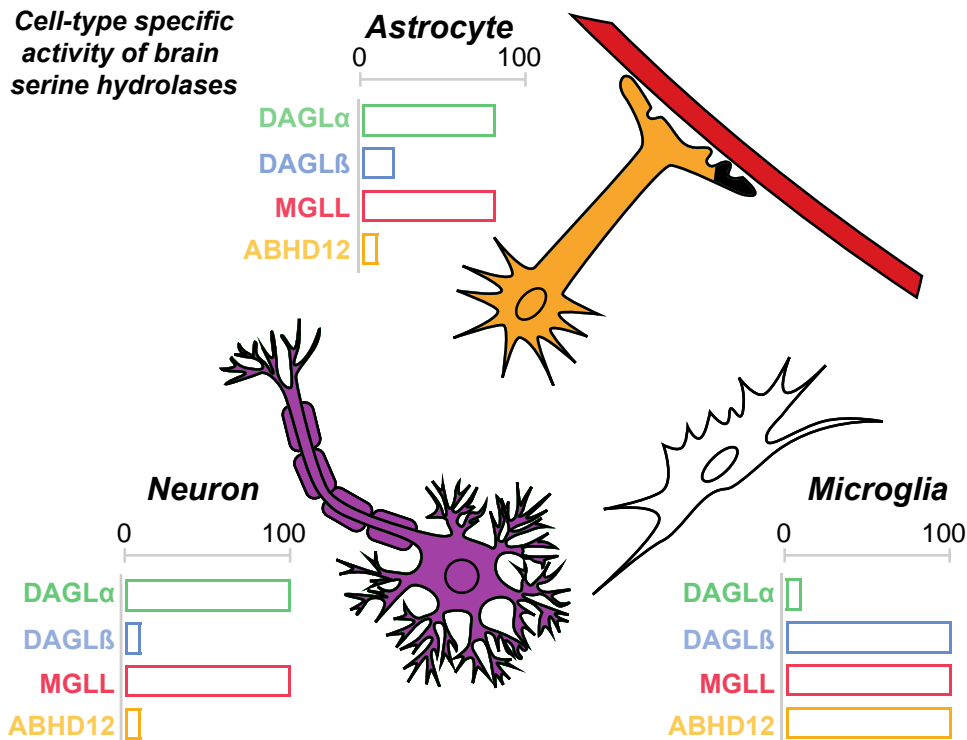


Figure 1.5 Distribution of 2-AG biosynthetic/hydrolytic serine hydrolases across cell types in brain 2-AG signaling in the central nervous system is regulated by differential expression of metabolic enzymes across cell types in the mammalian brain. DAGL α and MGLL activity is enriched in neurons, while DAGL β , MGLL, and ABHD12 regulate 2-AG metabolism and signaling in microglia. Astrocytes show similar activity profiles as neurons with the exception of increased contribution of DAGL β activity in this cell type.

1.1.8 Current DAGL inhibitors

Discovery of first-generation *in vivo*-active DAGL inhibitors was enabled by ABPP assays tailored for detection and quantitation of native DAGL activity^{52, 61}. In addition to enhanced sensitivity, the DAGL-tailored activity-based probe HT-01 allowed rapid evaluation of potency and selectivity of DAGL inhibitors directly in complex proteomes *in vitro* and *in vivo*⁵². Using ABPP-guided medicinal chemistry, the 1,2,3 triazole urea covalent inhibitor KT109 emerged as the first *in vivo*-active DAGL β inhibitor suitable for cell (IC₅₀ ~10 nM) and animal studies (EC₅₀ ~10 mg kg⁻¹ in animal pain models)^{52, 54, 62}. DAGL-inactive negative control inhibitor KT195 was also developed to distinguish DAGL β -specific from non-specific serine hydrolase inhibition^{52, 63}. Liposomal encapsulation of KT109 (i.e. liposomal KT109) enabled the targeted delivery of DAGL β inhibitors to macrophages and dramatically reduced compound amounts required to elicit anti-inflammatory effects in animal pain models⁶⁴.

KT172, a structural analog of KT109, was developed as a dual DAGL α and DAGL β inhibitor⁵². Further medicinal chemistry around the KT172 scaffold produced the CNS-active variants, DH376 and DO34, which permitted *in vivo* analysis of DAGL biology in the brain⁵³. DH376 and DO34 were used along with a negative-control probe (DO53) to demonstrate that acute blockade of DAGLs in mouse brain rapidly altered lipid profiles to impact synaptic plasticity, neuroinflammatory responses (50 mg kg⁻¹)⁵³, and fasting-induced refeeding behavior (50 mg kg⁻¹)⁶⁵. Exploration of reversible DAGL inhibitors, as opposed to covalent irreversible 1,2,3-triazole ureas, identified the α ketoheterocycle LEI104

(previously reported as a FAAH inhibitor) as a potential scaffold for developing DAGL α inhibitors⁶⁶. Future studies aimed at defining key structure-activity relationships that differentiate inhibitory activity against DAGL α versus DAGL β , as well as common serine hydrolase off-targets (e.g. ABHD6), will help guide development of DAGL α -selective inhibitors suitable for *in vivo* use in the CNS.

1.1.9 cPLA2 α regulation of arachidonic acid in inflammation

Cytosolic phospholipase A2 (cPLA2 α ; gene name of PLA2G4A) is a ~85 kDa cytosolic enzyme that is a member of a larger phospholipase A2 superfamily that directly hydrolyzes AA from the sn-2 position of membrane phospholipids^{67, 68}. Cell activation results in localization of cPLA2 α to the membrane and release of free AA, which are further converted to bioactive eicosanoid lipids that include PGE2⁶⁹. cPLA2 α preferentially hydrolyzes phosphatidylcholine (PC) with AA at the sn-2 position while still showing activity against PE and phosphatidylinositol (PI)⁷⁰⁻⁷². The unique substrate specificity of cPLA2 α can be partly explained by molecular dynamics (MD) simulations of cPLA2 α -PAPC (1-palmitoyl-2-arachidonoyl-PC) interaction, which show a deep channel binding pocket that confers cPLA2 α substrate specificity through π - π stacking unlike group VIA Ca²⁺-independent PLA2 (iPLA2; gene name of PLA2G6), which exhibits little specificity for sn-2 specific hydrolysis⁷³.

1.1.10 Functional cross-talk of cPLA2 α and DAGL β signaling pathways

Cross-talk between cPLA2 α and DAGL β pathways in macrophage lipid metabolism and signaling was recently revealed in model systems of inflammation.

Blockade of either cPLA2 α or DAGL β pathways resulted in partial reductions in cellular AA while the dual blockade of cPLA2 α /DAGL β resulted in near-complete depletion of AA in macrophages⁵². These metabolic effects were complemented by similar regulation of cytokine signaling where cPLA2 α /DAGL β -dual blockade provided a synergistic enhancement in TNF- α production. These metabolic and cell biological findings support distinct and complementary pathways for supplying AA utilized for COX-mediated production of proinflammatory lipid signals. cPLA2 α responds to calcium signaling by the nature of its Ca²⁺ binding C2 domain, which promotes membrane localization and direct release of AA from phospholipids. DAGL β hydrolyzes AA-esterified DAGs that likely arise from activation of phospholipase C (PLC) which releases DAG and IP3 during signal transduction^{74, 75}. Thus, the release of AA can occur through cPLA2 α hydrolysis of phospholipids or a PLC-DAGL-MGLL sequential metabolic pathway. Given the role of DAGL β in microglia biology⁵⁴, cross-talk with cPLA2 α pathways likely exists in the CNS where disruption of 2-AG metabolism (biosynthesis and degradation) can affect neuroinflammation^{54, 76}.

1.1.11 Dissertation Summary

There is an increasing interest in understanding how DAGL β is regulated, as well as the role that it plays in the context of inflammation. The effect of targeting DAGL β in a variety of pain models has been shown to be impactful even though the current understanding of the enzyme does not explain its efficacy in pain models. Elucidating the mechanisms involved DAGL β regulation could be of particular valuable as there is no pharmacological treatment available to treat

chronic pain syndromes. The goal of this dissertation to identify signaling pathways that DAGL β mediates in a biologically relevant environment. Chapter 2 discusses the approach to determine the cell type that contributes to pain signaling. This work utilized the encapsulation of DAGL β inhibitor in liposomes for targeted delivery to phagocytes. Chapter 3 demonstrates DAGL β inhibition as a unique target that could reduce dendritic cells' capacity to produce inflammatory cytokines without impacting its capacity for its adaptive immune function. Chapter 4 discusses the methods used to discover novel substrate specificity of DAGL β and signaling pathways contributing to the biological impact by DAGL β inhibition. Chapter 5 discusses a summary of the work presented in this dissertation and addresses limitations and future directions for studying the relevant signaling pathways of DAGL β and its relationship to inflammation.

1.2 References

1. Ashley, N.T., Z.M. Weil, and R.J. Nelson, *Inflammation: Mechanisms, Costs, and Natural Variation*. Annual Review of Ecology, Evolution, and Systematics, 2012. **43**(1): p. 385-406.
2. Kotas, Maya E. and R. Medzhitov, *Homeostasis, Inflammation, and Disease Susceptibility*. Cell, 2015. **160**(5): p. 816-827.
3. Karin, M., T. Lawrence, and V. Nizet, *Innate Immunity Gone Awry: Linking Microbial Infections to Chronic Inflammation and Cancer*. Cell, 2006. **124**(4): p. 823-835.
4. Mogensen, T.H., *Pathogen Recognition and Inflammatory Signaling in Innate Immune Defenses*. Clinical Microbiology Reviews, 2009. **22**(2): p. 240.
5. Wick, M.C., et al., *Relationship between inflammation and joint destruction in early rheumatoid arthritis: a mathematical description*. Annals of the rheumatic diseases, 2004. **63**(7): p. 848-852.
6. Brück, W. and C. Stadelmann, *Inflammation and degeneration in multiple sclerosis*. Neurological Sciences, 2003. **24**(5): p. s265-s267.
7. Fahy, E., et al., *Lipid classification, structures and tools*. Biochimica et biophysica acta, 2011. **1811**(11): p. 637-647.
8. German, J.B., *Dietary lipids from an evolutionary perspective: sources, structures and functions*. Maternal & Child Nutrition, 2011. **7**(s2): p. 2-16.
9. Bulbul, M.C., et al., *Disorders of Lipid Metabolism in Chronic Kidney Disease*. Blood Purification, 2018. **46**(2): p. 144-152.

10. Chiurchiù, V., A. Leuti, and M. Maccarrone, *Bioactive Lipids and Chronic Inflammation: Managing the Fire Within*. *Frontiers in immunology*, 2018. **9**: p. 38-38.
11. Rogerio, A.d.P., et al., *The Role of Lipids Mediators in Inflammation and Resolution*. *BioMed Research International*, 2015. **2015**: p. 2.
12. Sansone, R.A. and L.A. Sansone, *Pain, pain, go away: antidepressants and pain management*. *Psychiatry (Edgmont (Pa. : Township))*, 2008. **5**(12): p. 16-19.
13. Patetsos, E. and E. Horjales-Araujo, *Treating Chronic Pain with SSRIs: What Do We Know?* *Pain research & management*, 2016. **2016**: p. 2020915-2020915.
14. McEwen, B.S. and M. Kalia, *The role of corticosteroids and stress in chronic pain conditions*. *Metabolism - Clinical and Experimental*, 2010. **59**: p. S9-S15.
15. Vyvey, M., *Steroids as pain relief adjuvants*. *Canadian family physician Medecin de famille canadien*, 2010. **56**(12): p. 1295-e415.
16. Fields, H.L., *The doctor's dilemma: opiate analgesics and chronic pain*. *Neuron*, 2011. **69**(4): p. 591-594.
17. Rosenblum, A., et al., *Opioids and the treatment of chronic pain: controversies, current status, and future directions*. *Experimental and clinical psychopharmacology*, 2008. **16**(5): p. 405-416.

18. Blobaum, A.L. and L.J. Marnett, *Structural and Functional Basis of Cyclooxygenase Inhibition*. Journal of Medicinal Chemistry, 2007. **50**(7): p. 1425-1441.
19. Miller, S.B., *Prostaglandins in Health and Disease: An Overview*. Seminars in Arthritis and Rheumatism, 2006. **36**(1): p. 37-49.
20. Ricciotti, E. and G.A. FitzGerald, *Prostaglandins and inflammation*. Arteriosclerosis, thrombosis, and vascular biology, 2011. **31**(5): p. 986-1000.
21. Bushra, R. and N. Aslam, *An overview of clinical pharmacology of Ibuprofen*. Oman medical journal, 2010. **25**(3): p. 155-1661.
22. Pairet, M. and G. Engelhardt, *Distinct isoforms (COX-1 and COX-2) of cyclooxygenase: possible physiological and therapeutic implications*. Fundamental & Clinical Pharmacology, 1996. **10**(1): p. 1-15.
23. Meyer-Kirchrath, J. and K. Schror, *Cyclooxygenase-2 Inhibition and Side-effects of Non-steroidal Antiinflammatory Drugs in the Gastrointestinal Tract*. Current Medicinal Chemistry, 2000. **7**(11): p. 1121-1129.
24. Buttgerit, F., G.R. Burmester, and L.S. Simon, *Gastrointestinal toxic side effects of nonsteroidal anti-inflammatory drugs and cyclooxygenase-2-specific inhibitors*. The American Journal of Medicine, 2001. **110**(3): p. 13-19.
25. Parepally, J.M.R., H. Mandula, and Q.R. Smith, *Brain Uptake of Nonsteroidal Anti-Inflammatory Drugs: Ibuprofen, Flurbiprofen, and Indomethacin*. Pharmaceutical Research, 2006. **23**(5): p. 873-881.

26. Novakova, I., et al., *Transport rankings of non-steroidal antiinflammatory drugs across blood-brain barrier in vitro models*. PloS one, 2014. **9**(1): p. e86806-e86806.
27. Montilla-García, Á., et al., *Grip strength in mice with joint inflammation: A rheumatology function test sensitive to pain and analgesia*. Neuropharmacology, 2017. **125**: p. 231-242.
28. Sorkin, L.S. and M.S. Wallace, *ACUTE PAIN MECHANISMS*. Surgical Clinics of North America, 1999. **79**(2): p. 213-229.
29. Scholz, J., *Mechanisms of chronic pain*. Molecular Pain, 2014. **10**(Suppl 1): p. O15-O15.
30. Basbaum, A.I., et al., *Cellular and molecular mechanisms of pain*. Cell, 2009. **139**(2): p. 267-284.
31. Jensen, T.S. and N.B. Finnerup, *Allodynia and hyperalgesia in neuropathic pain: clinical manifestations and mechanisms*. The Lancet Neurology, 2014. **13**(9): p. 924-935.
32. Schäfers, M., et al., *Cyclooxygenase inhibition in nerve-injury- and TNF-induced hyperalgesia in the rat*. Experimental Neurology, 2004. **185**(1): p. 160-168.
33. Katz, J.A., *COX-2 Inhibition: What We Learned—A Controversial Update on Safety Data*. Pain Medicine, 2013. **14**(suppl_1): p. S29-S34.
34. Savage, R., *Cyclo-Oxygenase-2 Inhibitors*. Drugs & Aging, 2005. **22**(3): p. 185-200.

35. Carbone, C., T. Musumeci, and R. Pignatello, 9 - *Non-steroidal anti-inflammatory drugs*, in *Drug-Biomembrane Interaction Studies*, R. Pignatello, Editor. 2013, Woodhead Publishing. p. 281-303.
36. Broom, D.C., et al., *Cyclooxygenase 2 expression in the spared nerve injury model of neuropathic pain*. *Neuroscience*, 2004. **124**(4): p. 891-900.
37. Zhao, F.-Y., et al., *GW406381, a novel COX-2 inhibitor, attenuates spontaneous ectopic discharge in sural nerves of rats following chronic constriction injury*. *PAIN*, 2007. **128**(1).
38. Merrill, A.H., Jr. and M.C. Sullards, *Opinion article on lipidomics: Inherent challenges of lipidomic analysis of sphingolipids*. *Biochimica et biophysica acta. Molecular and cell biology of lipids*, 2017. **1862**(8): p. 774-776.
39. Glatz, J.F.C., *Challenges in Fatty Acid and lipid physiology*. *Frontiers in physiology*, 2011. **2**: p. 45-45.
40. Gijón, M.A. and C.C. Leslie, *Regulation of arachidonic acid release and cytosolic Phospholipase A2 activation*. *Journal of Leukocyte Biology*, 1999. **65**(3): p. 330-336.
41. Nomura, D.K., et al., *Endocannabinoid Hydrolysis Generates Brain Prostaglandins That Promote Neuroinflammation*. *Science*, 2011. **334**(6057): p. 809.
42. Hsu, K.-L., et al., *DAGL β inhibition perturbs a lipid network involved in macrophage inflammatory responses*. *Nat. Chem. Biol.*, 2012. **8**(12): p. 999-1007.

43. Wilkerson, J.L., et al., *Diacylglycerol lipase β inhibition reverses nociceptive behaviour in mouse models of inflammatory and neuropathic pain*. Br J Pharmacol, 2016. **173**(10): p. 1678-92.
44. Bisogno, T., et al., *Cloning of the first sn1-DAG lipases points to the spatial and temporal regulation of endocannabinoid signaling in the brain*. J. Cell Biol., 2003. **163**(3): p. 463.
45. Bisogno, T., et al., *Cloning of the first sn1-DAG lipases points to the spatial and temporal regulation of endocannabinoid signaling in the brain*. J Cell Biol, 2003. **163**(3): p. 463-8.
46. Reisenberg, M., et al., *The diacylglycerol lipases: structure, regulation and roles in and beyond endocannabinoid signalling*. Philosophical Transactions of the Royal Society B: Biological Sciences, 2012. **367**(1607): p. 3264-3275.
47. Shonesy, B.C., et al., *CaMKII regulates diacylglycerol lipase-alpha and striatal endocannabinoid signaling*. Nat Neurosci, 2013. **16**(4): p. 456-63.
48. Martin, B.R. and B.F. Cravatt, *Large-scale profiling of protein palmitoylation in mammalian cells*. Nat Methods, 2009. **6**(2): p. 135-8.
49. Yang, W., et al., *Proteome scale characterization of human S-acylated proteins in lipid raft-enriched and non-raft membranes*. Mol Cell Proteomics, 2010. **9**(1): p. 54-70.
50. Gao, Y., et al., *Loss of Retrograde Endocannabinoid Signaling and Reduced Adult Neurogenesis in Diacylglycerol Lipase Knock-out Mice*. J Neurosci, 2010. **30**(6): p. 2017-24.

51. Tanimura, A., et al., *The endocannabinoid 2-arachidonoylglycerol produced by diacylglycerol lipase alpha mediates retrograde suppression of synaptic transmission*. Neuron, 2010. **65**(3): p. 320.
52. Hsu, K.L., et al., *DAGLbeta inhibition perturbs a lipid network involved in macrophage inflammatory responses*. Nat Chem Biol, 2012. **8**(12): p. 999-1007.
53. Ogasawara, D., et al., *Rapid and profound rewiring of brain lipid signaling networks by acute diacylglycerol lipase inhibition*. Proc Natl Acad Sci U S A, 2016. **113**(1): p. 26-33.
54. Viader, A., et al., *A chemical proteomic atlas of brain serine hydrolases identifies cell type-specific pathways regulating neuroinflammation*. eLife, 2016. **5**: p. e12345.
55. Powell, D.R., et al., *Diacylglycerol Lipase alpha Knockout Mice Demonstrate Metabolic and Behavioral Phenotypes Similar to Those of Cannabinoid Receptor 1 Knockout Mice*. Front Endocrinol (Lausanne), 2015. **6**: p. 86.
56. Jenniches, I., et al., *Anxiety, Stress, and Fear Response in Mice with Reduced Endocannabinoid Levels*. Biol Psychiatry, 2015(0).
57. Shonesy, B.C., et al., *Genetic disruption of 2-arachidonoylglycerol synthesis reveals a key role for endocannabinoid signaling in anxiety modulation*. Cell Rep, 2014. **9**(5): p. 1644-53.

58. Zhou, Y., et al., *Regulated endosomal trafficking of Diacylglycerol lipase alpha (DAGLalpha) generates distinct cellular pools; implications for endocannabinoid signaling*. Mol Cell Neurosci, 2016. **76**: p. 76-86.
59. Jung, K.-M., et al., *A Key Role for Diacylglycerol Lipase-alpha in Metabotropic Glutamate Receptor-Dependent Endocannabinoid Mobilization*. Mol Pharmacol, 2007. **72**(3): p. 612-621.
60. Leslie, C.C., *Cytosolic phospholipase A(2): physiological function and role in disease*. J Lipid Res, 2015. **56**(8): p. 1386-402.
61. Hsu, K.L., et al., *Development and optimization of piperidyl-1,2,3-triazole ureas as selective chemical probes of endocannabinoid biosynthesis*. J Med Chem, 2013. **56**(21): p. 8257-69.
62. Wilkerson, J.L., et al., *Diacylglycerol lipase beta inhibition reverses nociceptive behaviour in mouse models of inflammatory and neuropathic pain*. Br J Pharmacol, 2016. **173**(10): p. 1678-92.
63. Yun, B., et al., *Serine Hydrolase Inhibitors Block Necrotic Cell Death by Preventing Calcium Overload of the Mitochondria and Permeability Transition Pore Formation*. Journal of Biological Chemistry, 2014. **289**(3): p. 1491-1504.
64. Shin, M., et al., *Liposomal Delivery of Diacylglycerol Lipase-Beta Inhibitors to Macrophages Dramatically Enhances Selectivity and Efficacy in Vivo*. Mol Pharm, 2018. **15**(3): p. 721-728.
65. Deng, H., et al., *Triazole Ureas Act as Diacylglycerol Lipase Inhibitors and Prevent Fasting-Induced Refeeding*. J Med Chem, 2017. **60**(1): p. 428-440.

66. Baggelaar, M.P., et al., *Development of an Activity-Based Probe and In Silico Design Reveal Highly Selective Inhibitors for Diacylglycerol Lipase- α in Brain*. *Angew Chem Int Ed Engl*, 2013.
67. Balboa, M.a.A., et al., *Expression and function of phospholipase A₂ in brain*. *FEBS Letters*, 2002. **531**(1): p. 12-17.
68. Balsinde, J., M.V. Winstead, and E.A. Dennis, *Phospholipase A₂ regulation of arachidonic acid mobilization*. *FEBS Letters*, 2002. **531**(1): p. 2-6.
69. Balsinde, J., et al., *Regulation and inhibition of phospholipase A₂*. *Annu Rev Pharmacol Toxicol*, 1999. **39**(1): p. 175-89.
70. Diez, E., et al., *Substrate specificities and properties of human phospholipases A₂ in a mixed vesicle model*. *J Biol Chem*, 1992. **267**(26): p. 18342-8.
71. Li-Stiles, B., H.-H. Lo, and S.M. Fischer, *Identification and characterization of several forms of phospholipase A₂ in mouse epidermal keratinocytes*. *Journal of Lipid Research*, 1998. **39**(3): p. 569-582.
72. Burke, J.E., et al., *A phospholipid substrate molecule residing in the membrane surface mediates opening of the lid region in group IVA cytosolic phospholipase A₂*. *J Biol Chem*, 2008. **283**(45): p. 31227-36.
73. Mouchlis, V.D., et al., *Membranes serve as allosteric activators of phospholipase A₂, enabling it to extract, bind, and hydrolyze phospholipid substrates*. *Proceedings of the National Academy of Sciences*, 2015. **112**(6): p. E516.

74. Tang, X., et al., *Role of phospholipase C and diacylglyceride lipase pathway in arachidonic acid release and acetylcholine-induced vascular relaxation in rabbit aorta*. Am J Physiol Heart Circ Physiol, 2006. **290**(1): p. H37-45.
75. Hokin, L.E., *Effects of calcium omission on acetylcholine-stimulated amylase secretion and phospholipid synthesis in pigeon pancreas slices*. Biochim Biophys Acta, 1966. **115**(1): p. 219-21.
76. Nomura, D.K., et al., *Endocannabinoid hydrolysis generates brain prostaglandins that promote neuroinflammation*. Science, 2011. **334**(6057): p. 809-13.

CHAPTER 2: Targeted Delivery of Diacylglycerol Lipase-Beta Inhibitors to macrophages *in vivo* using liposomal encapsulation

2.1 Overview

Diacylglycerol lipase-beta (DAGL β) hydrolyzes arachidonic acid (AA)-containing diacylglycerols to produce bioactive lipids including endocannabinoids and AA-derived eicosanoids involved in regulation of inflammatory signaling. Previously, we demonstrated that DAGL β inactivation using the triazole urea inhibitor KT109 blocked macrophage inflammatory signaling and reversed allodynic responses of mice in inflammatory and neuropathic pain models. Here, we tested whether we could exploit the phagocytic capacity of macrophages to localize delivery of DAGL β inhibitors to these cells *in vivo* using liposome encapsulated KT109. We used DAGL β -tailored activity-based probes and chemical proteomic methods to measure potency and selectivity of liposomal KT109 in macrophages and tissues from treated mice. Surprisingly, delivery of ~5 μ g of liposomal KT109 was sufficient to achieve ~80% inactivation of DAGL β in macrophages with no apparent activity in other tissues *in vivo*. Our macrophage-targeted delivery resulted in a >100-fold enhancement in antinociceptive potency compared with free compound in a mouse inflammatory pain model. Our studies describe a novel anti-inflammatory strategy that is achieved by targeted *in vivo* delivery of DAGL β inhibitors to macrophages.

2.2 INTRODUCTION

Macrophages are a key immune cell type that mediate inflammation and pain response¹. The primary functions of macrophages include engulfing foreign pathogens and releasing pro-inflammatory lipids and cytokines to neutralize pathogens^{2, 3}. Therefore, macrophages are often described as professional phagocytes. Here, we tested our hypothesis that targeted delivery of diacylglycerol lipase-beta inhibitors to macrophages *in vivo* could be achieved by liposomal encapsulation.

In brief, we demonstrated that liposomal encapsulation of the diacylglycerol lipase-beta inhibitor KT109 significantly improved *in vivo* inhibitor activity in macrophages. The increased inhibitor activity was accompanied by a remarkable increase in efficacy by >100-fold in preclinical inflammatory pain model. In this chapter, we further demonstrate that inflammation and pain sensitization is regulated by macrophages and targeted liposomal delivery this innate immune cell subset improves *in vivo* efficacy of diacylglycerol lipase-beta inhibitors.

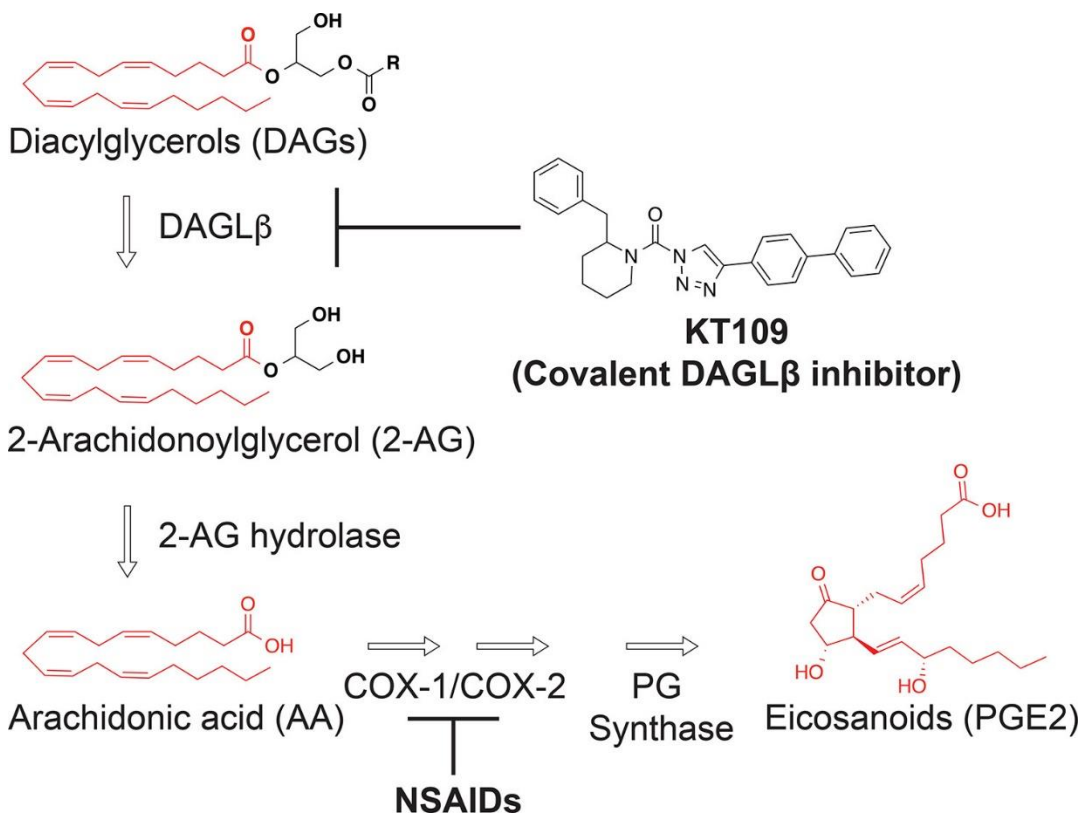


FIGURE 2.1 DAGL β hydrolyzes DAGs to regulate lipid precursors important for inflammation. DAGL β hydrolyzes diacylglycerol (DAG) to produce 2-arachidonoylglycerol (2-AG). DAG can signal by activating protein kinase pathways and 2-AG is the predominant lipid messenger for cannabinoid receptors. 2-AG can be further hydrolyzed by a downstream serine hydrolase (2-AG hydrolase) to produce arachidonic acid (AA), which is a substrate for cyclooxygenase 1 and 2 enzymes (COX1/2). COX1/2 along with PG synthases biosynthesize eicosanoids including PGE₂, which signal through prostaglandin receptors. Nonsteroidal anti-inflammatory drugs (NSAIDs) block COX1/2 activity.

Discovery of first generation DAGL β inhibitors was enabled by development of tailored activity-based protein profiling (ABPP) methods to overcome challenges with detection and quantitation of native DAGL activity^{1, 4}. In addition to being highly sensitive, ABPP methods allowed rapid evaluation of DAGL β inhibitor potency and selectivity directly in complex lysates. Using chemical proteomics to guide inhibitor optimization, the 1,2,3-triazole urea inhibitor KT109 emerged as the first *in vivo*-active DAGL β inhibitor suitable for cell and animal physiology studies^{1, 5}. Subsequent studies have since adopted this strategy to expand development of covalent as well as reversible DAGL inhibitors⁶⁻⁹. Cell biology studies using DAGL β inhibitors showed potent reductions in PGE₂ as well as TNF- α signaling in lipopolysaccharide (LPS)-stimulated macrophages treated with KT109¹. Treatment of mice with KT109 produced antinociceptive activity in the lipopolysaccharide (LPS) inflammatory pain model as well as in nerve injury and paclitaxel neuropathic pain models¹⁰. These results are consistent with established roles for PGE₂ and TNF- α inflammatory signaling in sensitization of peripheral sensory neurons in chronic pain and the effectiveness of KT109 to block these pathways *in vivo*. Results from the mouse pain models also showed that local injection of KT109 in the LPS-treated inflamed paw reversed allodynic pain responses, presumably through disruption of DAGL β function in macrophages that accumulate at inflammatory sites^{11, 12}.

Here, we set out to test whether we could use liposomes to localize delivery of DAGL β inhibitors to macrophages *in vivo*. We hypothesized that our approach would not only support macrophages as the site of action but also establish a new

strategy for development of targeted anti-inflammatory agents. We developed an encapsulation strategy compatible with the hydrophobic nature of KT109 to produce homogeneous liposomal formulations suitable for *in vivo* testing. We used DAGL β -tailored activity-based probes and chemical proteomic methods to evaluate potency and selectivity of liposomal KT109 across cells and tissues from treated mice. Finally, we tested whether enhanced delivery of liposomal KT109 to macrophages *in vivo* was sufficient to reverse nociceptive behavior in the mouse LPS inflammatory pain model.

2.3 Materials and Methods

Laboratory Animals

Subjects consisted of male C57BL/6J mice obtained from either Jackson Laboratories (Bar Harbor, Maine) or breeding pairs in the Virginia Commonwealth University vivarium for use in LPS pain studies. For selectivity studies, C57BL/6J mice were obtained from breeding pairs in the University of Virginia vivarium. Animal experiments were conducted in accordance with the guidelines of the Institutional Animal Care and Use Committee of each respective institution.

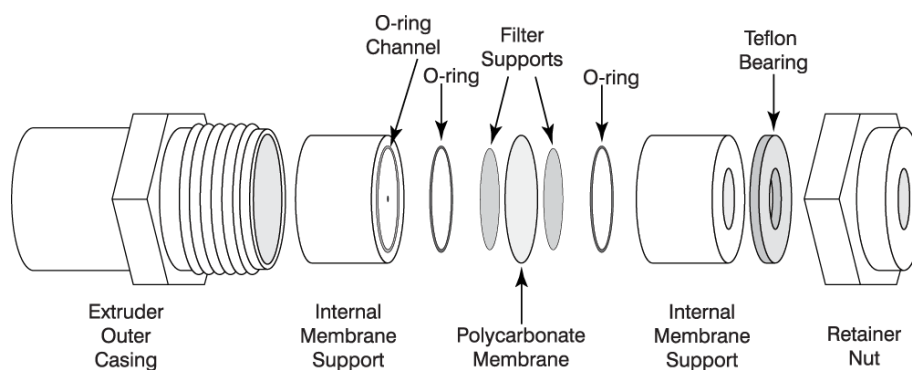
Materials

KT109, HT-01, and fluorophosphonate-rhodamine (FP-Rh) were synthesized and purity confirmed by $^1\text{H-NMR}$ and HPLC analysis as previously described^{1, 4, 13}. Isoflurane (Isothesia, Henry Schein) was purchased from the Center for Comparative Medicine at University of Virginia. Brewer thioglycollate medium was purchased from Fluka Analytical. The following lipids were purchased

from Avanti polar lipids as 25 mg/mL stock solutions in chloroform: 1,2-dioleoyl-*sn*-glycero-3-phosphoethanolamine (DOPE); 1,2-distearoyl-*sn*-glycero-3-phosphocholine (DSPC); and 1,2-dioleoyl-*sn*-glycero-3-phosphoethanolamine-*N*-[methoxy(polyethylene glycol)-2000] (ammonium salt) (PEG2000 PE). The liposome extrusion kit and polycarbonate membranes were also purchased through Avanti polar lipids. Sepharose beads (Sepharose CL-4B, 20% ethanol) were purchased from GE Health Care, Inc.

Preparation and Characterization of Liposomal KT109

Liposomal KT109 and matching “ghost” liposomes (containing the same lipid components but no compound) were prepared as described in detail in the methods section. Ghost liposomes were used as controls for *in vitro* and *in vivo* experiments. All liposomal KT109 stocks were made up as 1 mL sample sizes, limited by the 1 mL total volume of the extrusion syringes. However, multiple sets of liposomes were often made simultaneously to deliver larger quantities of liposomes for experimental use. Liposomal KT109 size and homogeneity were characterized via dynamic light scattering (DLS, Malvern Zetasizer, Nano Series) and nanoparticle tracking analysis (NTA, Malvern NanoSight LM10). KT109 concentrations in liposomes were determined by LC–MS as described below. Liposomes were kept refrigerated and used within a month.



SCHEME 2.1 Schematic diagram showing extruder assembly as provided by Avanti Polar Lipids Inc. Two Hamilton syringe with 1mL capacity were placed at each end of the extruder. The polycarbonate membrane with 100nm pore size was placed in between two filters for support. Extruder was assembled and liposomes were pushed from one syringe to the other till the liposome sizes were narrowed down to 100nm in diameter.

Detailed procedure for preparation of liposomal KT109. DSPC, DOPE and PEG2000 PE were added to a test tube with molar ratios of 56.6, 28.7, 14.7 respectively, to a total volume of 1 mL. KT109 compound was dissolved in chloroform to a concentration of 5 mg/mL and 1mL of this solution was added to the lipid sample. The chloroform was evaporated slowly under nitrogen stream for 2 hrs, leaving a thin film of lipid bilayers and entrapped KT109 around the bottom and sides of the test tube. These dried lipid films were then typically stored overnight in a -20 °C freezer. The following day, the lipid films were removed from the freezer and allowed to warm to room temperature. PBS was added to the dried down lipids in the test tube, the lipid mixture vortexed briefly, and then placed in a heat shaker at 60 °C (900 RPM) for 2 hrs. Parafilm was tightly secured over the top of the test tube to prevent evaporation. The samples were periodically vortexed over that two-hour period to further encourage stripping of the lipids from the side walls and hence formulation of the liposomes within the aqueous media. As the liposomes form, KT109 is likely entrapped, undissolved, within the hydrophobic fatty acid bilayer and/or within the inner core. After 2 hrs, the test tube was taken out of the heat shaker and placed in a bath sonicator for ~ 5 min (or until the samples became opalescent). The extruder casing was then assembled as shown in **Scheme 2.1** using 0.1 µm polycarbonate membrane pores.

A 1 mL extrusion syringe was filled with the liposomal KT109 mixture and carefully positioned through the extruder casing port into the internal membrane support chamber. Another empty 1 mL extrusion syringe was placed into the internal membrane support at the other side. Slowly the liposomal solution was

passed back and forth between syringes, eleven times, collecting the final sample in the opposite syringe. This sample was then passed through a sepharose-packed exclusion column to remove any remaining free drug. To prepare the exclusion column, ethanol was first removed from the sepharose by centrifugation, making up a final volume of sepharose in a 1:1 ratio with PBS. The sepharose was then packed and washed with an additional 5 mL of PBS prior to use.

Quantification of KT109 in Liposomal KT109 Stocks by LC–MS LC–MS was performed on an I-class Acquity coupled to a TQ-S mass spectrometer (Waters Corporation, Milford, MA). Samples were analyzed on a 2.1 mm ID × 5 cm C8 Kinetex column (Phenomenex) with the column oven set to 50 °C. Mobile phases consisted of water with 0.1% formic acid (A) and methanol with 0.1% formic acid (B). A gradient of 50% B to 99% B over 1 min was held for 0.5 min before re-equilibration at 0.5 mL/min. KT109 was detected by multiple reaction monitoring (MRM) analysis using the 423.3 > 202.1 transition with a collision energy of 10 using argon as the collision gas. Concentrations of KT109 in liposomal KT109 stocks were estimated to be ~20 µg/mL by LC–MS (**Figure 2.2**)

Compound name: KT109
Correlation coefficient: $r = 0.999159$, $r^2 = 0.998318$
Calibration curve: $4.93539 * x + -0.00137393$
Response type: Internal Std (Ref 1), Area * (IS Conc. / IS Area)
Curve type: Linear, Origin: Exclude, Weighting: 1/x, Axis trans: None

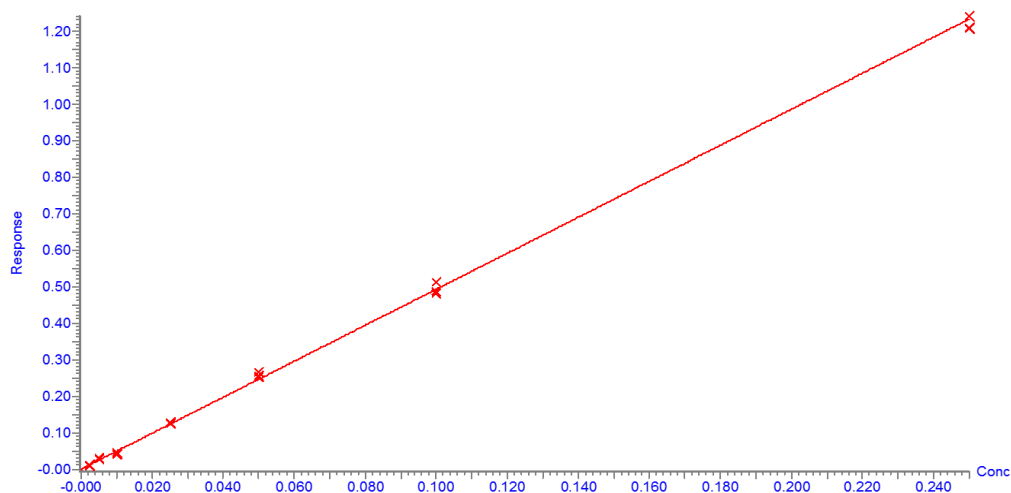


FIGURE 2.2. LC-MS analyses to measure KT109 concentrations in liposomes.

Stock solutions of free KT109 at respective concentrations were prepared and analyzed using LC-MS to generate a standard curve for estimating KT109 concentrations in liposomes. The MRM intensity values for KT109 standards were linear from 0.0025 to 0.25 $\mu\text{g/mL}$. Liposomes were diluted using acetonitrile and analyzed by LC-MS MRM analysis. Linear regression was used to calculate the concentration of KT109 in liposomal KT109 stocks. Independent replicate analyses are shown for a representative liposomal KT109 stock.

***In Vivo* Studies Using Liposomal KT109** C57BL/6J mice were injected with thioglycollate solution (4% w/v) in the peritoneal cavity 4 days prior to compound treatment in order to recruit sufficient macrophages for analyses. Mice were treated with ghost or liposomal KT109 (2.5 or 5 μ g; intraperitoneal, i.p.; 4 h), anesthetized with isoflurane, sacrificed, and thioglycollate-elicited macrophages harvested as previously described. For selectivity profiling, other tissues were harvested at the same time as macrophages. Macrophages and tissues were either used immediately or flash frozen in liquid nitrogen and stored at -80 °C until use.

Preparation of Tissue Proteomes Tissues were washed twice with ice cold lysis buffer (0.25 M sucrose, 20 mM HEPES, and 2 mM DTT in ddH₂O). Tissues were processed using dounce homogenization and placed in ice for 15 min. Tissue homogenates were centrifuged at $800 \times g$ for 5 min at 4 °C. The resulting supernatant was isolated to remove debris. Supernatants were centrifuged at $100,000 \times g$ for 45 min at 4 °C. The supernatant was removed and remaining pellet resolubilized in assay buffer (20 mM HEPES in ddH₂O) by passing through a 26-gauge syringe multiple times, and referred to as soluble and membrane fractions, respectively. Protein concentrations were determined using a Bio-Rad DC protein assay.

Gel-Based Competitive Activity Based Protein Profiling (ABPP) Proteomes (1 mg/mL) were treated with either HT-01 or FP-Rh at 1 μ M final concentration for 30 min at 37 °C. The reaction was quenched using SDS-PAGE loading buffer. After

separation by SDS-PAGE (10% acrylamide), samples were visualized by in-gel fluorescence scanning using a Chemidoc MP imaging system.

Evaluation of Liposomal KT109 in LPS Model of Inflammatory Pain Mice were given an injection of 2.5 µg of LPS from *Escherichia coli* (026:B6, Sigma), in 20 µL of physiological sterile saline (Hospira Inc., Lake Forest, IL, USA) into the plantar surface of the right hind paw. As previously reported, this dose of LPS elicits mechanical allodynia without producing measurable increases in paw thickness¹⁴. Mice were returned to their home cages after the LPS injection. Twenty-two hours following LPS administration, each mouse was given an intraperitoneal (i.p.) injection of ghost liposome or liposomal KT109 (8, 4, or 1 µg) and tested for mechanical allodynia at 24 h.

Behavioral Assessment of Mechanical Allodynia Baseline responses to light mechanical touch were assessed using von Frey filaments following habituation to the testing environment, as described elsewhere¹⁵. In brief, mice were acclimated to the testing conditions in which they were given a daily 30 min habituation session for 4 days. They were placed under an inverted wire mesh basket, which allowed unrestricted air flow, that was on top of a wire mesh screen, with spaces 0.5 mm apart. During acclimation and testing, each mouse was unrestrained and singly housed. The von Frey test utilizes a series of calibrated monofilaments, (2.83–4.31 log stimulus intensity; North Coast Medical, Morgan Hills, CA, USA) applied randomly to the left and right plantar surfaces of the hind paw for 3 s. Lifting, licking, or shaking the paw was considered a response.

Statistical Analysis Enzyme activity remaining was determined by comparing integrated band intensities of inhibitor with vehicle-treated samples for gel-based ABPP assays. Linear regression analysis was used to generate KT109 standard curves from LC–MS studies. In the LPS inflammatory pain study, Holm–Sidak’s multiple comparisons test was used for post hoc analysis following a significant one-way ANOVA. The antinociceptive ED₅₀ value 95% confidence limit of liposomal KT109 was calculated using least-squares linear regression analysis. The potency ratio with 95% confidence limit of KT109 between its formulation in liposomes (present study) and free compound in a standard vehicle (previous study⁵) was calculated using linear regression. Data are shown as mean ± SEM. For analysis of DAGLβ inhibition in paw, significance was determined by unpaired Student’s *t* test. All statistical analyses were performed using GraphPad Prism or Excel.

2.4 RESULTS

2.4.1 Encapsulation of KT109 in Liposomes As KT109 is insoluble in aqueous media, typical passive loading mechanisms for liposomal encapsulation were ineffective. We therefore explored whether KT109 could be trapped within the lipid bilayer during the dry-down step of the liposome formulation process. In brief, KT109 was dissolved in chloroform along with a cocktail of natural and unnatural phospholipids. Next, the KT109/lipid mixture was dried down under a nitrogen stream. Addition of aqueous buffer (PBS) followed by shaking and vortexing produced liposomal KT109 (**see Methods section**). Although this method provided us a route for liposomal KT109 formulation, the method proved to be very

inefficient with a large portion of compound remaining suspended within the PBS solution rather than entrapped within the lipid bilayer during spontaneous liposome formation upon rehydration. To counter this issue, we used a higher starting concentration of KT109 (5 mg/mL) to overcome limitations resulting from encapsulation inefficiency. More than 99% of the non-encapsulated KT109 is separated from liposomal KT109 during the liposome extrusion step, remaining trapped on one side of the polycarbonate membrane. The remaining free drug is separated from the liposome portion during size-exclusion chromatography to yield pure liposomal KT109.

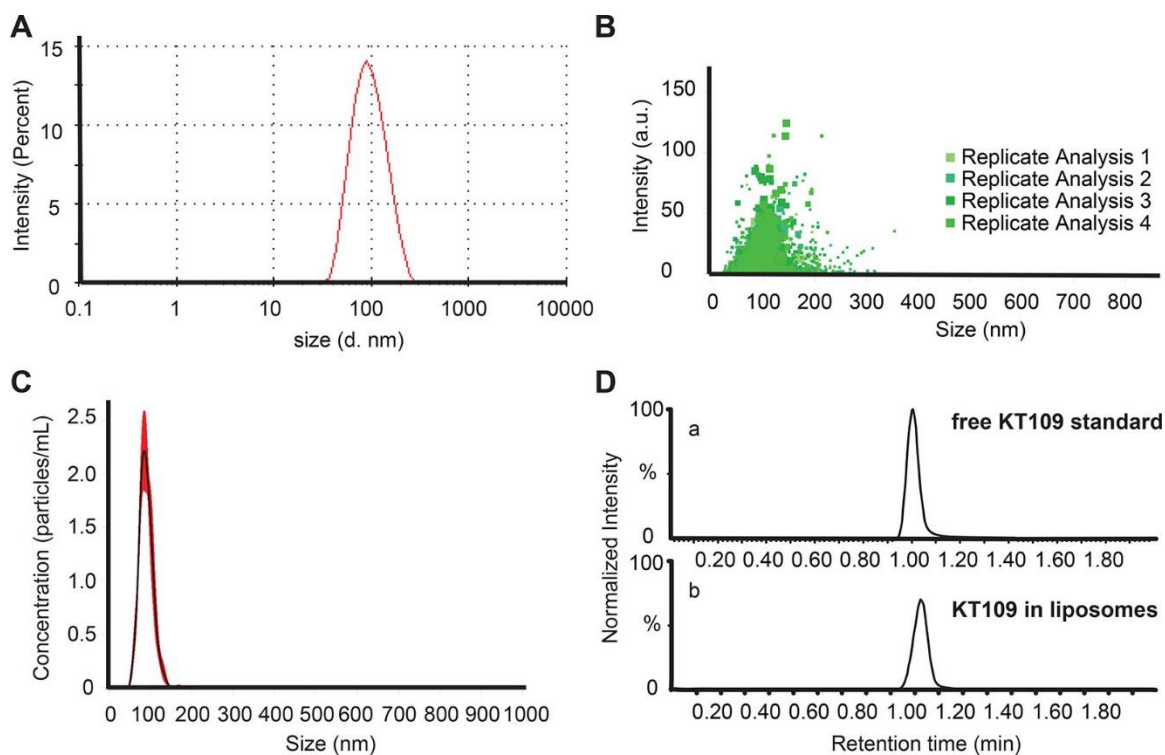


FIGURE 2.3 Characterization of liposomal KT109 by DLS, NTA, and LC-MS. (A) Graph showing the average size distribution by intensity of liposomal KT109 as determined by dynamic light scattering (DLS). Liposomal KT109 was diluted 1:100 for this analysis. The peak average is 101 ± 2 nm, which corresponds to a Z-average of 89 ± 0.3 nm. (B) Liposomal KT109 size and homogeneity as characterized by nanoparticle tracking analysis (NTA). Representative scatter graph of four replicate analyses of liposomal KT109 intensity (absorbance unit, a.u.) as a function of size (nm). (C) Finite track length adjustment (FTLA) analysis of scatter graphs is used to calculate average particle concentration ($9 \pm 0.5 \times 10^8$ particles/mL) and mean particle size (91 ± 2 nm). (D) Representative extracted ion chromatogram from MRM analysis by LC-MS of free KT109 standard compared with KT109 in liposomes. The equivalent retention times confirm the identity of KT109 encapsulated in liposomes. MRM analysis was performed using a 423 to 202 transition for KT109.

2.4.2 Characterization of Liposomal KT109 To determine the size and homogeneity of liposomal KT109, we measured these parameters by both dynamic light scattering (DLS) and nanoparticle tracking analysis (NTA). As shown in **Figure 2.3A**, the DLS profile revealed a single peak that centers around 101 ± 2 nm in diameter, which corresponds to a Z-average value of 89 ± 0.3 nm in diameter. Like DLS, NTA measures the Brownian motion of particles in a suspension and their speed related to the Stokes–Einstein equation. However, unlike DLS, which can only measure time-dependent fluctuations in scattering intensity, NTA can measure individual particle motion by video. NTA, therefore, is able to provide a more quantitative analysis as well as enhanced size resolution. For NTA, a laser beam is passed through the liposomal suspension. As the liposomes scatter light, they may be visualized by microscope. A representative distribution plot of liposome intensity as a function of size as measured by NTA is shown in **Figure 2.3 B**. As shown in **Figure 2.3C**, we used NTA finite track length adjustment (FTLA) analysis to calculate the average particle concentration ($9 \pm 0.5 \times 10^8$ particles/mL) and a mean particle size (91 ± 2 nm) for a typical liposomal KT109 sample. In summary, characterization of liposomal KT109 using complementary DLS and NTA techniques confirm that stable, homogeneous liposomes of desired diameter are routinely and reproducibly fabricated.

To determine the concentration of KT109 encapsulated in liposome, we developed a targeted multiple-reaction monitoring (MRM) LC–MS method to quantify KT109 concentrations in liposome samples (423 to 202 MRM transition, **Figure 2.3 D**). We first generated a standard curve of free KT109 and

showed high correlation between KT109 concentrations and MRM signal intensities from 0.0025 to 0.25 $\mu\text{g/mL}$ ($R^2 = 0.99$, **Figure 2.2**). Using our standard curve, we were able to estimate the concentration of encapsulated KT109 as ~ 20 $\mu\text{g/mL}$ (**Figure 2.2**). We calculated encapsulation efficiency based on the ratio of total encapsulated (20 μg) versus starting (5 mg) KT109 amounts, which results in an estimated efficiency of $\sim 0.4\%$. Future studies will be required to improve the formulation process and increase the amount of KT109 that is effectively incorporated into liposomes.

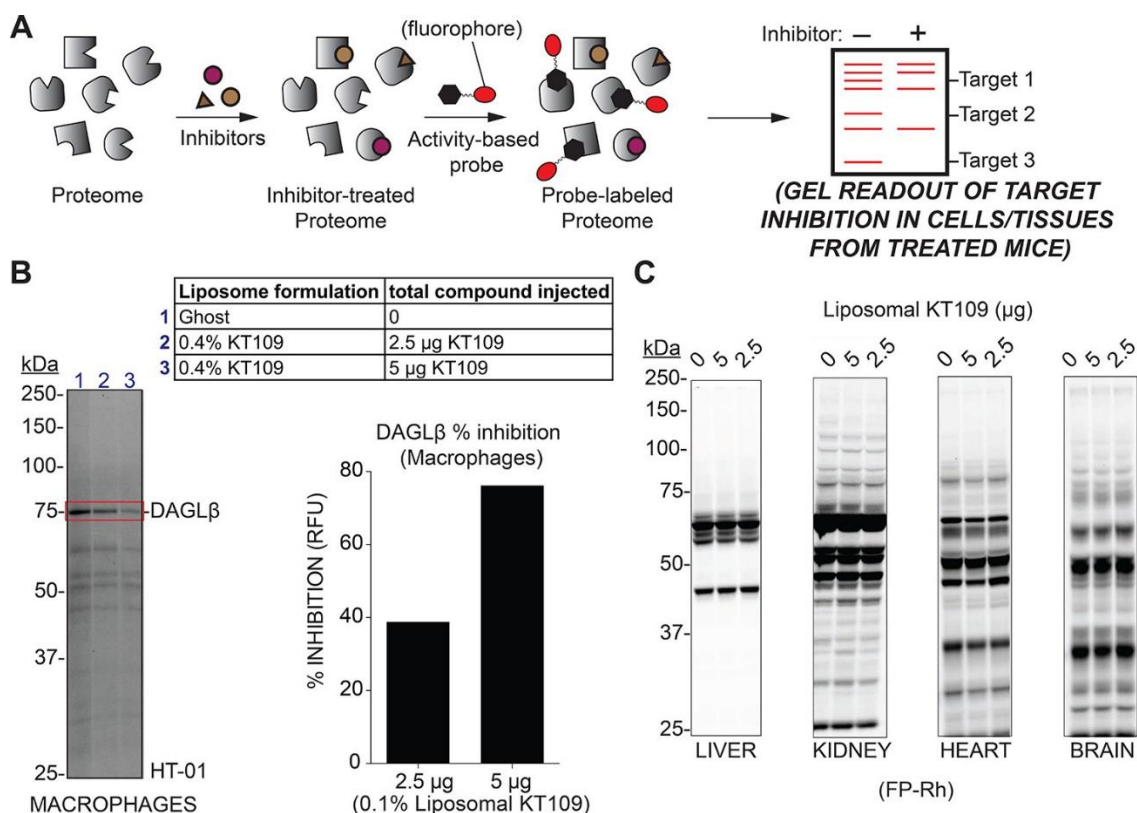


FIGURE 2.4 Chemical proteomic evaluation of liposomal KT109 potency and selectivity *in vivo*. (A) General scheme of competitive gel-based activity based protein profiling (ABPP). Proteomes were pretreated with inhibitors (30 min at 37 °C) followed by labeling with activity based probe (HT-01 or FP-Rh, 1 μ M, 30 min at 37 °C). Probe-labeled proteomes were separated by SDS-PAGE and analyzed by in-gel fluorescence scanning. (B) Thioglycollate-elicited macrophages were isolated after 4 h treatment with ghost liposomes or liposomal KT109 at the indicated doses. Cells were lysed and membrane proteomes subjected to gel-based ABPP analysis using HT-01. The degree of inactivation (% inhibition) was quantified using integrated band intensities from fluorescence gel analyses. (C) Activity and selectivity of liposomal KT109 against serine hydrolases detected in tissues from treated mice using gel-based ABPP with FP-Rh. Treatment with liposomal KT109 resulted in negligible activity across measured tissues.

KIDNEY

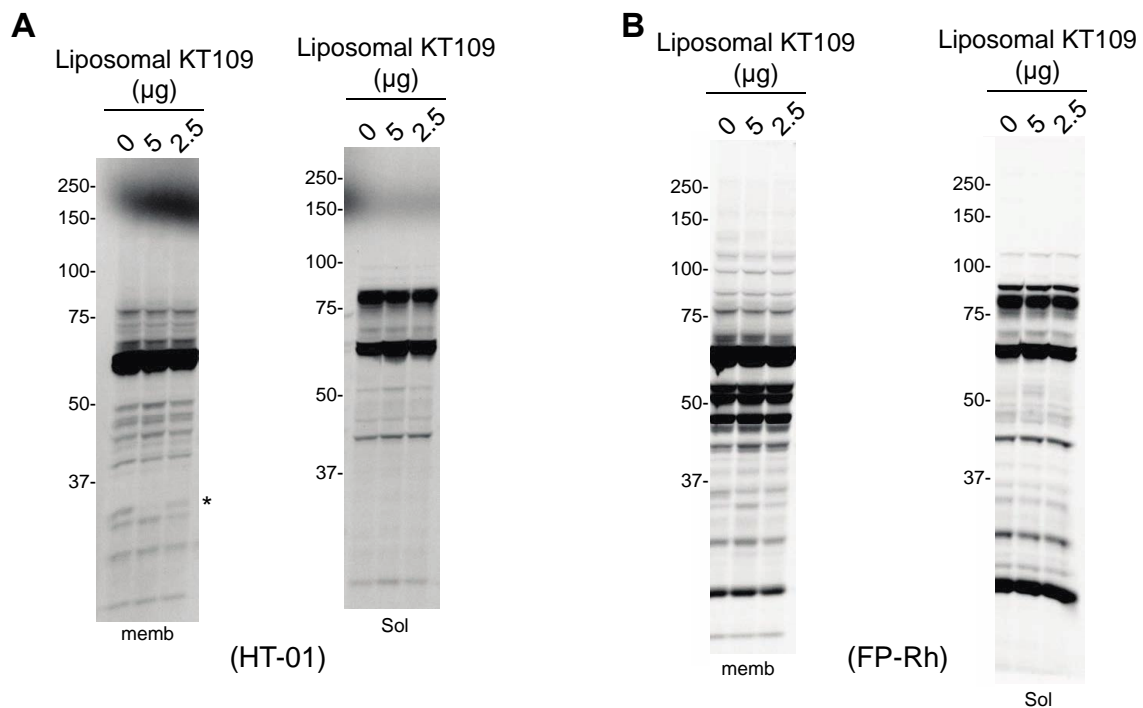


FIGURE 2.4.1 Gel-based activity-based protein profiling (ABPP) of kidney proteomes from mice treated with ghost liposomes or liposomal KT109. Mice were treated with ghost liposome or liposomal KT109 at the indicated doses for 4 hrs, animals sacrificed, and kidney tissue processed for gel-based ABPP analysis as described in **Experimental Section**. Proteomes were treated with either HT-01 (1 μM) or FP-Rh (1 μM) for 30 min at 37 $^{\circ}\text{C}$. Samples were separated by SDS PAGE and gels analyzed by in-gel fluorescence scanning using a Chemidoc MP imaging system.

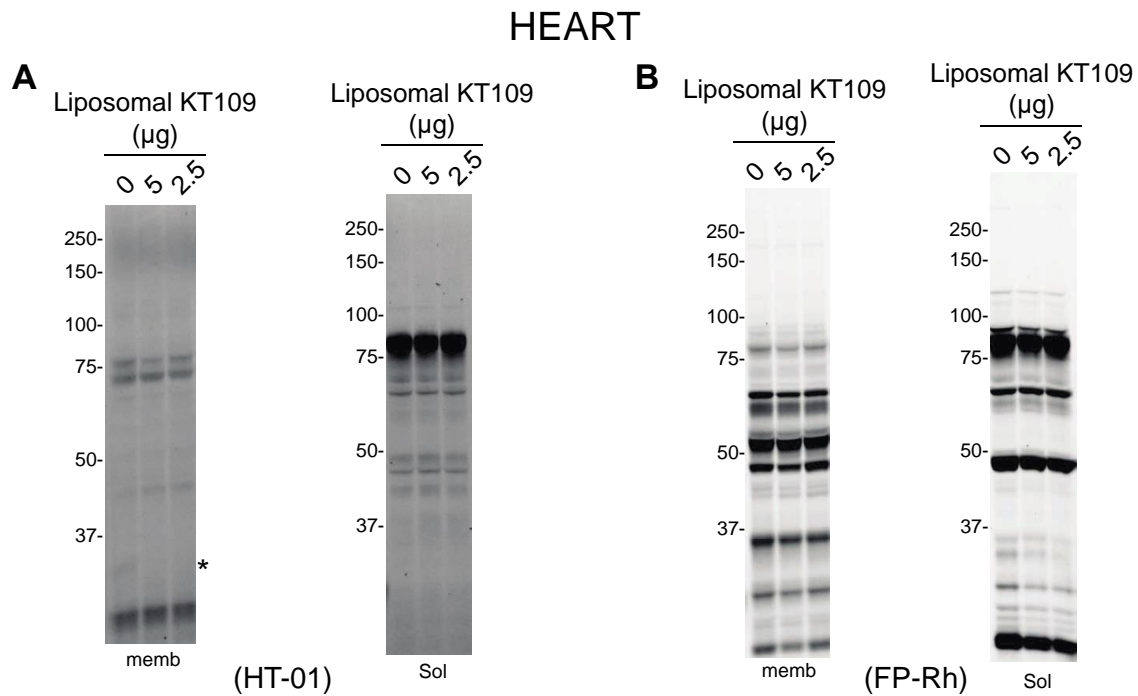


FIGURE 2.4.2 Gel-based activity-based protein profiling (ABPP) of heart from mice treated with liposomes. Activity and selectivity of liposomal KT109 in heart proteomes from ghost liposome- or liposomal KT109-treated mice were evaluated by gel-based ABPP.

BRAIN

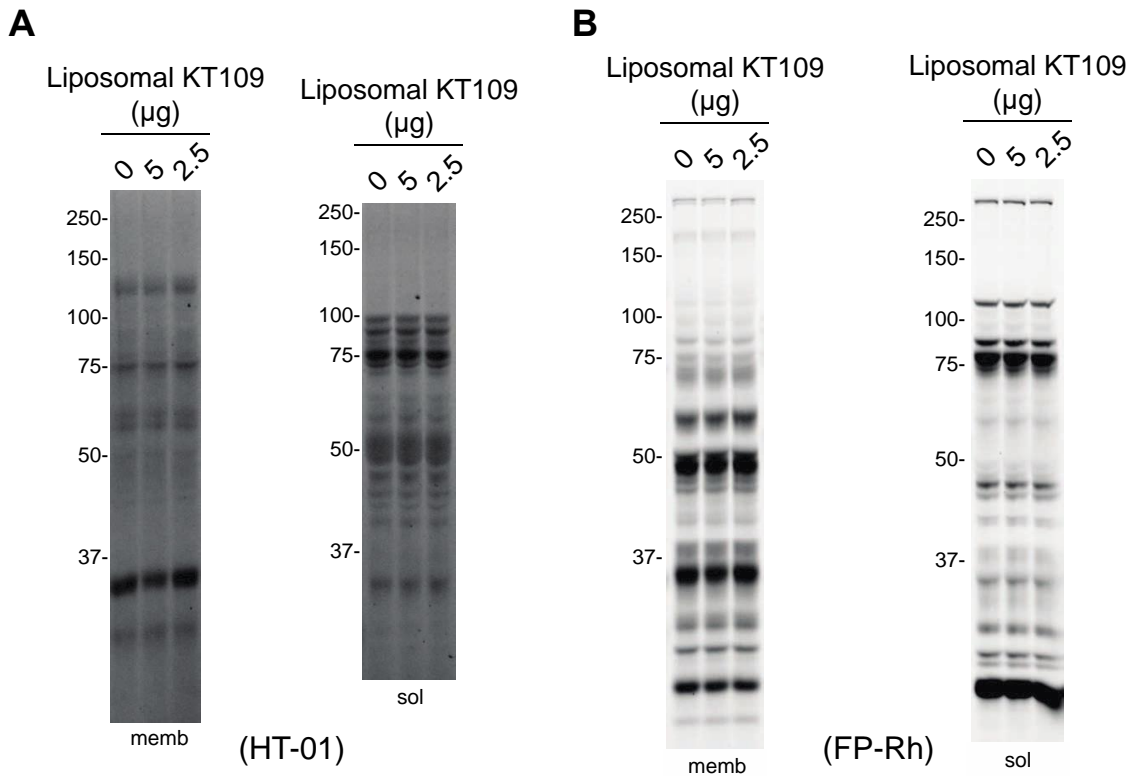


FIGURE 2.4.3 Gel-based activity-based protein profiling (ABPP) of brain from mice treated with liposomes. Activity and selectivity of liposomal KT109 in brain proteomes from ghost liposome- or liposomal KT109-treated mice were evaluated by gel-based ABPP.

LIVER

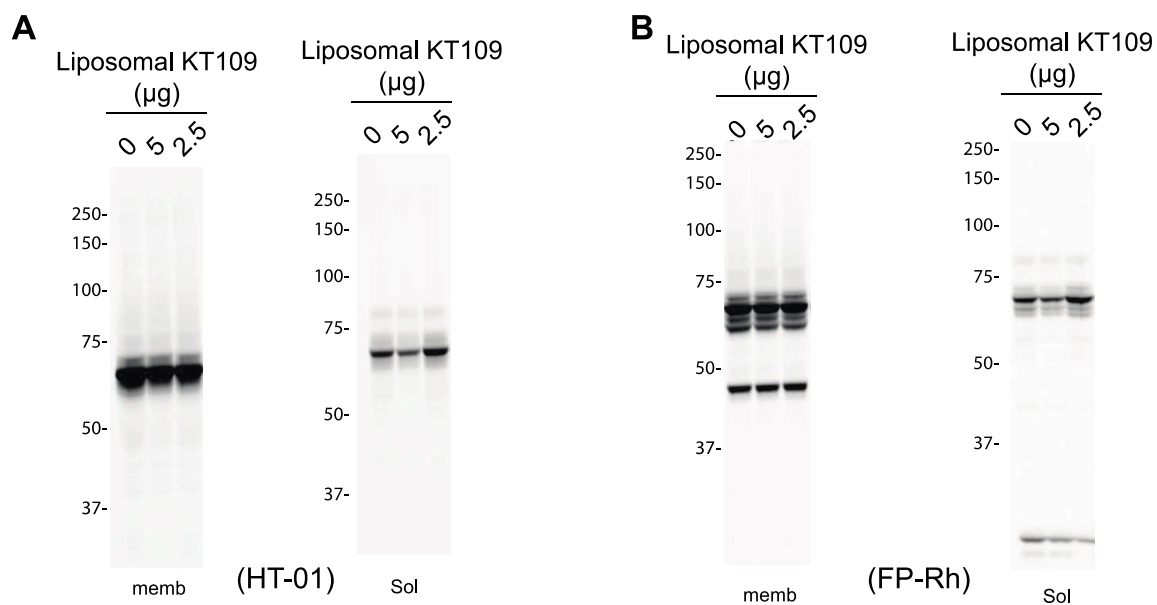


FIGURE 2.4.4 Gel-based activity-based protein profiling (ABPP) of liver from mice treated with liposomes. Activity and selectivity of liposomal KT109 in liver proteomes from ghost liposome- or liposomal KT109-treated mice were evaluated by gel-based ABPP.

2.4.3 Chemical Proteomic Analysis of Liposomal KT109 Using our first generation liposomal KT109 formulation, we asked how liposome delivery would impact KT109 potency and selectivity *in vivo*. For these analyses, we evaluated native DAGL β and other serine hydrolase (SH) activities by gel-based competitive ABPP using DAGL-tailored (HT-01¹) and broad spectrum (FP-Rh¹⁶) SH probes (**Figure 2.4 A**). ABPP analysis provides a molecular snapshot of liposomal KT109 bioavailability and selectivity *in vivo* because covalent enzyme inactivation by KT109 during treatment is not affected by tissue lysis and processing. Mice were treated with ghost liposome or liposomal KT109 (2.5 or 5 μ g) for 4 h, animals sacrificed, and tissues processed and analyzed by gel-based ABPP assay (**Figure 2.4 A**). Remarkably, we observed dose-dependent inhibition of DAGL β in peritoneal macrophages despite these low amounts of administered KT109 with ~80% inhibition observed at the 5 μ g dose (**Figure 2.4 B**). Compared with administration of free KT109 (5 mg kg⁻¹ dose¹), liposomal delivery reduced the amount of total KT109 required for comparable DAGL β inactivation in peritoneal macrophages by >20-fold (~120 vs 5 μ g of KT109 in free- compared with liposomal-delivery, respectively).

We observed excellent selectivity for liposomal KT109 across other tissues profiled (**Figure 2.4 C** and **Figure 2.4.1- Figure 2.4.4**). We measured tissues where DAGL β is known to be active (liver^{1, 17}, brain¹⁸) as well as tissues that are potential liabilities for compound toxicity (kidney, heart). In all tissues profiled, we observed negligible cross-reactivity with the exception of a minor off-target activity against a ~35 kDa serine hydrolase in kidney (**Figure 2.4.1**) and heart (**Figure**

2.4.2) proteomes that is likely ABHD6 based on molecular weight and reactivity with HT-01 probe. ABHD6 is a known off-target for several mechanism-based inhibitors including triazole ureas like KT109¹. Gel-based ABPP analysis of brain and liver proteomes from liposomal KT109-treated mice did not reveal any overt off-target activity (**Figure 2.4** and **Figure 2.4.3- Figure 2.4.4**). In summary, we discovered that liposomal delivery of KT109 dramatically enhances potency against DAGL β in macrophages while minimizing cross-reactivity in other tissues where DAGL β is active.

2.4.4 Liposomal KT109 exhibits high potency in reversing LPS-induced mechanical allodynia Next, we examined whether liposomal KT109 would reverse LPS-induced mechanical allodynia with increased potency compared with free compound from our recent study⁵. As shown in **Figure 2.5 A**, KT109 significantly reversed LPS-induced allodynia [$F(4,33) = 32, p < 0.0001$]. Post hoc testing revealed that treatment with 4 and 8 μg of liposomal KT109 significantly attenuated LPS-induced allodynia compared with mice receiving LPS and ghost liposomes. At 8 μg of KT109, we observed full reversal of LPS-induced allodynia (**Figure 2.5 A**). Using these data, the calculated ED₅₀ value for liposomal KT109 was 11 $\mu\text{g}/\text{kg}$ (9–13 $\mu\text{g}/\text{kg}$; 95% confidence limits), which represents a >100-fold enhancement in potency compared with treatments using free KT109⁵.

We also confirmed that liposomal KT109 was active in the LPS-injected paw by directly measuring native DAGL β activity at this site by gel-based ABPP using HT-01 (**Figure 2.5 B**). First, we confirmed that the ~70 kDa band detected in paw proteomes represented endogenous DAGL β by demonstrating that pretreatment

with KT109 (DAGL β inhibitor) but not KT195 (DAGL β -inactive control inhibitor) *in vitro* blocked HT-01 probe labeling (left panel, **Figure 2.5 B**). Next, we measured DAGL β activity in contralateral (control) and LPS-injected paws of mice treated with ghost liposome or liposomal KT109. We observed a modest but significant decrease in endogenous DAGL β activity (~20% inhibition, $P = 0.037$) in the LPS-injected but not contralateral control paw (right panels, **Figure 2.5 B**). Future studies are needed to determine whether increased accumulation of macrophages at inflammatory sites is a likely mechanism explaining why liposomal KT109 blocks DAGL β activity only in the LPS-injected paw. In contrast to activity in the LPS-injected paw, we observed no apparent inhibition of other SHs in central (brain and spinal cord) and peripheral (liver and spleen) tissues from liposomal KT109-treated mice as measured by gel-based ABPP (**Figure 2.5 C, D**). Collectively, our results help support that liposomal delivery of KT109 dramatically enhances *in vivo* efficacy and selectivity and that the LPS-injected paw is the likely site of action for reversal of LPS-induced allodynia.

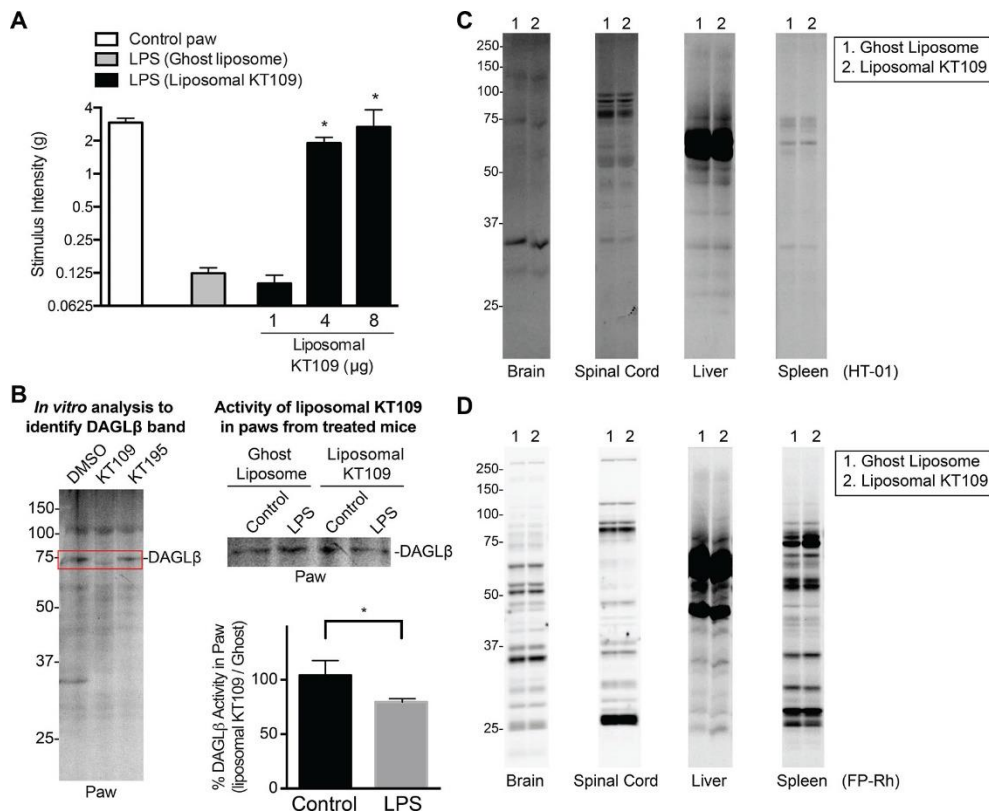


FIGURE 2.5 Efficacy and selectivity of liposomal KT109 in the LPS inflammatory pain model. (A) Intraperitoneal (i.p.) administration of liposomal KT109 reverses LPS-induced allodynia in C57BL/6J mice. $*P < 0.05$ vs LPS + ghost liposome-treated paw. Data reflect mean \pm SEM, $n = 13$ (control paw), 10 (LPS + ghost liposome), 6 (LPS + liposomal KT109 (1 μg)), 6 (LPS + liposomal KT109 (4 μg)), and 3 (LPS + liposomal KT109 (8 μg)). (B) Native DAGL β activity in LPS-treated and contralateral hind paws (control) from representative mice was measured by gel-based ABPP using HT-01. The identity of the DAGL β band detected in paws was confirmed by *in vitro* treatment of paw proteomes using free KT109 (DAGL β specific inhibitor) compared with the DAGL β -inactive control inhibitor KT195 (left panel). Native DAGL β activity was quantified in paws of mice treated with ghost liposome or liposomal KT109 under basal and inflammatory states (LPS-injected paw). Intraperitoneal administration of liposomal KT109 (4 μg) resulted in $\sim 20\%$ inhibition of total DAGL β activity in the LPS-treated paw (estimated by ratio of fluorescent signals of DAGL β band from paws of liposomal KT109- compared with ghost liposome-treated mice). Liposomal KT109 (4 μg) did not inhibit DAGL β activity in contralateral paw (no LPS treatment). $*P < 0.05$ for DAGL β activity remaining in LPS-injected versus contralateral paws. Liposomal KT109 (4 μg , i.p.) showed negligible activity against serine hydrolases in brain, spinal cord, liver, and spleen of treated mice (under inflammatory states) as measured by gel-based ABPP using HT-01 (C) and FP-Rh (D).

2.5 DISCUSSION

DAGL β expression and activity is enriched in macrophages¹, providing an opportunity to exploit the phagocytic capacity of these immune cells¹⁹ for targeted delivery of inhibitors. We explored liposomal delivery of KT109 with the goal of lowering the total amount of compound required for DAGL β inactivation in macrophages *in vivo*. The effective increase in potency using liposomal KT109 would allow for more localized blockade of PGE2 and TNF- α signaling at inflammatory sites where macrophages are known to accumulate^{11, 12}.

We discovered that systemic delivery of ~ 5 μg of KT109 in liposomes was sufficient to achieve $\sim 80\%$ inactivation of DAGL β in macrophages. Enhanced delivery of liposomal KT109 to macrophages *in vivo* was sufficient to reverse nociceptive behavior in the mouse LPS inflammatory pain model. The calculated ED₅₀ value for liposomal KT109 was 11 $\mu\text{g}/\text{kg}$ (9–13 $\mu\text{g}/\text{kg}$; 95% confidence limits), which represents a >100 -fold enhancement in potency compared with treatments using free KT109⁵. While active in macrophages, the use of liposomal delivery resulted in negligible activity of KT109 in central as well as peripheral tissues under basal (**Figure 2.4 C** and **Figure 2.4.1 - Figure 2.4.4**) and inflammatory states (**Figures 2.5 C, D**). The dramatic increase in potency supports our hypothesis that systemic administration of liposomal KT109 results in accumulation and targeted disruption of DAGL β activity in macrophage *in vivo*. As a result, we can reduce the total amount of KT109 required for efficacy to minimize cross-reactivity in other tissues and improve overall selectivity *in vivo*.

We also demonstrated that chemical proteomic methods were critical for evaluating the cells and tissues where liposomal KT109 is active. Importantly, the use of HT-01-based ABPP analysis allowed us to confirm potent inactivation of DAGL β in macrophages as well as to measure general off-target activity against other detected SHs in central and peripheral tissues. An interesting finding from our chemical proteomics analyses was detection of DAGL β inhibition by liposomal KT109 only in the LPS-injected paw (**Figure 2.5 B**). While we cannot fully explain why DAGL β activity was unaffected in control paws, our current findings support macrophages as the likely site of action for the antinociceptive activity of liposomal KT109. Future studies will focus on isolation of macrophages from paws of treated mice to further clarify the specificity of liposomal KT109 for targeting macrophages versus other cell types at inflammatory sites. We are also cognizant that DAGL β inactivation at other sites in addition to the paw may contribute to the observed efficacy *in vivo*. Future studies are needed to investigate whether changes in macrophage trafficking and/or phagocytic capacity affects liposomal KT109 access and clearance during inflammation, and whether this could represent a general strategy to target compounds to inflammatory sites. Incorporation of targeting agents, e.g., antibodies against the macrophage-specific marker F4/80²⁰, in future studies should further enhance the utility of this approach to target specific macrophage subsets.

While our preliminary studies using liposomal KT109 were successful, we recognize the low encapsulation efficiency of our current formulation process. Currently the encapsulation efficiency of KT109 within the formulated liposomes is

~0.4%. Concentrating liposomes can increase the effective dose administered *in vivo* but does not address the substantial loss of KT109 during formulation. Future studies therefore, in addition to the incorporation of targeting agents, should also address the suboptimal encapsulation efficiencies. Different methods of liposomal loading and/or lipid formulation are presently being considered. Other nanoparticle materials, specifically block copolymers such as PLGA and PLA/PEO formulations^{21, 22}, are also being considered for potential improvement of KT109 encapsulation.

2.6 ACKNOWLEDGEMENTS

We thank all members of the Hsu Lab and colleagues at the University of Virginia for helpful discussions and review of the manuscript. This work was supported by the University of Virginia (start-up funds to K.-L.H.), VCU School of Pharmacy (start-up funds to A.H.L.), NanoSTAR (to H.S.), and National Institutes of Health (DA035864 to K.-L.H.; 1F31NS095628 to L.D.S.; T32DA007027, P30DA033934, and R01NS093990 to A.H.L.).

2.7 References

1. Hsu, K.-L., et al., *DAGL β inhibition perturbs a lipid network involved in macrophage inflammatory responses*. Nat. Chem. Biol., 2012. **8**(12): p. 999-1007.
2. Rosales, C. and E. Uribe-Querol, *Phagocytosis: A Fundamental Process in Immunity*. BioMed Research International, 2017. **2017**: p. 18.
3. Dale, D.C., L. Boxer, and W.C. Liles, *The phagocytes: neutrophils and monocytes*. Blood, 2008. **112**(4): p. 935.
4. Hsu, K.-L., et al., *Development and Optimization of Piperidyl-1,2,3-Triazole Ureas as Selective Chemical Probes of Endocannabinoid Biosynthesis*. J. Med. Chem., 2013. **56**(21): p. 8257-8269.
5. Wilkerson, J.L., et al., *Diacylglycerol lipase β inhibition reverses nociceptive behaviour in mouse models of inflammatory and neuropathic pain*. Br. J. Pharmacol., 2016. **173**(10): p. 1678-1692.
6. Baggelaar, M.P., et al., *Highly Selective, Reversible Inhibitor Identified by Comparative Chemoproteomics Modulates Diacylglycerol Lipase Activity in Neurons*. J. Am. Chem. Soc., 2015. **137**(27): p. 8851-8857.
7. Baggelaar, M.P., et al., *Development of an Activity-Based Probe and In Silico Design Reveal Highly Selective Inhibitors for Diacylglycerol Lipase- α in Brain*. Angewandte Chemie International Edition, 2013. **52**(46): p. 12081-12085.
8. Deng, H., et al., *Triazole Ureas Act as Diacylglycerol Lipase Inhibitors and Prevent Fasting-Induced Refeeding*. J. Med. Chem., 2017. **60**(1): p. 428-440.
9. Janssen, F.J., et al., *Discovery of Glycine Sulfonamides as Dual Inhibitors of sn-1-Diacylglycerol Lipase α and α/β -Hydrolase Domain 6*. J. Med. Chem., 2014. **57**(15): p. 6610-6622.
10. Ogasawara, D., et al., *Rapid and profound rewiring of brain lipid signaling networks by acute diacylglycerol lipase inhibition*. Proc. Natl. Acad. Sci. U. S. A., 2016. **113**(1): p. 26-33.
11. Costigan, M., J. Scholz, and C.J. Woolf, *Neuropathic pain: a maladaptive response of the nervous system to damage*. Annu. Rev. Neurosci., 2009. **32**: p. 1-32.
12. Marchand, F., M. Perretti, and S.B. McMahon, *Role of the Immune system in chronic pain*. Nat. Rev. Neurosci., 2005. **6**(7): p. 521-532.
13. Patricelli, M.P., et al., *Direct visualization of serine hydrolase activities in complex proteomes using fluorescent active site-directed probes*. Proteomics, 2001. **1**(9): p. 1067-71.
14. Booker, L., et al., *The fatty acid amide hydrolase (FAAH) inhibitor PF-3845 acts in the nervous system to reverse LPS-induced tactile allodynia in mice*. Br. J. Pharmacol., 2012. **165**(8): p. 2485-2496.
15. Murphy, P.G., et al., *Endogenous interleukin-6 contributes to hypersensitivity to cutaneous stimuli and changes in neuropeptides associated with chronic nerve constriction in mice*. Eur J Neurosci, 1999. **11**(7): p. 2243-53.
16. Jessani, N., et al., *Enzyme activity profiles of the secreted and membrane proteome that depict cancer cell invasiveness*. Proc. Natl. Acad. Sci. U. S. A., 2002. **99**(16): p. 10335-10340.
17. Gao, Y., et al., *Loss of retrograde endocannabinoid signaling and reduced adult neurogenesis in diacylglycerol lipase knock-out mice*. J. Neurosci., 2010. **30**(6): p. 2017-2024.
18. Viader, A., et al., *A chemical proteomic atlas of brain serine hydrolases identifies cell type-specific pathways regulating neuroinflammation*. eLife, 2016. **5**: p. e12345.

19. Van, R.N. and A. Sanders, *Liposome mediated depletion of macrophages: mechanism of action, preparation of liposomes and applications*. J Immunol Methods, 1994. **174**(1-2): p. 83-93.
20. Laroui, H., et al., *Fab'-bearing siRNA TNF α -loaded nanoparticles targeted to colonic macrophages offer an effective therapy for experimental colitis*. J. Controlled Release, 2014. **186**: p. 41-53.
21. McDaniel, D.K., et al., *TIPS pentacene loaded PEO-PDLLA core-shell nanoparticles have similar cellular uptake dynamics in M1 and M2 macrophages and in corresponding in vivo microenvironments*. Nanomedicine (N. Y., NY, U. S.), 2017. **13**(3): p. 1255-1266.
22. Pustulka, K.M., et al., *Flash Nanoprecipitation: Particle Structure and Stability*. Mol. Pharmaceutics, 2013. **10**(11): p. 4367-4377.

Chapter 3. Diacylglycerol lipase-beta is required for TNF-alpha response but not CD8+ T cell priming capacity of dendritic cells

3.1 Overview

We utilized DAGL-tailored activity-based protein profiling and genetic disruption models to discover that DAGL β regulates inflammatory lipid and protein signaling pathways in primary dendritic cells (DCs). DCs serve as an important link between innate and adaptive immune pathways by relaying innate signals and antigen to drive T cell clonal expansion and prime antigen-specific immunity. We discovered that disruption of DAGL β in DCs lowers cellular 2-AG and AA that is accompanied by reductions in lipopolysaccharide (LPS) stimulated TNF- α secretion. Cell-based vaccination studies revealed DC maturation *ex vivo* and immunogenicity *in vivo* was surprisingly unaffected by DAGL β inactivation. Collectively, we identify DAGL β pathways as a means for attenuating DC inflammatory signaling while sparing critical adaptive immune functions and further expands the utility of targeting lipid pathways for immunomodulation.

3.2 INTRODUCTION

We sought to investigate the role of DAGL β in dendritic cells. We used DAGL-tailored ABPP studies with HT-01 to demonstrate that DAGL β was expressed and active in primary dendritic cells¹. The innate immune functions in response to LPS were analyzed by ELISA measurements of cytokines released by dendritic cells generated from DAGL $\beta^{-/-}$ and DAGL $\beta^{+/+}$ mice. Lastly, the adaptive immune function of dendritic cells was investigated using dendritic cell vaccinations in mice and evaluation of OVA peptide-specific T cell priming using dendritic cells derived from DAGL $\beta^{-/-}$ and DAGL $\beta^{+/+}$ mice.

3.3 Materials and methods

Reagents. Unless otherwise specified, reagents used were purchased from Fisher Scientific. Arachidonic acid-d8 (CaymanChemical Company, catalog# 390010, 2-Arachidonyl glycerol-d5 (Cayman Chemical Company, catalog# 362162. CD11c antibody-APC (Clone: N418, Biolegend, catalog# 117310), CD70 antibody-PE (Clone: FR70, eBioscience, catalog# 12-0701-82), CD86 antibody-FITC (Clone: B7-2, eBioscience, catalogue# 11-0862-82), OVA257 Dextramer-APC (Immudex, Catalog# JD2163-APC, Lot# 20150316-LL2). Fetal Bovine serum (FBS) were obtained from Omega scientific.

Animals. All studies were conducted in 8-12-week-old C57BL/6J mice. Mice were housed in the MR6 animal facility (UVa), and Gilmer animal facility (UVa). All studies were carried out under a protocol approved by the ACUC/University of Virginia. All animals were allowed free access to a standard chow diet and water. The animals were housed according to the ACUC policy on social housing of animals.

Bone marrow derived dendritic cells (BMDCs) differentiation. C57BL/6J mice were sacrificed and femur and tibia were isolated from hindlegs. Bone marrow was extracted by cutting each end of the bone and flushed with serum free RPMI. Red blood cells were lysed with red blood cell lysis buffer and cultured in DC differentiation media (200 U/mL GM-CSF, 10% FBS, 2mM L-Glutamine (Thermo Fisher Scientific), 10 units and 100 $\mu\text{g mL}^{-1}$ penicillin-streptomycin (Sigma-Aldrich), 50 μM beta-mercaptoethanol (Sigma-Aldrich), 20 mM HEPES). At day 3, an additional 10 mL of DC differentiation media was added. At day 6 and 8, half of the

media was exchanged to DC differentiation media that contains 30 U/mL instead 200 U/mL of GM-CSF. BMDCs were harvested by gently harvesting non-adherent suspension cells.

BMDC activation/maturation. At day 10 of differentiation, suspension cells were gently harvested by centrifugation at 600 x *g* for 5 min and resuspended in DC differentiation media. BMDCs were re-plated in a 10 cm petri-dish and activated for 8 hrs with PAM3CSK4 (1 µg/mL), FGK45 (1 µg/mL), and OVA257 (10 µg/mL). At the end of the 8 hr activation, cells were gently collected and centrifuged at 600 x *g* for 5 min. Cells were resuspended in DC differentiation media and analyzed by flow cytometry for activation and maturation.

BMDC and splenocyte flow cytometry analysis. BMDCs were analyzed using the following BMDC surface marker panel: CD11c-APC (1:500), CD70-PE (1:250), and CD86-FITC (1:500). Antibodies were diluted with FACS buffer (0.5% BSA, 2 mM EDTA, in PBS). Cells (1×10^5 cells) were resuspended in a 96-well plate (V-bottom plate) and stained with Live/Dead dye (Aqua Dead cell stain; ThermoFisher L34957). Live/Dead reagent was washed with PBS twice before being blocked with FC-block (anti-CD16/32; Invitrogen) for 10 min at 4 °C. Following FC-block, BMDC antibody panels were added and stained for 30 min at 4 °C. Count beads (ThermoFisher 01-1234-42) (51,000 beads) were added after the staining was completed in order to accurately count the number of activated dendritic cells per C57BL/6J mouse. FMO (fluorescence Minus One) controls were prepared by leaving out one of each stain in the staining panel. Activated BMDCs (CD70+, CD86+, CD11c+) cells were injected into C57BL/6J (100,000 activated cells) in

PBS by tail vein (i.v.). Spleens were harvested 7 days after BMDC injection. Splenocyte analysis was performed after spleens were dounce-homogenized briefly and filtered through a mesh filter (100 μ m). Splenocytes were labeled with Live/Dead stain, and FC-block. A splenocyte panel (CD8-FITC (1:500), CD44-PE (1:1000), and OVA_dex-APC (1:20) (Immudex) was used to stain CD8⁺ T cells that are specific for OVA₂₅₇. FMO controls were prepared as above. Samples were analyzed using BDFACS CANTO II flow cytometer. Flow cytometric analysis was performed using FlowJo software version 10 (Ashland OR).

Gating strategy for FACS analysis of bone-marrow derived dendritic cells (BMDCs)

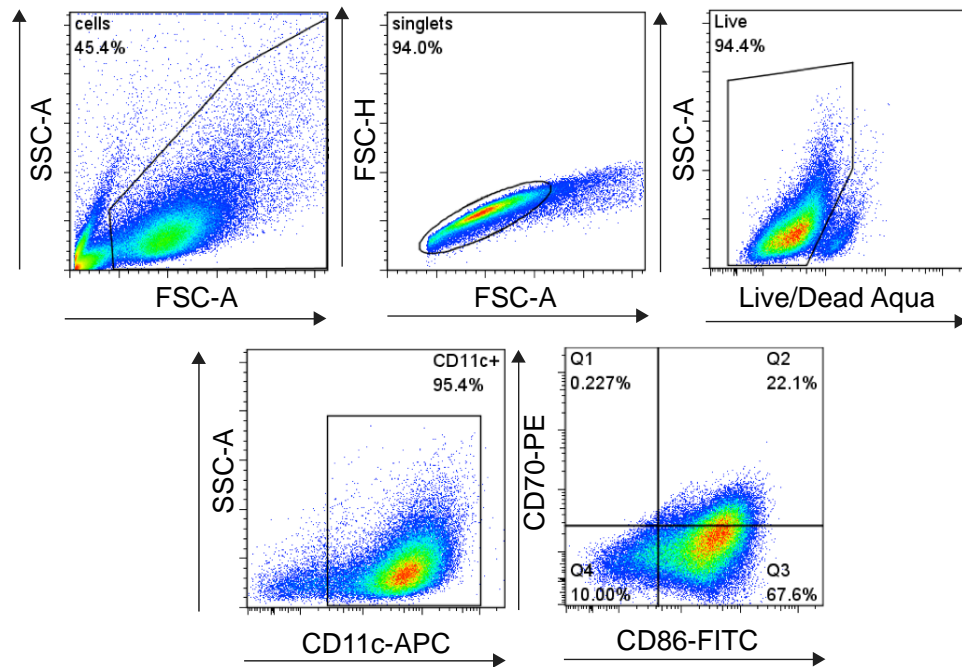


Figure 3.1 Gating strategy for flow cytometry analysis of dendritic cells. BMDCs (10^5 cells) were stained with BMDC antibody panels as shown in plots and described in methods. Cells were initially identified based on FSC-A and SSC-A for their size and granularity. Selected population was gated with FSC-A, and FSC-H for doublet exclusion. A live/dead stain (AQUA) was used to gate for live cells that were further analyzed for CD11c⁺ populations. BMDC activation/maturation was evaluated based on CD11c, CD70, and CD86 surface markers.

Gating strategy for evaluating OVA-specific CD8+ T cells from spleens of BMDC-vaccinated mice

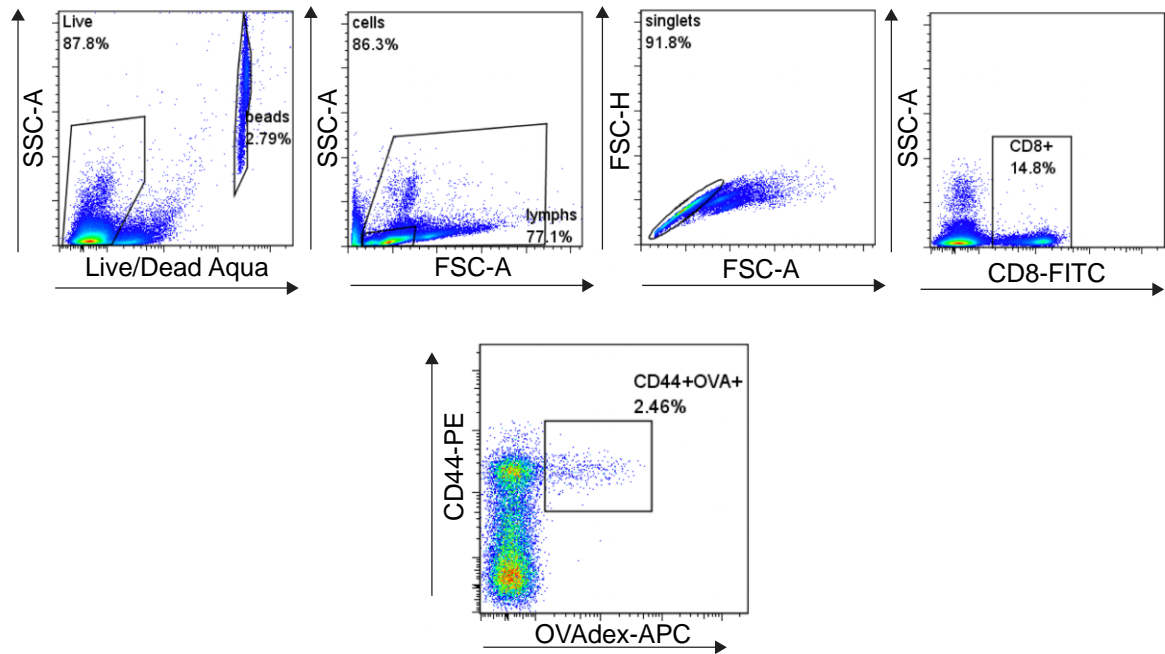


Figure 3.2 Gating strategy for flow cytometry analysis of OVA-specific CD8+ T cells from spleens of mice vaccinated with BMDCs. Splenocytes were isolated from spleens by dounce homogenization and filtered through a 100 μ m mesh filter. Isolated splenocytes were stained with the splenocyte antibody panel as shown in plots and described in methods. A live/dead stain (AQUA) was used to identify live cells that were further gated with FSC-A and SSC-A for their size and granularity. Doublets were excluded using FSC-A, and FSC-H gate. Cells were gated for CD8, CD44, and OVADex markers to identify antigen-specific T cells.

Activity-based protein profiling (ABPP) of BMDCs. BMDCs were lysed by dounce homogenization in cold lysis buffer (0.25 M sucrose, 20 mM HEPES, and 2 mM DTT in ddH₂O) with Protease and Phosphatase inhibitor (ThermoFisherScientific, A32959). After cell lysis, samples were allowed to sit in ice for 15 min. Lysates were centrifuged at 100,000 x *g* for 45 min at 4 °C. The supernatant was labeled as soluble fraction. The remaining pellet (membrane fraction) was washed with assay buffer (20mM HEPES in H₂O) and resuspended by passing through a 26-gauge needle in assay buffer. Protein concentrations were measured using a Bio-Rad DC protein assay and lysates were standardized to 1 mg/mL for ABPP analysis. Proteomes (1mg/mL) were treated with either HT-01 (1 μM) or FP-Rh (1 μM) for 30 min at 37 °C. Probe labeling was quenched using gel loading buffer containing 2-mercaptoethanol. Samples were separated by SDS-PAGE and analyzed by in-gel fluorescence scanning using a Chemidoc MP imaging system. The protease inhibitor cocktail is essential for DAGLβ analysis because protease activity in BMDC lysates can result in substantial proteolytic fragments of native DAGLβ.

Lipid extraction. Folch method (Chloroform:Methanol:Water/2:1:1) were used to extract lipids from BMDC pellets (3 x 10⁶ cells). Antioxidant BHT (butylated hydroxy toluene) was added at 50 μg/mL during extraction. Chloroform (2 mL), and Methanol (1 mL) were added with 1 mL of ddH₂O containing resuspended BMDCs. Samples were vortexed and centrifuged at 2,000 x *g* for 5 min. Lipid standards used for quantitation include arachidonic acid-d8 (Cayman Chemical Company, Catalog # 390010) and 2-arachidonylglycerol-d5 (Cayman Chemical Company,

catalog # 362162). Lipid standards (10 pmol of each standard) were added to organic solvents prior to mixing and lipid extraction of BMDCs. The organic layer was transferred and aqueous layer extracted with addition of 1.5 mL of 2:1 chloroform:methanol solution. The extracted organic layers were combined and dried down under nitrogen stream. Samples were resuspended in 120 μ L of 1:1 methanol:isopropanol and stored at -80 °C until further analysis.

Mass spectrometry-based lipid analysis of BMDCs. The lipid samples were analyzed by LC-MS. Dionex Ultimate 3000 RS UHPLC system was used with the analytical column (Kinetex® 1.7 μ m C18 100 Å, Phenomenex, LC column 100 x 2.1mm) and reverse phase LC (FA: 0.05% acetic acid, H₂O, B: 0.05% acetic acid, Acetonitrile) with the following gradient: Flowrate 0.25 mL/min, 0 min 25%B, 5 min 40%B, 6 min 58%B, 9 min 68%B, 12 min, 90%B, 13 min 90%B, 15 min 100% B. The eluted lipids were ionized through electrospray using a HESI-II probe into an Orbitrap Q-Exactive Plus mass spectrometer (Thermo Scientific). Data acquisition was performed through (parallel reaction monitoring) PRM targeting arachidonic acid (303.2318 m/z), arachidonic acid-d8 (311.2820 m/z), 2-arachidonyl glycerol (379.2842 m/z), 2-arachidonyl glycerol-d5 (384.3157 m/z). Through PRM monitoring, fragments of the lipid precursors were monitored (arachidonic acid (259.2434 m/z), arachidonic acid-d8 (267.2935 m/z), 2-arachidonyl glycerol (287.2365 m/z), 2-arachidonyl glycerol-d5 (287.2365 m/z)). Intensities were measured using Tracefinder™ software, which targeted list of lipids and aligned them according to the intensities of the ion species found in each raw file. For 2-AG measurements, 4 technical replicates per samples were taken and averaged

together to give better approximation of the lipid concentration. Semi-quantitative measurements were performed by taking intensities for 2-AG and 2-AG-d5 and normalized based on the amount of standards doped into the sample and the cell number (10pmol, 2.5million cells). *P < 0.05 for DAGL β KO versus wild-type group. *Data were represented as mean \pm s.e.m.; n = 2~3.* For arachidonic acid, fragment ion intensities for both endogenous AA and AA-d8 were measured for better approximation of accurate AA level in the sample. Semi-quantitative measurements were performed by normalizing with AA, and AA-d8 followed by normalization with doped standard amount and cell number (10pmol, 2.5million cells). *Data were represented as mean \pm s.e.m.; n = 3.* Aligned intensities were exported and analyzed using Prism Graphpad version 7.03.

Inflammatory activation of BMDCs and multiplex cytokine analysis. After BMDCs were differentiated, suspension cells were seeded in a 96-well plate in 50 μ L volume at 100,000 cells per well in complete DC differentiation media. 50 μ L of lipopolysaccharide (LPS) in complete DC differentiation media was added to designated wells for a final LPS concentration of 100 ng/mL and incubated for 6 hrs at 37 °C. Supernatant was collected in V-bottom 96 well plate and centrifuged at 1,400 x g for 5 min to pellet residual BMDCs. Supernatant was transferred to a separate 96 well plate and stored at -80°C until further analysis. Cytokine profiling was performed at the UVa flow cytometry core. In brief, antibody-immobilized beads were prepared by sonication/vortexing for 1 min with 60 μ L of each individual antibody-bead: anti-Mouse IL-1 β (catalog# MIL1B-MAG), anti-Mouse TNF α (catalog# MCYTNFA-MAG), anti-Mouse IL-12 (p70) (catalog# MIL12P70-

MAG), and anti-Mouse IL-6 (catalog# MCYIL6-MAG) and combining them in a total volume of 3.0 mL of assay buffer (Millipore corporation, catalog# L-AB). Wells were washed, detected, and analyzed using the Luminex MAGPIX system following manufacturer's recommended protocols. Samples were analyzed using median fluorescent intensity (MFI) data using a 5-parameter logistic for calculating the cytokine concentrations in samples. Exported data were analyzed using Prism Graphpad version 7.03 and statistical significance was calculated using unpaired t-test.

Data and Software Availability

The Repository ID for the flow cytometry data regarding the dendritic cell experiments as well as splenocytes analysis of OVA-DEX positive CD8 T cells is FR-FCM-Z2ZQ, data stored at FlowRepository. The mass spectrometry data for lipidomics analysis can be found at Mendeley data published at doi:10.17632/45csyctfbn.1. Data sets are divided into two parts, one for 2-AG analysis, and the other for arachidonic acid.

3.4 RESULTS

3.4.1 Chemoproteomic discovery of DAGL β activity in primary dendritic cells

We generated bone marrow-derived dendritic cells (BMDCs) from *Daglb*^{-/-} mice following previous reported procedures² and as detailed in the Methods section. We also included *Dagla*^{-/-} BMDCs to directly compare whether DAGL function in BMDCs is isoform specific. In brief, bone marrow cells were harvested from femurs

and tibias of mice and cultured in the presence of GM-CSF for 10 days followed by enrichment for BMDCs by separating suspension (fraction containing BMDCs) from adherent cells. We used flow cytometry and established surface markers of DCs (CD11c³) to confirm >95% of BMDCs were CD11c⁺ dendritic cells (**Figure 3.3A**).

Next, we confirmed that BMDCs expressed active DAGL β using our DAGL-tailored activity-based protein profiling (**ABPP, Figure 3.3B**) probe, HT-01⁴⁻⁶. We detected prominent HT-01 labeling of an ~70 kDa protein band corresponding to endogenous DAGL β activity that was present in *Daglb*^{+/+} but absent from *Daglb*^{-/-} BMDC membrane proteomes as measured by gel-based ABPP (**Figure 3.3B**). We could not detect native DAGL α activity in BMDC proteomes as evidenced by the lack of any detectable fluorescent band in the ~120 kDa molecular weight range (**Figure 3.3B**). We also compared activity profiles of other serine hydrolases (SHs) detected in BMDC proteomes by exchanging HT-01 for a broad SH-reactive ABPP probe, fluorophosphonate-rhodamine (FP-Rh⁷). As shown in **Figure 3.3B**, we did not observe any substantial differences in SH activity profiles in gel-based ABPP analysis of *Daglb*^{+/+} compared with *Daglb*^{-/-} BMDC proteomes labeled with FP-Rh.

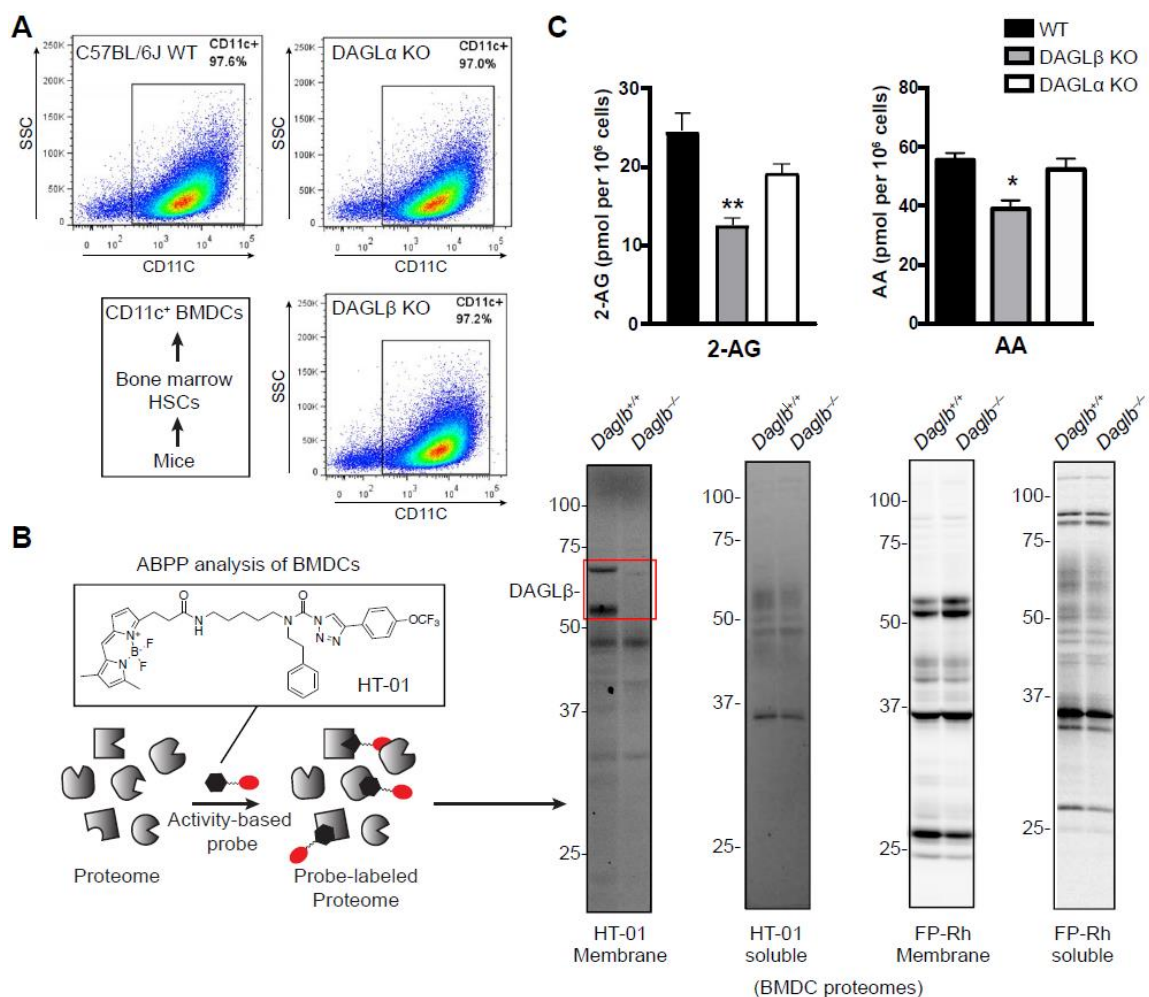


Figure 3.3 Chemical proteomic and metabolomic analysis of BMDCs (A) BMDCs were differentiated from bone marrow of C57BL/6J mouse and dendritic cell phenotype and purity determined by flow cytometry analysis of a dendritic cell surface marker (CD11c). BMDCs derived from DAGL α and DAGL β mice were comparable with wild-type counterparts. See Fig S1 for gating strategy used in flow cytometry analyses. (B) Schematic of activity-based protein profiling (ABPP) of BMDCs. BMDC proteomes were treated with DAGL-directed ABPP probe HT-01 or broad-spectrum serine hydrolase probe FP-Rh (1 μ M of probes, 30 min, 37 $^{\circ}$ C). Probe-labeled samples were analyzed by SDS-PAGE and in-gel fluorescence scanning to confirm active DAGL β in BMDC proteomes with no discernable changes in other detectable serine hydrolase activities. The lower molecular weight band represents a proteolytic fragment of DAGL β that is sometimes generated and observed during sample processing. (C) Targeted metabolomics analysis of BMDCs showed that 2-arachidonylglycerol (2-AG) and downstream lipid product, arachidonic acid (AA) is reduced in DAGL β -disrupted BMDCs. * P < 0.05 for DAGL β KO versus wild-type groups. Data are mean \pm s.e.m.; n = 3 per group.

3.4.2 DAGL β regulates endocannabinoid and arachidonic acid metabolism in BMDCs

Previous studies established that both DAGL α and DAGL β hydrolyze arachidonic acid (AA)-esterified diacylglycerols (DAGs) to produce the principal endocannabinoid, 2-arachidonoylglycerol (2-AG)^{4, 8}. Although DAGL α and DAGL β are capable of catalyzing the same lipid biochemistry, their respective metabolic functions in living systems are segregated by tissue- and cell type-specific expression⁹. Here, we employed targeted metabolomics to compare lipid composition of BMDCs from DAGL α and DAGL β knockout (KO) mice compared with wild-type (WT) counterparts. Total lipids (i.e. lipidome) were extracted from BMDCs using the Folch method¹⁰ and analyzed by liquid chromatography-mass spectrometry (LC-MS) on a high-resolution Q-Exactive Plus mass spectrometer configured for parallel reaction monitoring acquisition¹¹. We observed a reduction in cellular 2-AG in *Daglb*^{-/-} compared with *Daglb*^{+/+} BMDCs (~50% reduction in 2-AG, **Figure 3.3C**). In agreement with previous findings in macrophages, we also observed a corresponding ~30% reduction in cellular AA in *Daglb*^{-/-} BMDCs, which supports DAGL β biosynthesis of 2-AG pools utilized for AA production (**Figure 3.3C**). In contrast, cellular 2-AG and AA was largely unchanged between *Dagla*^{+/+} and *Dagla*^{-/-} BMDC lipidomes (**Figure 3.3C**). In summary, our metabolomics findings identify DAGL β as a key 2-AG biosynthetic enzyme in dendritic cells.

3.4.3 DAGL β regulates LPS-stimulated TNF- α release of BMDCs

To understand how DAGL β metabolism affects BMDC signaling, we evaluated cytokine response of DAGL-disrupted BMDCs exposed to the inflammatory stimuli, lipopolysaccharide (LPS). DCs express toll-like receptors (e.g. TLR1, TLR2, TLR4) that can sense pathogens in order to rapidly activate innate immune responses through production of proinflammatory cytokine and lipid signals¹². To examine the effects of DAGL inactivation on the inflammatory response of DCs, BMDCs were treated with LPS (100 ng/mL, 6 hrs) followed by multiplex bead-based Luminex immunoassay of secreted cytokines in media from treated cells. LPS-stimulated BMDCs showed a marked increase in secreted TNF- α , IL-1 β and IL-6, as well as a modest enhancement in IL-12 compared with non-stimulated dendritic cells as quantified by multiplex immunoassay of their conditioned media (**Figure 3.4**).

Interestingly, *Daglb*^{-/-} BMDCs exhibited significantly reduced secreted TNF- α in response to LPS when compared with wild-type counterparts (**Figure 3.4A**). DAGL β regulation of TNF- α appeared specific given that levels of other cytokines including IL-6, IL-12 and IL-1 β remained largely unchanged (**Figure 3.4A**). Our current data match previous findings in macrophages showing disruption of DAGL β reduced levels of secreted TNF- α in LPS-stimulated macrophages⁴. In contrast, secreted TNF- α was largely unchanged in *Dagla*^{-/-} compared with *Dagla*^{+/+} BMDCs stimulated with LPS (**Figure 3.4B**). Further analysis showed cytokine response of BMDCs to LPS was largely unaffected by DAGL α inactivation with the exception of a slight decrease in secreted IL-12 that did not reach statistical significance ($P = 0.0805$, Fig 2B). In summary, our findings identify a role

for DAGL β in specific regulation of TNF- α response of DCs exposed to inflammatory stimuli.

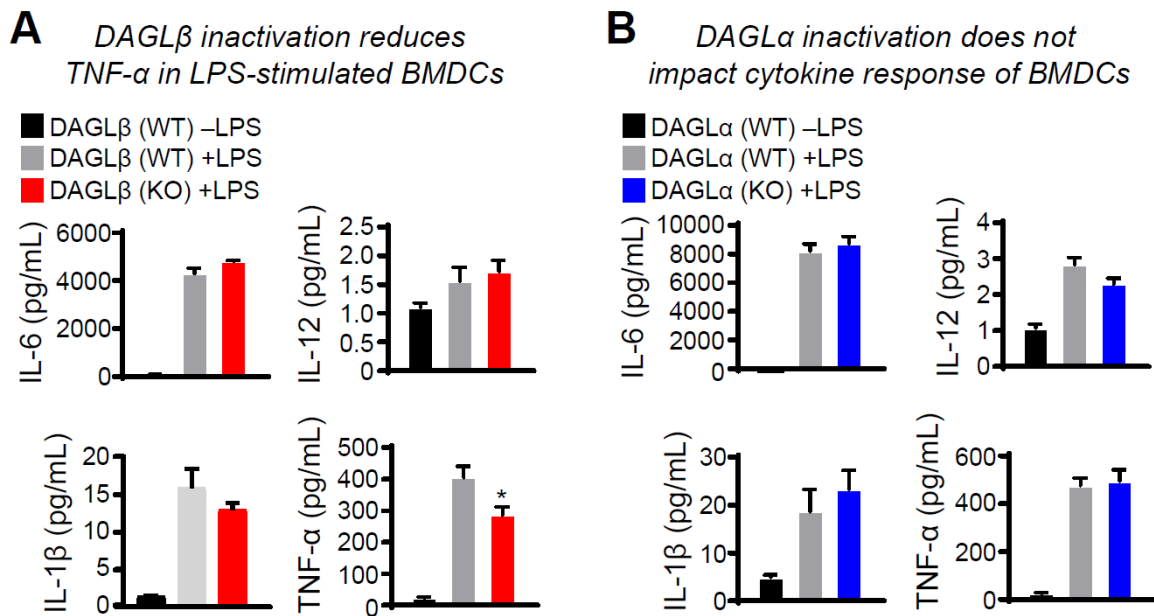


Figure 3.4 DAGL β regulates TNF- α response of LPS-stimulated BMDCs. Cytokine secretion by BMDCs exposed to vehicle or lipopolysaccharide (LPS, 100 ng/mL, 6 hrs) were detected using a Luminex MAGPIX system for multiplex evaluation of secreted TNF- α , IL-12, IL-6, and IL-1 β from LPS-stimulated BMDCs. The results showed disruption of DAGL β (A) but not DAGL α (B) suppressed TNF- α secretion in LPS-stimulated BMDCs. * $P < 0.05$ for WT+LPS versus KO+LPS groups. Data are mean \pm s.e.m.; $n = 4$ per group.

3.4.4 DAGL β inactivation does not affect DC-mediated T cell priming *in vivo*

Next, we examined the capacity of DAGL-disrupted BMDCs to prime antigen-specific T cell responses by cell-based vaccination *in vivo*. Here, BMDCs were activated and loaded with peptide antigens *ex vivo* followed by injection into mice, initiation of immunity, and detection of antigen-specific T cells from spleens of vaccinated mice. We chose ovalbumin peptide (OVA257) for eliciting antigen-specific responses because this peptide is presented by class I major histocompatibility complex (MHC) to elicit a robust OVA-specific CD8⁺ T cell response *in vivo*, which can be quantified by flow cytometry using OVA-specific MHC dextramers (see Methods for additional details).

First, we asked whether DAGL inactivation impacts activation/maturation of BMDCs. These studies evaluated whether BMDC maturation in the presence of peptide antigen is impaired with DAGL inactivation. For these studies, we chose *ex vivo* maturation conditions optimized for eliciting CD8⁺ T cell responses in mice. BMDCs were exposed to PAM3CSK4 (TLR1/TLR2 agonist), FGK45 (CD40 agonistic antibody), and OVA257 (10 μ g/mL) and the degree of activation determined by expression of DC maturation markers, CD70 and CD86^{3, 13-15} (**Figure 3.5A**). Activation of BMDCs resulted in a large increase in CD11c⁺CD70⁺CD86⁺ dendritic cells (from ~0.1% to ~14% in basal versus activated, respectively, **Figure 3.5B**). The degree of activation, as judged by the number of CD11c⁺CD70⁺CD86⁺ BMDCs, was comparable across all genotypes with the exception of a slight increase in the number of activated *Daglb*^{-/-} BMDCs that did not reach statistical significance ($P = 0.0834$, **Figure 3.5B**).

Next, we tested the impact of DAGL disruption on immunogenicity of BMDCs *in vivo*. We vaccinated mice with CD11c⁺CD70⁺CD86⁺ BMDCs pulsed with OVA257-264 peptide (10 µg/mL), followed by enumerating OVA257-264-specific CD8⁺ T cells within the spleen 7 days later using MHC-dextramer staining and flow cytometry (**Figure 3.6A**). We observed comparable numbers of antigen-specific CD8⁺ T cells from mice vaccinated with *Daglb*^{+/+} and *Daglb*^{-/-}BMDCs (**Figure 3.6B and C**). These *in vivo* findings were important given that our *ex vivo* experiments suggested a possible enhancement in maturation of *Daglb*^{-/-} BMDCs (**Figure 3.5B**). We also showed that inactivation of DAGL α does not impact the CD8⁺ T cell priming capacity of vaccinated BMDCs (**Figure 3.6B and C**). Collectively, our results demonstrate that disruption of DAGLs does not affect maturation *ex vivo* and T cell priming capacity of DCs *in vivo*.

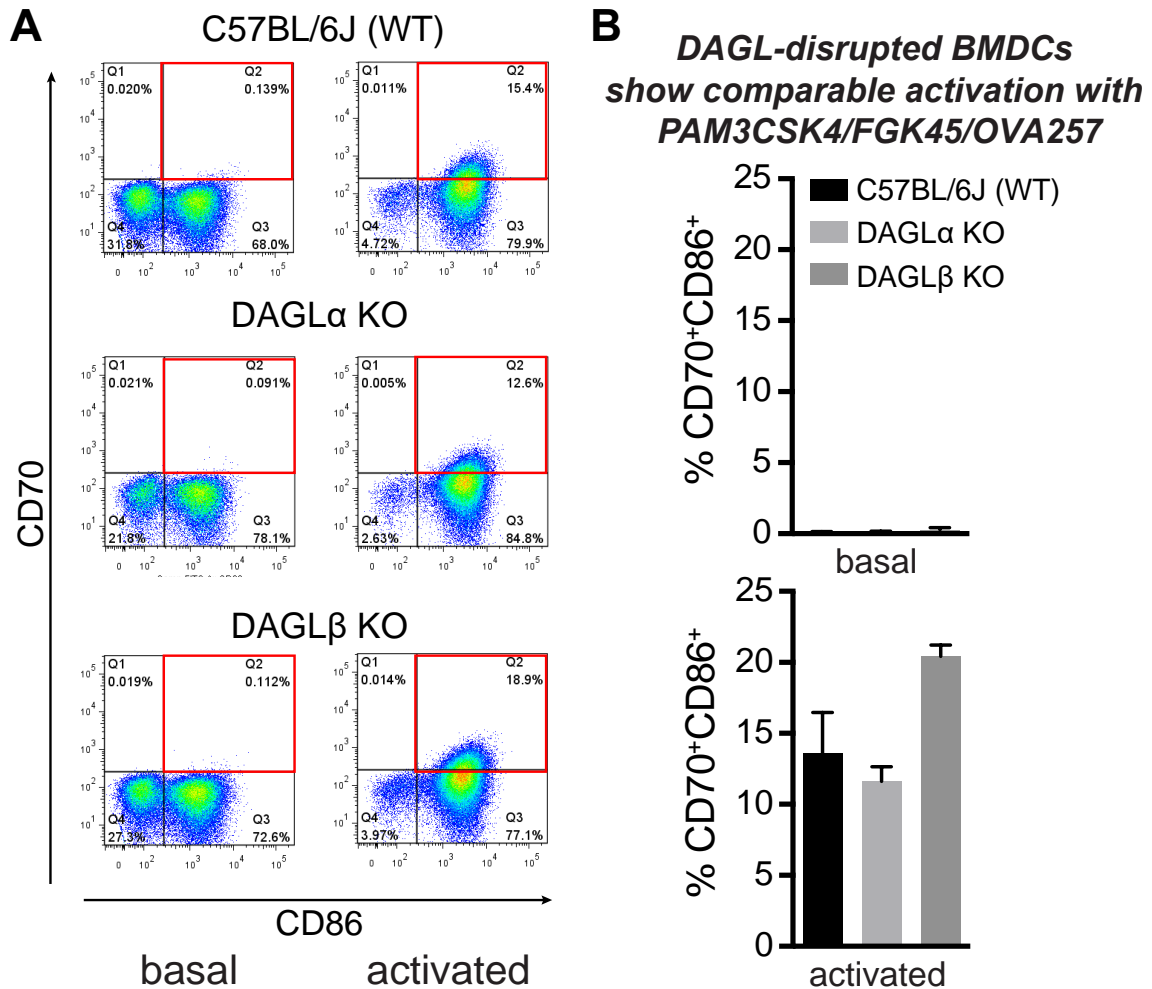


Figure 3.5 DAGL inactivation does not impair BMDC activation/maturation. BMDCs (3×10^6 cells) were stimulated using PAM3CSK4 (1 $\mu\text{g}/\text{mL}$), FGK45 (1 $\mu\text{g}/\text{mL}$), and OVA257 (10 $\mu\text{g}/\text{mL}$) for 8 hrs at 37 $^{\circ}\text{C}$. (A) BMDC phenotype was confirmed with anti-CD11c (APC). The degree of BMDC activation/maturation was determined by flow cytometry analysis of increased surface expression of CD70 (PE) and CD86 (FITC). See Fig S1 for gating strategy used in flow cytometry analyses. (B) Bar plot comparing percentage of CD11c⁺CD70⁺CD86⁺ BMDCs from basal and activated BMDCs, which was used to evaluate activation/maturation across genotypes tested. Data are mean \pm s.e.m.; $n = 3$ per group.

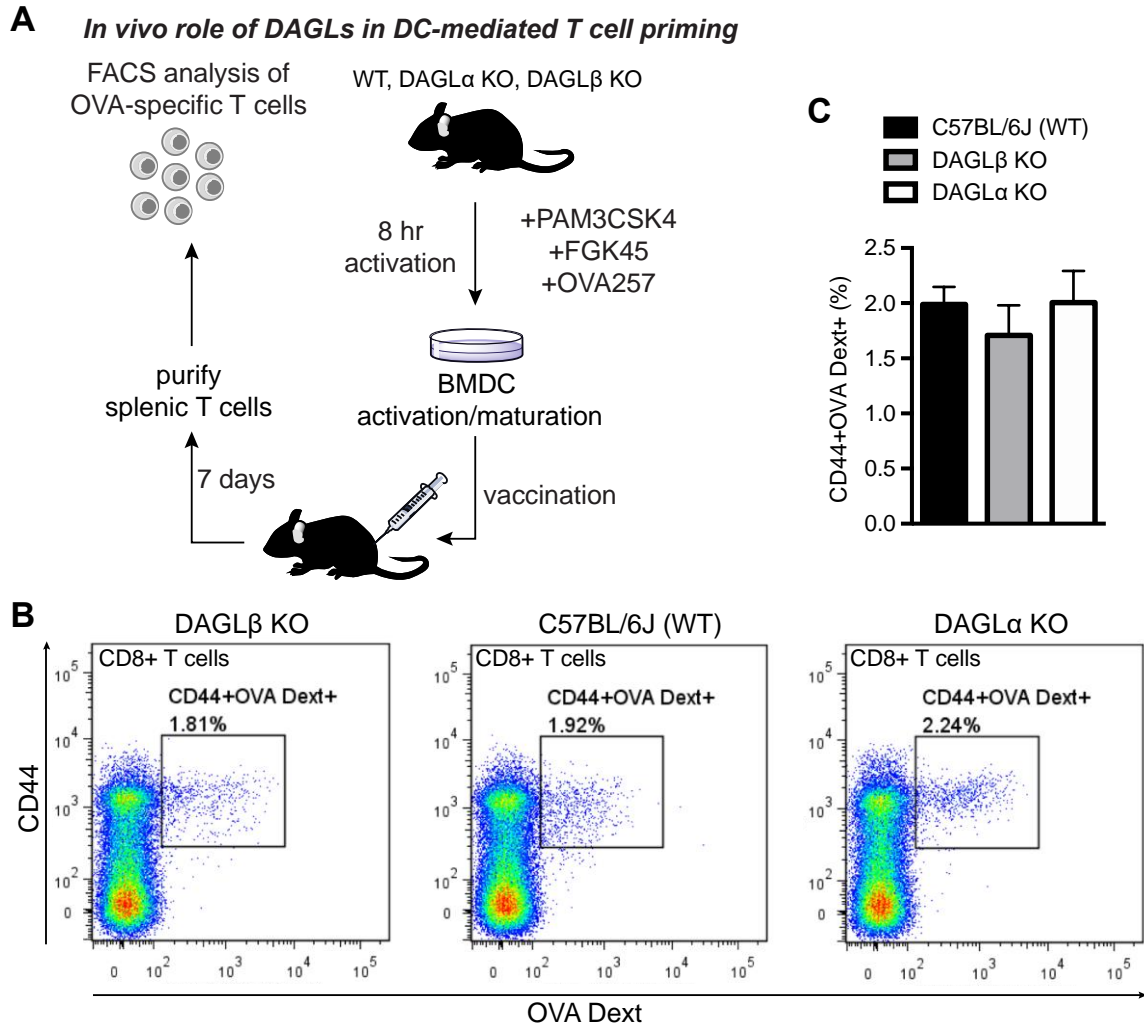


Figure 3.6 DAGL inactivation does not affect BMDC priming of antigen-specific CD8⁺ T cells *in vivo*. (A) BMDCs activation/maturation was achieved by incubation with PAM3CSK4 (1 μ g/mL), FGK45 (1 μ g/mL), and OVA257 (10 μ g/mL) for 8 hrs at 37 °C *ex vivo*. Afterwards, C57BL/6J mice were vaccinated (tail vein by i.v. injection) with 100,000 CD11c⁺CD70⁺CD86⁺ BMDCs. Mice were sacrificed after 7 days, spleens harvested, and splenic cells isolated for flow cytometry analysis. (B) An OVA-specific MHC1 dextramer (OVA Dextrin) was used to quantify percentage of OVA-specific CD8⁺CD44⁺OVA Dextrin⁺ T cells using flow cytometry. See Figure 2 for gating strategy used in flow cytometry analyses. (C) No significant differences in percentage of CD8⁺CD44⁺OVA Dextrin⁺ splenic T cells from vaccinated mice across genotypes tested. Data is representative of cell vaccination experiments from 2 independent cohorts of mice ($n = 3-5$ mice per group).

3.5 DISCUSSION

DCs serve as a critical link between innate and adaptive immunity and form the basis of new cellular immunotherapies against cancer in the clinic ¹². Identifying molecular pathways that modulate DC inflammatory and immunogenic functions is important for basic understanding of innate regulation of immunity. Here, we apply chemical proteomics, mass spectrometry metabolomics, and cell-based vaccination *in vivo* to identify DAGL β regulation of lipid signaling pathways that uncouple the cytokine response and T cell priming capacity of DCs. Our findings are significant given that proinflammatory cytokines including TNF- α produced by DCs are directly involved in the pathogenesis of chronic inflammation ¹⁶.

We overcame challenges with detecting endogenous DAGL activity, which are typically expressed in low abundance in cells and tissues, in BMDCs using activity-based probes tailored for measuring DAGL β and DAGL α activity ⁴⁻⁶. Our chemical proteomic studies revealed that DAGL β but not DAGL α is expressed and active in BMDCs (**Figure 3.3B**). Our findings are in agreement with previous reports demonstrating that DAGL β is the principal isoform found in innate immune cells including macrophages and microglia ^{4, 9}. The isoform specificity of DAGLs was further validated through MS-metabolomics and cytokine profiling, which showed reduced cellular 2-AG/AA (**Figure 3.3C**) and TNF- α (**Figure 3.4**), respectively, in *Daglb*^{-/-} but not *Dagla*^{-/-} BMDCs compared to wild-type counterparts. The impaired LPS-stimulated TNF- α response of *Daglb*^{-/-} BMDCs was intriguing given these cells did not show defects in maturation (**Figure 3.5**) and could efficiently prime antigen-specific CD8⁺ T cell responses in animal vaccination

studies (**Figure 3.6**). Thus, disruption of DAGL β pathways is a potential route towards selective regulation of DC inflammatory responses.

Our findings are noteworthy given the potential for targeting DAGL β for inflammation. Chemical or genetic disruption of DAGL β provides anti-inflammatory effects in animal models of pain and neuroinflammation^{6, 17}. While inhibiting DAGL α provides similar anti-inflammatory effects *in vivo*^{8, 9}, long-term disruption of this isoform results in massive alterations in brain lipids that are associated with behavioral defects and seizures in knockout mice¹⁸⁻²⁰. In contrast, DAGL β knockout mice do not exhibit gross differences in brain lipids and appear to develop and behave normally^{9, 17, 19}. Our current findings extend the utility of targeting DAGL β for inflammation (and potentially chronic inflammation) by showing disruption of this lipase does not appear to impact immunity, which is important given defects in regulating DC immunogenicity has been associated with allergy and autoimmunity¹². In summary, our findings identify a unique lipid pathway regulated by DAGL β that modulates an inflammatory cytokine response without affecting maturation and T cell priming capacity of DCs *in vivo*.

3.6 SIGNIFICANCE

Chemical proteomics has greatly enabled discovery and annotation of new lipid signaling pathways important for physiology and disease. Among these candidates, diacylglycerol lipase-beta (DAGL β) has emerged as a promising target for inflammation because of its restricted activity in innate immune cells including

macrophages and microglia where it regulates proinflammatory lipid and cytokine signaling in neuroinflammation and pain. Here, we apply activity-based protein profiling (ABPP) and mass spectrometry metabolomics to discover that DAGL β inactivation in dendritic cells reduces arachidonic acid and secreted TNF- α in response to inflammatory stimuli. The anti-inflammatory effects from DAGL β disruption did not impair the ability of dendritic cells to prime antigen-specific CD8 $^+$ T cell responses *in vivo*. These findings were surprising given that inflammatory signals induce dendritic cell activation/maturation to enhance T cell priming capacity. The ability to suppress dendritic cell inflammatory pathways while sparing adaptive immune functions is important given that defects in DC immunogenicity has been associated with allergy and autoimmunity. Our findings support DAGL β as a molecular pathway that can be targeted to selectively suppress dendritic cell inflammatory TNF- α responses.

3.7 ACKNOWLEDGMENTS

We thank all members of the Hsu Lab and colleagues for careful review of this manuscript. This work was supported by the University of Virginia (start-up funds to K.-L.H.) and National Institutes of Health (DA035864 and DA043571 to K.-L.H.; CA166458 to T.N.J.B.).

3.8 References

1. Hsu, K.-L., et al., *DAGL β inhibition perturbs a lipid network involved in macrophage inflammatory responses*. Nat. Chem. Biol., 2012. **8**(12): p. 999-1007.
2. Lutz, M.B., et al., *An advanced culture method for generating large quantities of highly pure dendritic cells from mouse bone marrow*. J Immunol Methods, 1999. **223**(1): p. 77-92.
3. Keller, A.M., et al., *Expression of costimulatory ligand CD70 on steady-state dendritic cells breaks CD8+ T cell tolerance and permits effective immunity*. Immunity, 2008. **29**(6): p. 934-46.
4. Hsu, K.L., et al., *DAGLbeta inhibition perturbs a lipid network involved in macrophage inflammatory responses*. Nat Chem Biol, 2012. **8**(12): p. 999-1007.
5. Hsu, K.L., et al., *Development and optimization of piperidyl-1,2,3-triazole ureas as selective chemical probes of endocannabinoid biosynthesis*. J Med Chem, 2013. **56**(21): p. 8257-69.
6. Shin, M., et al., *Liposomal Delivery of Diacylglycerol Lipase-Beta Inhibitors to Macrophages Dramatically Enhances Selectivity and Efficacy in Vivo*. Mol Pharm, 2018. **15**(3): p. 721-728.
7. Bachovchin, D.A., et al., *Superfamily-wide portrait of serine hydrolase inhibition achieved by library-versus-library screening*. Proc Natl Acad Sci U S A, 2010. **107**(49): p. 20941-6.
8. Ogasawara, D., et al., *Rapid and profound rewiring of brain lipid signaling networks by acute diacylglycerol lipase inhibition*. Proc Natl Acad Sci U S A, 2016. **113**(1): p. 26-33.
9. Viader, A., et al., *A chemical proteomic atlas of brain serine hydrolases identifies cell type-specific pathways regulating neuroinflammation*. Elife, 2016. **5**: p. e12345.
10. Folch, J., M. Lees, and G.H. Sloane Stanley, *A simple method for the isolation and purification of total lipides from animal tissues*. J Biol Chem, 1957. **226**(1): p. 497-509.
11. Peterson, A.C., et al., *Parallel Reaction Monitoring for High Resolution and High Mass Accuracy Quantitative, Targeted Proteomics*. Molecular & Cellular Proteomics, 2012. **11**(11): p. 1475-1488.
12. Steinman, R.M., *Decisions about dendritic cells: past, present, and future*. Annu Rev Immunol, 2012. **30**: p. 1-22.
13. Reis e Sousa, C., *Dendritic cells in a mature age*. Nat Rev Immunol, 2006. **6**(6): p. 476-83.
14. Bullock, T.N. and H. Yagita, *Induction of CD70 on dendritic cells through CD40 or TLR stimulation contributes to the development of CD8+ T cell responses in the absence of CD4+ T cells*. J Immunol, 2005. **174**(2): p. 710-7.
15. Van Deusen, K.E., R. Rajapakse, and T.N. Bullock, *CD70 expression by dendritic cells plays a critical role in the immunogenicity of CD40-independent, CD4+ T cell-dependent, licensed CD8+ T cell responses*. J Leukoc Biol, 2010. **87**(3): p. 477-85.
16. Connolly, M.K., et al., *In liver fibrosis, dendritic cells govern hepatic inflammation in mice via TNF-alpha*. J Clin Invest, 2009. **119**(11): p. 3213-25.
17. Wilkerson, J.L., et al., *Diacylglycerol lipase beta inhibition reverses nociceptive behaviour in mouse models of inflammatory and neuropathic pain*. Br J Pharmacol, 2016. **173**(10): p. 1678-92.
18. Jenniches, I., et al., *Anxiety, Stress, and Fear Response in Mice With Reduced Endocannabinoid Levels*. Biol Psychiatry, 2016. **79**(10): p. 858-868.

19. Powell, D.R., et al., *Diacylglycerol Lipase alpha Knockout Mice Demonstrate Metabolic and Behavioral Phenotypes Similar to Those of Cannabinoid Receptor 1 Knockout Mice*. *Front Endocrinol (Lausanne)*, 2015. **6**: p. 86.
20. Cavener, V.S., et al., *Inhibition of Diacylglycerol Lipase Impairs Fear Extinction in Mice*. *Front Neurosci*, 2018. **12**: p. 479.

Chapter 4. Investigation of diacylglycerol lipase-beta function inflammation by activity-based protein profiling (ABPP) and lipidomics

4.1 Overview

DAGL β is a principal endocannabinoid biosynthetic enzyme that regulates proinflammatory signaling pathways in macrophages. Although DAGL β inhibitors mediate anti-inflammatory effects in part through reducing arachidonic acid-derived prostanoids, the mode of action for these small molecules remain largely underexplored. Here, we discover functional cross-talk between DAGL β and the metabolic energy sensor AMP-activated protein kinase (AMPK) in primary macrophages. Chemical or genetic inactivation of DAGL β resulted in phosphorylation (threonine 172) and activation of AMPK as evidenced by inhibition of downstream substrates (acetyl-CoA carboxylase and fatty acid synthase). Metabolomic discovery of PUFA-specific triacylglycerol lipase activity by DAGL β supports reduced DAG-PKC signaling that blocks an inhibitory AMPK phosphorylation site (serine 485/491). Treatment of *Daglb*^{-/-} mice with AMPK inhibitors reversed the anti-inflammatory phenotypes observed in lipopolysaccharide-induced pain models. Collectively, our findings suggest that AMPK activation could explain the anti-inflammatory effects mediated by DAGL β inhibitors *in vivo*, as well as a metabolomic changes that could be explained by the discovery of PUFA containing TAGs as novel substrates in BMDMs.

4.2 Introduction

We have described how DAGL β regulates inflammation through subsets of cell population called phagocytes and how it could be taken advantage to improve selectivity and potency of the small molecule delivery to inhibit DAGL β ¹. In addition, we have shown that inhibition of DAGL β does not result in hampered adaptive immune function by dendritic cells (Chapter 3). However, we have not addressed the mechanistic understanding of how DAGL β inhibition leads to potent anti-nociceptive effects outside arachidonic acid reduction.

The current understanding of the DAGL β shows that arachidonic acid is produced from 2-AG by processing 1-steroyl-2-arachidonyl glycerol (SAGs)². The inhibition of DAGL β activity leads to reduction in 2-AG as well as subsequent arachidonic acid and prostaglandins². The efficacy of DAGL β inhibition has been highlighted in pain models including inflammatory pain, chemotherapy induced peripheral neuropathy (CIPN), and Chronic Constriction Injury (CCI) neuropathic pain models³. The inhibition of DAGL β reversed allodynia elicited by the pain experiments tested in mice. One of the most surprising finding in this work was the effectiveness against the allodynia.

The chronic treatment of NSAIDs accompanies number of side effects such as internal bleeding, ulcer development, hypersensitivity reactions, among others. Thus, it is well-accepted that NSAIDs are unsuitable for chronic pain management⁴⁻⁶. However, NSAIDs have shown efficacy in providing relief for acute pain and inflammation. Non-Steroid Anti-inflammatory drugs (NSAIDs)

treatment for inflammatory pain model showed moderate efficacy against inflammatory pain. Subsequently, analysis of tissues in mice showed significant reduction in prostaglandins⁷. However, NSAIDs have no beneficial effects against neuropathic pains such as CIPN or CCI, which indicates that reduction in prostaglandins is beneficial in providing relief to acute inflammation but ineffective against neuropathic pain^{8, 9}. There arose a discrepancy in understanding the proposed mechanism behind the efficacies of the NSAIDs versus DAGL β inhibition. Inhibiting prostaglandin production via COX-inhibitors was much more effective in reducing prostaglandin production compared to DAGL β inhibition. Therefore, we hypothesized that there are additional pathways that DAGL β is associated with other than the pathway involving 2-AG, AA, and the prostaglandins pathway.

Here, we present a chemoproteomics strategy and untargeted lipidomics to elucidate the lipids that are regulated by DAGL β , with an emphasis in how these could control alternative lipid substrates and protein signaling pathways. We initially profiled bone marrow derived macrophages (BMDMs) using tailored activity-based probe (ABP) HT-01^{2, 10, 11} to demonstrate that primary DAGL activity in BMDMs between DAGL β and DAGL α derives from DAGL β . In order to address potential lipid signaling pathways that DAGL β is involved in, we utilized untargeted lipidomics to get an idea about the biologically relevant lipid species that are affected upon DAGL β inhibition. After observing sub-populations of triacylglycerol species accumulation in DAGL β KO BMDMs, we hypothesized that DAGL β selectively processes triacylglycerols with poly-unsaturated fatty acid (PUFA). We confirmed the specificity for TGs by using our mass-spec based substrate assay

against DAGL β . To our surprise, we found that there was no increase in activation of PKC upon DAGL β inhibition. Lastly, we showed that DAGL β disruption in BMDMs shows an increase in activation of AMPK which leads to an anti-inflammatory phenotype. Given the lack of studies on DAGL β , our study shows the utilization of untargeted lipidomics to better understand the signaling pathways that could be further investigated for development of pain studies.

4.3 Materials and methods

Animals All studies were conducted in 2-3 months old C57BL/6J mice. Mice were housed in the Gilmer animal facility (UVa). All studies were carried out under a protocol approved by the ACUC/University of Virginia. All animals were allowed free access to a standard chow diet and water. The animals were housed according to the ACUC policy on social housing of animals.

Materials Unless otherwise specified, reagents used were purchased from Fisher Scientific. Bio-beads SM-2 Absorbants (Catalogue #1528920, Bio-Rad), Phospho-AMPK α 1 (Ser485)/AMPK α 2 (Ser491) Antibody (Catalogue #4185S, Cell signaling technology), Phospho-AMPK α (Thr172) (40H9) Rabbit mAb (Catalogue #2535S, Cell signaling technology), Phospho-(Ser) PKC Substrate Antibody (Catalogue #2261S, Cell signaling technology), DAG Lipase β (D4P7C) Rabbit mAb (Catalogue #12574S, Cell signaling technology), Triacylglycerol species were purchased from Nuchek prep. Tritetradecanoin (C14:0, Catalogue #T-140), Trihexadecanoin (C16:0, Catalogue #T-150), Trioctadecanoin (C18:0, Catalogue # T-160), Trieicosanoin (C20:0, Catalogue #T-70), Tridocosanoin (C22:0, Catalogue #T-180), Triarachidonin (C20:4, Catalogue # T-295),

Tricosapentaenoic (C20:5, Catalogue #T-160), Tricosahexaenoic (C22:6, Catalogue #T-310),

Western blot analysis

Cell lysates were separated via centrifugation at 100,000 x *g* for 45 min at 4 °C. Proteins separated by SDS-PAGE (4-20% polyacrylamide, TGX Stain-Free MIDI Gel). Gel transfers were performed using the Bio-Rad Trans-Blot Turbo RTA Midi Nitrocellulose Transfer Kit with a Bio-Rad Trans-Blot Turbo Transfer System. After incubation with 5% milk in TBST (1.5 M NaCl, 0.25 M Tris pH 7.4, 0.1% Tween 20, in ultrapure water (ddH₂O)) for 1 hr. The membrane was incubated with primary antibody p-AMPK Thr172 (1:1000), p-AMPK α 1 (Ser485)/AMPK α 2(Ser491) (1:1000), DAG lipase β , phospho-(Ser) PKC substrates (1:1000) for 12 hrs at 4 °C. After the primary antibody incubation, membranes were washed 5 times for 5 min with TBST and incubated with secondary antibody (1:10,000) for 2 hrs at 25 °C. The membrane was washed 5 times for 5 minutes with TBST and imaged with Chemidoc MP Imaging system.

Bone Marrow Isolation and Culture

C57BL/6J mice were sacrificed and tibia and femur were isolated from both hind legs. Both ends of the tibia and femurs were cut and bone marrow was extracted by flushing through serum free RPMI. Bone marrow was pelleted at 600 xg for 5 minutes and resuspended in red blood cell (RBC) lysis buffer for 1 min. After RBC buffer was removed, cells were plated with BMDM differentiation media (RPMI, 10% L929 media, 10% FBS, 2mM L-Glutamine (Thermo Fisher Scientific), 10 units and 100 μ g mL⁻¹ penicillin-streptomycin (Sigma-Aldrich), 50 μ M beta-

mercaptoethanol (Sigma-Aldrich), 20mM HEPES) on petri dishes. At day 3, an additional 10mL of DC differentiation media was added. BMDMs finished differentiation at day 7 and cells were used for subsequent experiments.

Whole cell BMDM lipid extraction BMDM cell pellets (3 million cells) were extracted using folch extraction method (2:1:1 chloroform:methanol:water). BHT (50 μ g/mL) was added to organic solvents used for extraction. Chloroform/methanol solution (2mL) was added with 1mL of resuspended cells in water. Samples were briefly vortexed and centrifuged at 2,000 xg for 5 minutes. Organic layer was transferred and aqueous layer was added with 1.5mL of additional 2:1 chloroform:methanol solution for extraction followed by centrifugation at 2,000 xg for 5 minutes. Organic layers were combined and dried under stream of nitrogen gas. Samples were resolubilized in 120 μ L of 1:1 methanol:Isopropanol solution.

LC-MS/MS analysis of lipidomics samples for untargeted lipid identification

Data dependent The lipid samples were analyzed by LC-MS. Dionex Ultimate 3000 RS UHPLC system was used with the analytical column (Kinetex $\text{\textcircled{R}}$ 1.7 μ m C18 100 \AA , LC column 100X2.1mm) and reverse phase LC (A: 0.1% formic acid, 10mM ammonium formate, 50% water, 50% acetonitrile, B: 0.1% formic acid, 10mM ammonium formate, 10% acetonitrile, 88% isopropanol, 2% water) with the following gradient: 0-4 min, 35% to 60% B; 4-12min, 60% to 85% B; 12-24 min, 85% to 100% B, flow rate at 250 μ L/min. The eluted lipids were electrosprayed using HESI-II probe into an Orbitrap Q-Exactive Plus mass spectrometer (Thermo Scientific), which was operated with a top 10 data-dependent acquisition method

that consisted of one full MS1 scan (250-1,200 m/z) followed by 10 MS2 scans of the most abundant ions recorded in the MS1 scan. Isolation window was set at 1.2 m/z. Data acquisitions were performed on both positive and negative mode to enhance confidence of species identification. Data analysis performed using the lipidsearch™ software package. Software matched MS1 monoisotopic precursor ions for the *in-silico* database search followed by the product ions search from MS2 spectra (search parameters: Target database:Q Exactive, Searchtype: product, ExpType LC-MS, Precursor tol 5.0 ppm, product tol 5.0 ppm, intensity threshold: product ion 1.0%, m-score threshold 2.0). Two results are were merged to generate matched lipid dataset. The searched data were aligned with selected parameters (ExpType:LC-MS, Alignment Method: Median, Toprank Filter: on, Main node Filter: Main isomer peak, m-Score Threshold: 5.0, ID quality filter: A, B, C, D) and curated with species that have grade score “A” and “B” for further analysis.

Overexpression of DAGL β in HEK293T cells

Recombinant DAGL β protein was produced by transient transfection of HEK293T cells with recombinant DNA. The transient transfection was performed as described previously². In short, HEK293T cells were seeded in 10cm cell culture treated plate at 400,000 cells in complete RPMI (RPMI, 10% FBS, Penstrep, L-Glutamine). After cells were allowed to grow to 40-60% confluency, 20 μ L of sterilized polyethylenimine (PEI) solution (1mg/mL, pH 7.4) and 2.6 μ g of DNA were added to 600 μ L of RPMI and incubated at 25°C for 30 minutes. The combined solution was added to 10cm plate dropwise and mixed gently. Cells were

harvested after two days of growth and snap frozen in liquid nitrogen and stored at -80°C freezer till the further analysis.

Mass spec-based lipid substrate assay

Cell pellets were dounce homogenized in lysis buffer (0.25M sucrose, 20mM HEPES at pH 7.4, 2mM DTT) and ultracentrifuged at 100,000 xg for 45 minutes at 4C. Pellets are resuspended by sonication in activity buffer (50mM HEPES at pH 7.4, 100mM NaCl, 5mM CaCl₂, 0.1% Triton X-100 v/v, 10% DMSO and 0.5mM DTT). Protein concentrations were normalized between mock transfect and DAGLB overexpressed HEK293T cells. Protein concentration was standardized to 0.37mg/mL (membrane fraction) and treated with respective inhibitors for 30 minutes (KT109 2 μ M, KT195 2 μ M). 40uL of the pre-treated lysates were added with 250pmol of respective lipid species at final volume of 500uL with activity buffer. The reaction was continued at room temperature for 4 hours. The reaction was quenched via organic extraction. The extraction carried out by adding 1.5mL of hexane (3:1 hexane: H₂O) with 80mg of biobeads. Reaction mixture was vortexed and centrifuged at 2,000 xg for 5 minutes. Additional wash with 1.5mL of hexane was performed and hexane layers were combined. Hexane layer was transferred to a new dram vial and added with 1mL of water, and 80mg of biobeads. After vortex/centrifugation, hexane layer was transferred to a clean dram vial and dried down under nitrogen. Samples were resuspended in 1:1 isopropanol:methanol and stored at -80°C till the analysis.

Modification to LC analysis of substrate assay LC-MS/MS conditions used for the substrate assay lipid identification is identical to the conditions described in

“LC-MS/MS analysis of lipidomics samples for untargeted lipid identification” with slight changes in LC configuration. External hardware divert valves were used to discard eluents from initial 6 minutes of the analysis in order to prevent residual triton X-100 from being introduced to mass spectrometer.

Sample preparation for gel based Competitive Activity Based Protein Profiling (ABPP). Cell pellets were processed using dounce homogenizer. Supernatant was isolated and centrifuged at 100,000 g for 45 minutes. Resulting supernatant fraction and resuspended pellet solution were referred as soluble and membrane fraction, respectively. Proteomes (1mg/mL) were treated with HT-01 at 1 μ M final concentration for 30 minutes at 37°C. The reaction was quenched using SDS-PAGE loading buffer. After separation by SDS-PAGE (10% acrylamide), samples were visualized by in-gel fluorescence scanning using Chemidoc MP imaging system.

Tissue histology

Liver sections were fixed in 10% formaldehyde solution in PBS and paraffin embedded prior to sectioning. Hematoxylin eosin (H&E) staining was performed by Research Histology Core at UVA. The H&E staining was performed using automated Varistain Gemini and Hematoxylin 360 system. In brief, slides were deparaffinized and re-hydrated with water. Hematoxylin solution was added to completely cover the tissue section and was incubated for 10 minutes. Sections were rinsed in DI water for 20 – 30 seconds. Bluing reagent was added and incubated for 30 seconds and washed with DI water. Sections were dehydrated and mounted on slides.

4.4 RESULTS

4.4.1 ABPP analysis of BMDM shows enriched activity of DAGL β but not

DAGL α Activities of DAGL α are enriched in central nervous system whereas DAGL β is expressed in immune cells. We tested the enrichment of the DAGL activities in brain tissue and BMDMs using the DAGL tailored activity-based probe (ABP) HT-01 to investigate the differential expression of the DAGLs (**Figure 4.1**). In brief, brains were harvested from wildtype, DAGL α knockout, and DAGL β mice. For BMDMs, bone marrows were isolated from wildtype, DAGL α knockout, and DAGL β mice and differentiated into BMDMs for 7 days. After the differentiation, BMDMs were harvested and analyzed along with brain proteome. Each sample was dounce homogenized and ultracentrifuged for 45 minutes at 4C. Resulting pellets were resuspended and labeled with tailored DAGLs ABP HT-01. Samples were analyzed using SDS-PAGE and band at ~120kDa and ~70kDa were identified as DAGL α and DAGL β , respectively. In brain tissue, both DAGL α and DAGL β were able to be detected. This was further confirmed by the disappearance of the ~120kDa band on DAGL α knockout mouse brain (**Figure 4.1**). On the other hand, the BMDM analysis of the DAGLs showed that macrophages show enriched activities of DAGL β . However, DAGL α was not able to be detected (**Figure 4.1**).

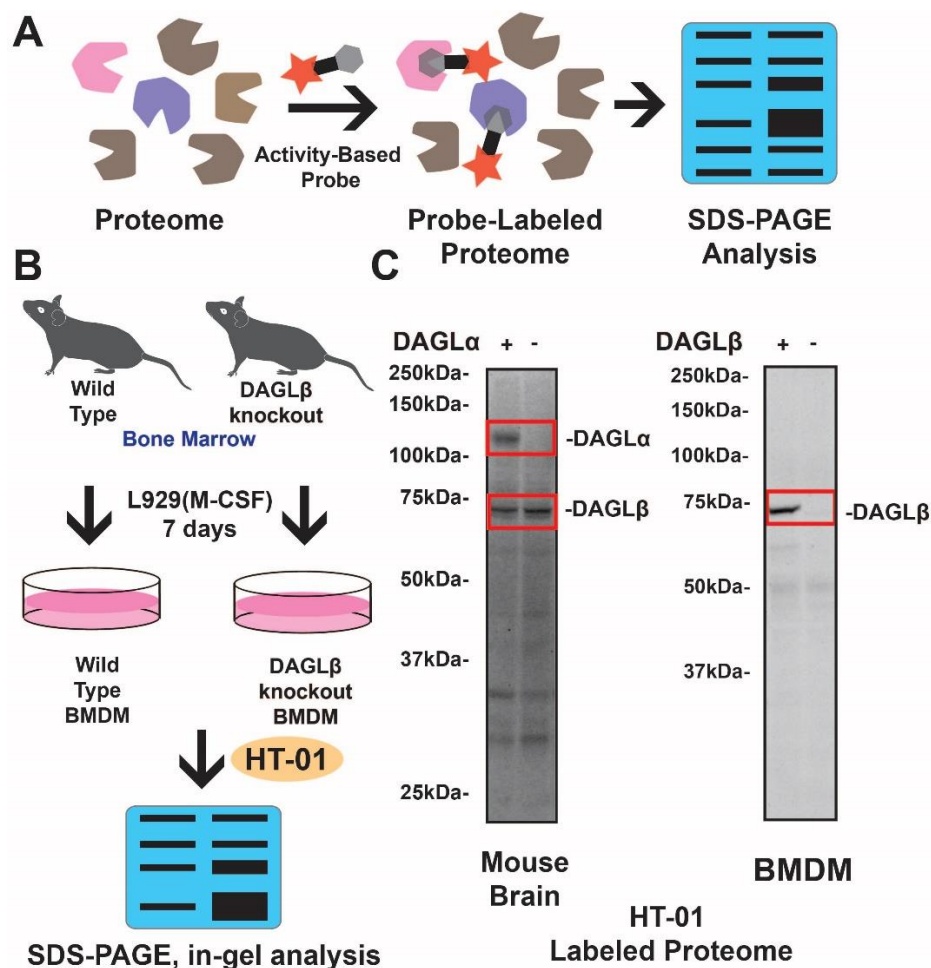


Figure 4.1 Activity-Based Protein Profiling (ABPP) of DAGLs using HT-01 in mouse brain and Bone marrow derived macrophages The schematics of the ABPP on proteome. The proteome is labeled with tailored DAGL ABP HT-01. Following labeling, samples were analyzed with SDS-PAGE (A). The schematics of the sample preparation using BMDMs. Bone marrow from mice were cultured with L929 supplemented media. The cells were lysed and membrane fractions were enriched. Membrane fractions were resuspended and labeled with tailored DAGLs ABP. Samples were analyzed using 10% acrylamide SDS-PAGE gel (B). The brain tissues from DAGL α wildtype and knockout mice, and BMDMs from DAGL β wildtype and knockout were labeled with HT-01 and analyzed with SDS-PAGE.

4.4.2 DAGL β disruption does not result in PKC hyperactivation. Given the role of DAGL β in modulating cellular DAG levels, either through TAG (this study) or DAG lipase activity², we explored protein kinase C (PKC) activation in DAGL β -disrupted BMDMs. PKC activation is mediated in part by C1 domains that bind DAGs to allow membrane localization during cell signaling¹². To assess activity against DAG-sensitive PKCs, we used a general antibody that recognizes phosphorylated substrates of PKC based on conserved motifs surrounding the phospho-serine residue¹³⁻¹⁵. Initially, we measured PKC phospho-substrate profiles under basal conditions (non-activated BMDMs) and observed negligible differences in *Daglb*^{-/-} and *Daglb*^{+/+} proteomes (**Figure 4.2, 4.2.1, 4.2.2**). Activation of BMDMs with lipopolysaccharide (LPS, 100 ng/mL, 1 hr) resulted in enhanced phosphorylation of several PKC substrates across the molecular weight range in soluble and membrane fractions (~30kDa, and ~20kDa for membrane fraction, and ~120kDa, 80kDa, ~70kDa, and ~60kDa for soluble fraction, phospho-bands; **Figure 4.1**). Interestingly, disruption of DAGL β globally reduced the degree of LPS-stimulated phosphorylation of PKC substrates as measured by western blot of *Daglb*^{-/-} and *Daglb*^{+/+} proteomes (**Figure 4.1**).

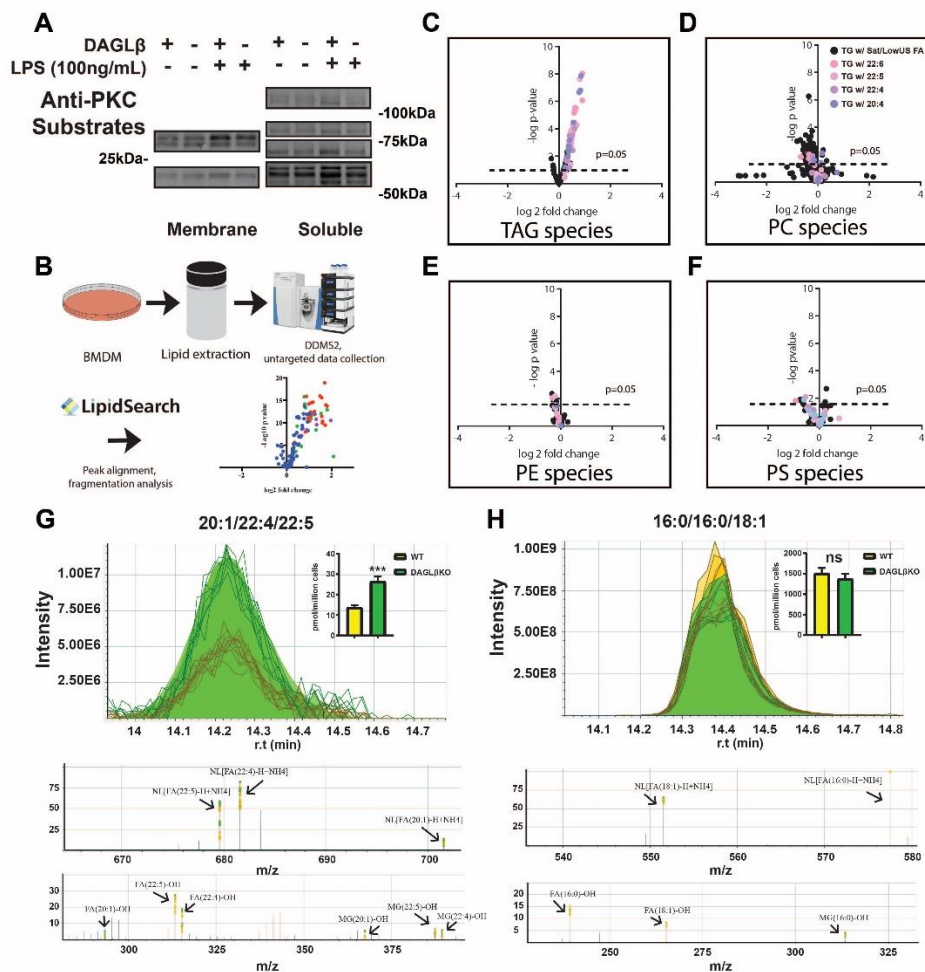


Figure 4.2 Phosphorylated PKC substrate changes in BMDMs with DAGL β disruption and untargeted lipidomics analysis. BMDMs from DAGL $\beta^{+/+}$ and DAGL $\beta^{-/-}$ were treated with either vehicle or LPS (100ng/mL) for 1 hour at 37°C. Cells were lysed and separated into membrane and soluble fractions using ultracentrifugation. Protein concentrations were normalized and separated using SDS-PAGE. Samples were analyzed with western blot analysis using antibody recognizing phosphorylated PKC substrates (**A**). Schematics of the sample preparation for the untargeted lipidomics analysis. In brief, BMDMs were extracted using folch method and analyzed using Q-Exactive Plus. Lipids were searched and aligned using LipidSearch™ (**B**). Various lipid classes were analyzed including triacylglycerol (TAG, +NH₄ ion adduct, **C**), phosphatidylcholine (PC, +H ion adduct, **D**), Phosphatidylethanolamine (PE, +H ion adduct, **E**), and phosphatidylserine (PS, -H ion adduct, **F**). each lipid species was colored-coded based on the fatty acids (PUFA FA were labeled (4 unsaturated or more) with color and saturated FA or FA with low unsaturation units (unsaturation units 3 or less). The fragmentation analysis as well as peak alignments of the lipid species across tested samples were performed in LipidSearch™ for triacylglycerol species (PUFA containing TAG (**G**), and saturated FA TAG (**H**)).

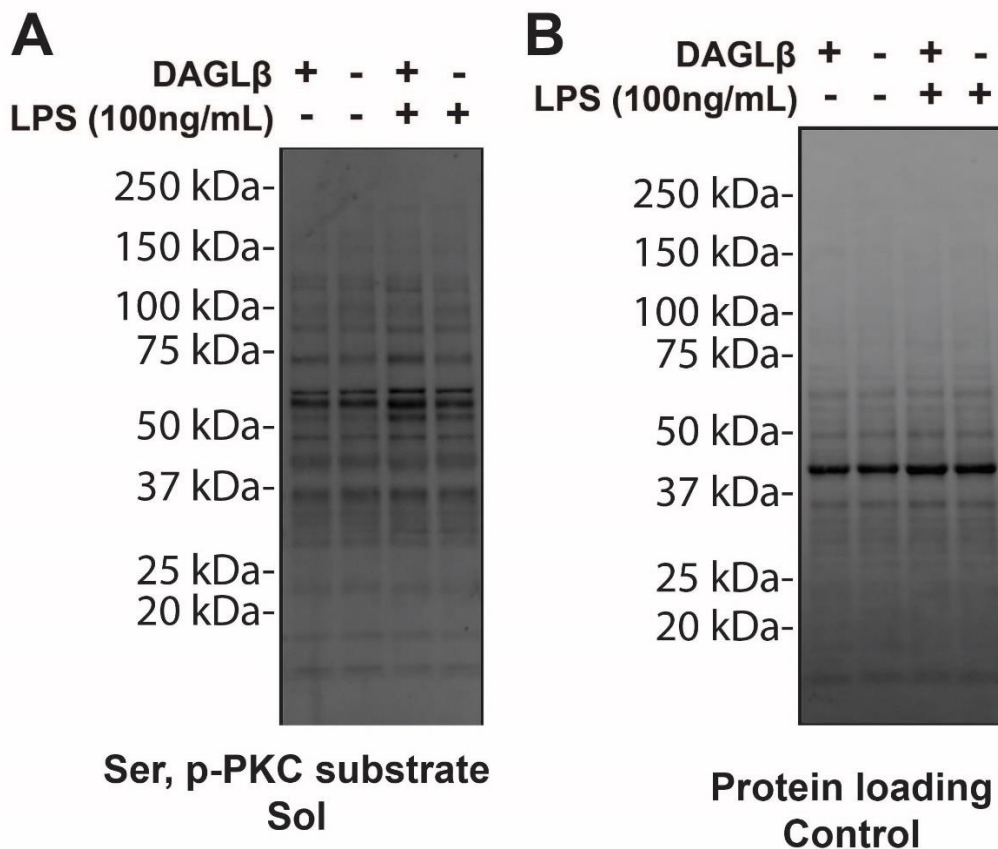


Figure 4.2.1 Western blot analysis of phosphorylated PKC substrates on soluble fractions from BMDMs generated from DAGL $\beta^{+/+}$ and DAGL $\beta^{-/-}$ mice. BMDMs from DAGL $\beta^{+/+}$ and DAGL $\beta^{-/-}$ mice were treated with either vehicle or LPS (100ng/mL) for 1 hour at 37°C. cells were lysed and separated into soluble and membrane fractions using ultracentrifugation. The protein concentrations were normalized with BioRad DC assay. Soluble fraction Western blot analysis was performed with p-PKC substrate antibody. pPKC substrate antibody labels protein substrates that have been phosphorylated by PKC (A). The protein loading control was analyzed using stain free gel.

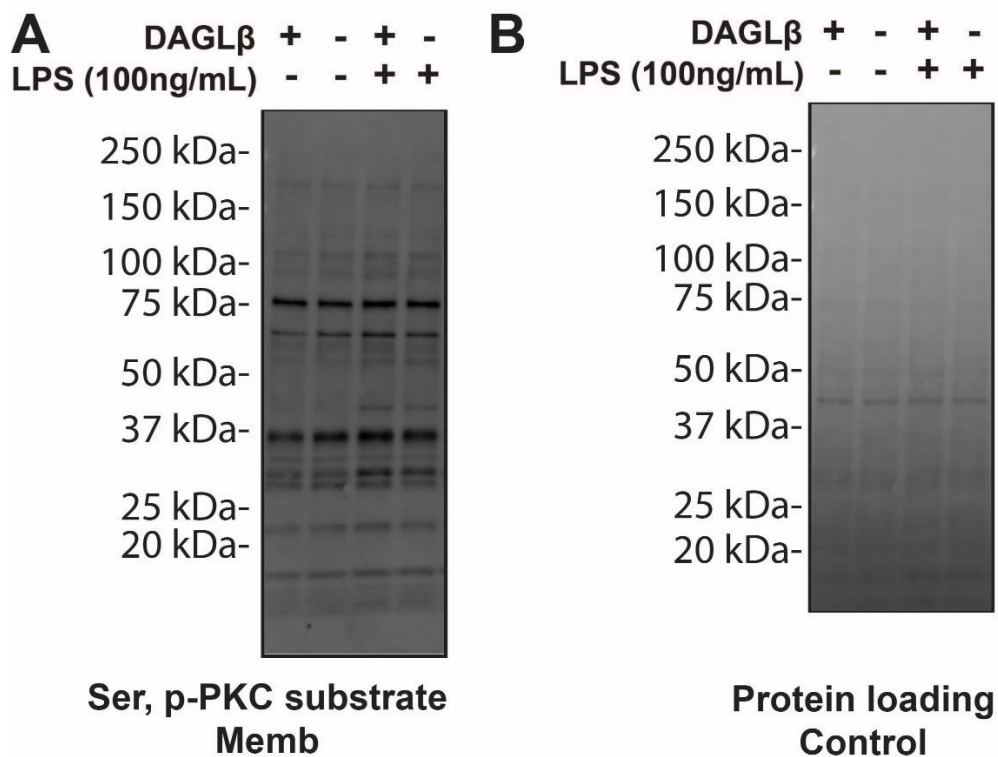


Figure 4.2.2 Western blot analysis of phosphorylated PKC substrate antibody for membrane fraction from BMDMs generated from DAGL $\beta^{+/+}$ and DAGL $\beta^{-/-}$ mice. BMDMs from DAGL $\beta^{+/+}$ and DAGL $\beta^{-/-}$ mice were treated with either vehicle or LPS (100ng/mL) for 1 hour at 37°C. cells were lysed and separated into soluble and membrane fractions using ultracentrifugation. The protein concentrations were normalized with BioRad DC assay. Membrane fraction Western blot analysis was performed with p-PKC substrate antibody. pPKC substrate antibody labels protein substrates that have been phosphorylated by PKC (A). The protein loading control was analyzed using stain free gel.

4.4.3 Untargeted lipidomics analysis of BMDMs shows selective accumulation of triacylglycerols composed of PUFAs Here, we employed untargeted MS-metabolomics¹⁶⁻¹⁸ to gain an unbiased global evaluation of alterations in lipid composition of DAGL β -disrupted BMDMs. Total lipids (i.e. lipidome) were extracted from *Daglb*^{+/+} and *Daglb*^{-/-} BMDMs using the Folch method¹⁹ and analyzed by liquid chromatography-mass spectrometry (LC-MS) on a high-resolution Q-Exactive mass spectrometer configured for untargeted data-dependent acquisition (ddMS2, **Figure 4.2**). Precursor ions (MS1) of lipids selected for fragmentation were identified using LipidSearch identification algorithm²⁰ that matches precursor (MS1) and fragment (MS2) spectra to an in-silico database of >1.5 million lipid ions and their predicted fragment ions. Identified lipids were scored based on annotation of FA chain composition, which are deduced from neutral loss scans, and only those with high quality (Grade A or B signifying 2-4 lipid class-specific diagnostic fragment ions) and <5 ppm mass accuracy was selected for further manual evaluation (see Method section for details of LC-MS data analyses).

We detected on average ~1600 lipids per analyses (n = 3 – 6 sample) across both positive and negative mode analyses of BMDM lipidomes. From these data, we could quantitate >900 distinct species after filtering for lipids with high quality annotations of FA composition. Our findings show a striking alteration in TAG lipid profiles in DAGL β -disrupted BMDMs. Specifically, we observed statistically significant accumulation of TAG species that contain polyunsaturated fatty acids (PUFAs) in *Daglb*^{-/-} compared with *Daglb*^{+/+} BMDMs (**Figure 4.2**). Fatty

acid compositions of accumulated TAGs include those containing omega-6 (arachidonic acid, C20:4) and omega-3 fatty acids (docosahexaenoic acid, C22:6; **Figure 4.2 C**). TAGs containing saturated fatty acids (C16:0 and C18:0) showed negligible differences in *Daglb*^{-/-} compared with *Daglb*^{+/+} lipidomes. The identities of the TAGs species were further confirmed by the fragmentation pattern based on the MS2 fragments from the precursor mass as well as the peak-alignment (**Figure 4.2 G, H**). To determine if PUFA-TAG changes were due to general alterations in macrophage lipidomes, we compared levels of phospholipids between *Daglb*^{-/-} and *Daglb*^{+/+} lipidomes and observed little to no change in phosphatidyl-ethanolamine (PE), -choline (PC), and -serine (PS) species (**Figure 4.2**).

We also confirmed TAG alterations observed in *Daglb*^{-/-} BMDMs using our previously published DAGLβ-selective inhibitor KT109 and matching negative control probe KT195^{2, 10}. We first confirmed by gel-based ABPP using HT-01 that treatment of BMDMs with KT109 but not KT195 resulted in concentration-dependent blockade of DAGLβ (**Figure 4.3**). From these studies, we selected optimal treatment conditions (200 nM compounds, 4 hrs, 37 °C) for untargeted metabolomics analyses. We observed statistically significant PUFA-TAG accumulations in KT109- but not KT195-treated BMDMs (**Figure 4.4**). Finally, to assess the impact of DAGLβ inactivation on bulk TAG levels in BMDMs, we compared the abundance of PUFA- and saturated-TAGs detected in BMDM lipidomes based on ion intensities of MS1 peaks. Unlike PC, PE, and PS lipids, the abundance of PUFA-TAGs represented a very minor fraction of total TAGs,

indicating that disruption of DAGL β does not result in massive accumulations of TAGs as observed with other TAG lipases.

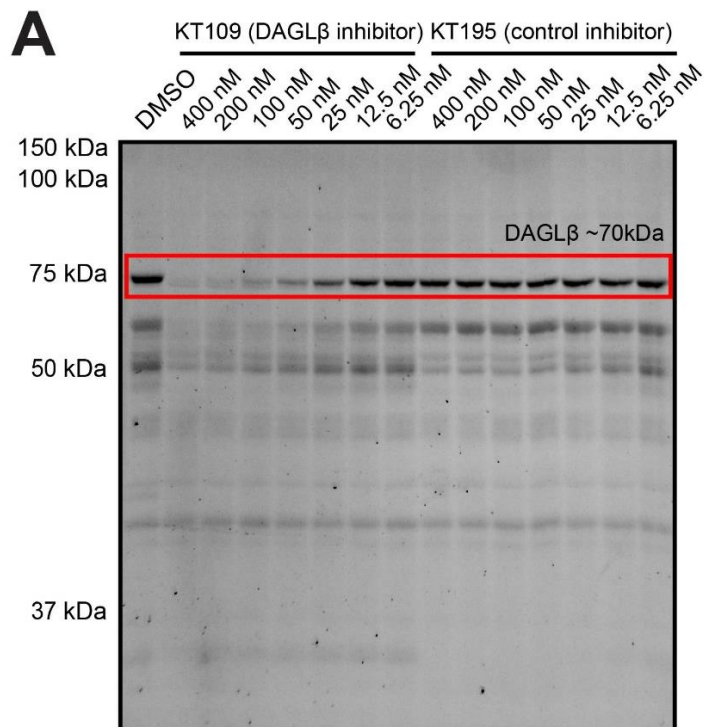
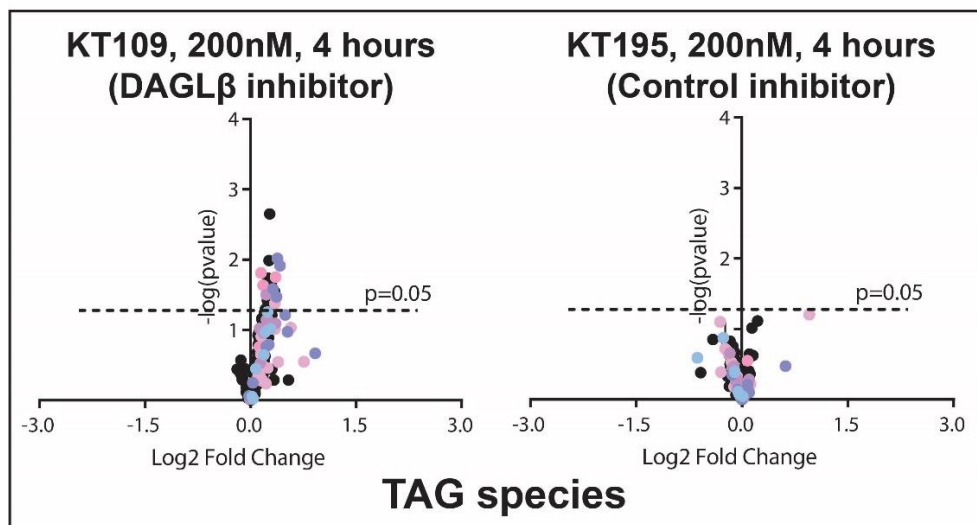
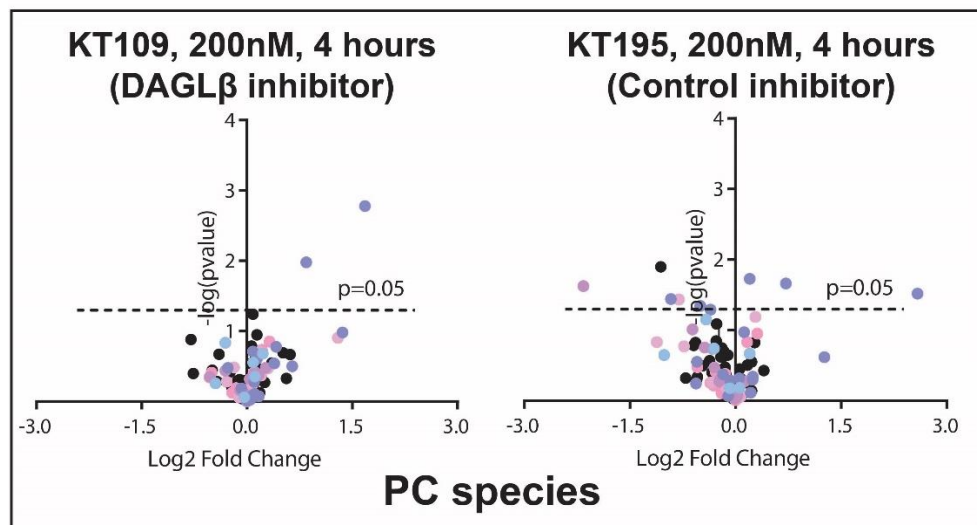


Figure 4.3 Activity based protein profiling analysis of the BMDMs with in-situ compound treatment for dose dependent inhibition of DAGL β BMDMs were treated with KT109 (DAGL β specific inhibitor) or KT195 (control inhibitor) at different concentrations in live cell for 4 hours at 37°C. Cells were harvested and lysed with dounce homogenizer. The membrane fractions were isolated with ultracentrifugation. The protein concentrations for the membrane fractions were normalized using BioRad DC assay. Standardized proteomes were labeled with HT-01(1 μ M) for 30 minutes at 37°C. Samples were analyzed using 10% acrylamide SDS-PAGE gel.

A**B**

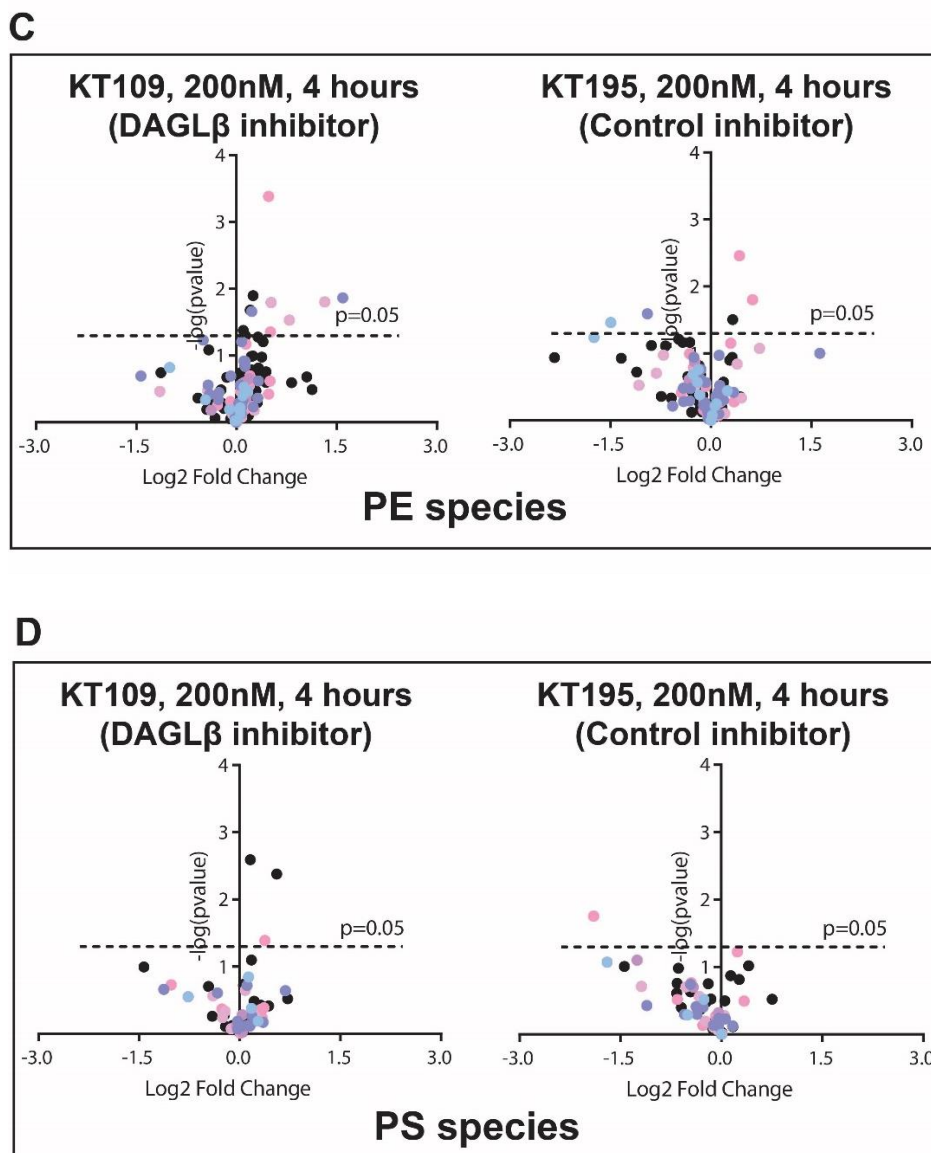


Figure 4.4 Untargeted lipidomics analysis of DAGL β ^{+/+} BMDMs treated with KT109 (200 nM) or KT195 (200 nM) at for 4 hours The concentration of the KT109 treatment condition was determined based on the gel-based ABPP analysis shown in 3.3. The complete inhibition of the DAGL β activity was achieved at 200nM KT109. BMDMs were treated with KT109 as well as KT195 at 200nM for 4 hours. Cells were harvested and lipid extractions were performed using the folch method. Samples were analyzed using Q-Exactive Plus mass spectrometer. Lipids were searched and aligned using LipidSearchTM. Various lipid classes were analyzed including triacylglycerol (TAG, +NH₄ ion adduct, **A**), phosphatidylcholine (PC, +H ion adduct, **B**), Phosphatidylethanolamine (PE, +H ion adduct, **C**), and phosphatidylserine (PS, -H ion adduct, **D**). each lipid species was colored-coded based on the fatty acids (PUFA FA were labeled (4 unsaturated or more) with color and saturated FA or FA with low unsaturation units (unsaturation units 3 or less).

4.4.4 Biochemical validation that DAGL β functions as a PUFA-specific TAG lipase We next examined whether DAGL β could hydrolyze TAGs by substrate assay. We transiently overexpressed DAGL β in HEK293T cells, confirmed recombinant DAGL β activity in membrane fractions by gel-based ABPP with HT-01, and showed recombinant DAGL β was inhibited by KT109 but not KT195 treatments (2 μ M compounds, 30 min, 37 °C; **Figure 4.5**). We also confirmed catalytic activity of recombinant DAGL β by demonstrating robust hydrolysis activity using a fluorogenic lipase substrate assay that could be blocked by >90% with KT109 but not KT195 using treatment conditions from our gel-based ABPP analyses.

Next, we tested recombinant DAGL β activity against TAGs with varying FA composition ranging from short-chain saturated FAs (C14:0) to long-chain PUFAs (C22:6). Incubation of recombinant DAGL β membrane proteomes with PUFA-TAG substrates (both C20 and C22 species) resulted in statistically significant depletion of TAG substrate and production of corresponding DAG products in recombinant overexpressed compared with non-transfected mock samples as measured by MS-metabolomics (**Figure 4.5**). In contrast, recombinant DAGL β showed negligible activity against saturated TAG substrates regardless of FA composition (**Figure 4.5**). We compared saturated and unsaturated TAG pairs to directly test the importance of FA unsaturation on TAG lipase activity of DAGL β . Incubation of recombinant DAGL β proteomes with triarachidonin (C20:4 FA) or tridocosahexaenoin (C22:6 FA) resulted in robust hydrolysis activity that could be blocked with KT109 but not KT195 pretreatment, which supports DAGL β -specific

activity (**Figure 4.5**). The saturated TAG counterparts (C20:0 and C22:0 FA) were not processed by DAGL β to any appreciable degree. In summary, our findings support DAGL β as a TAG lipase with high specificity for species containing PUFAs.

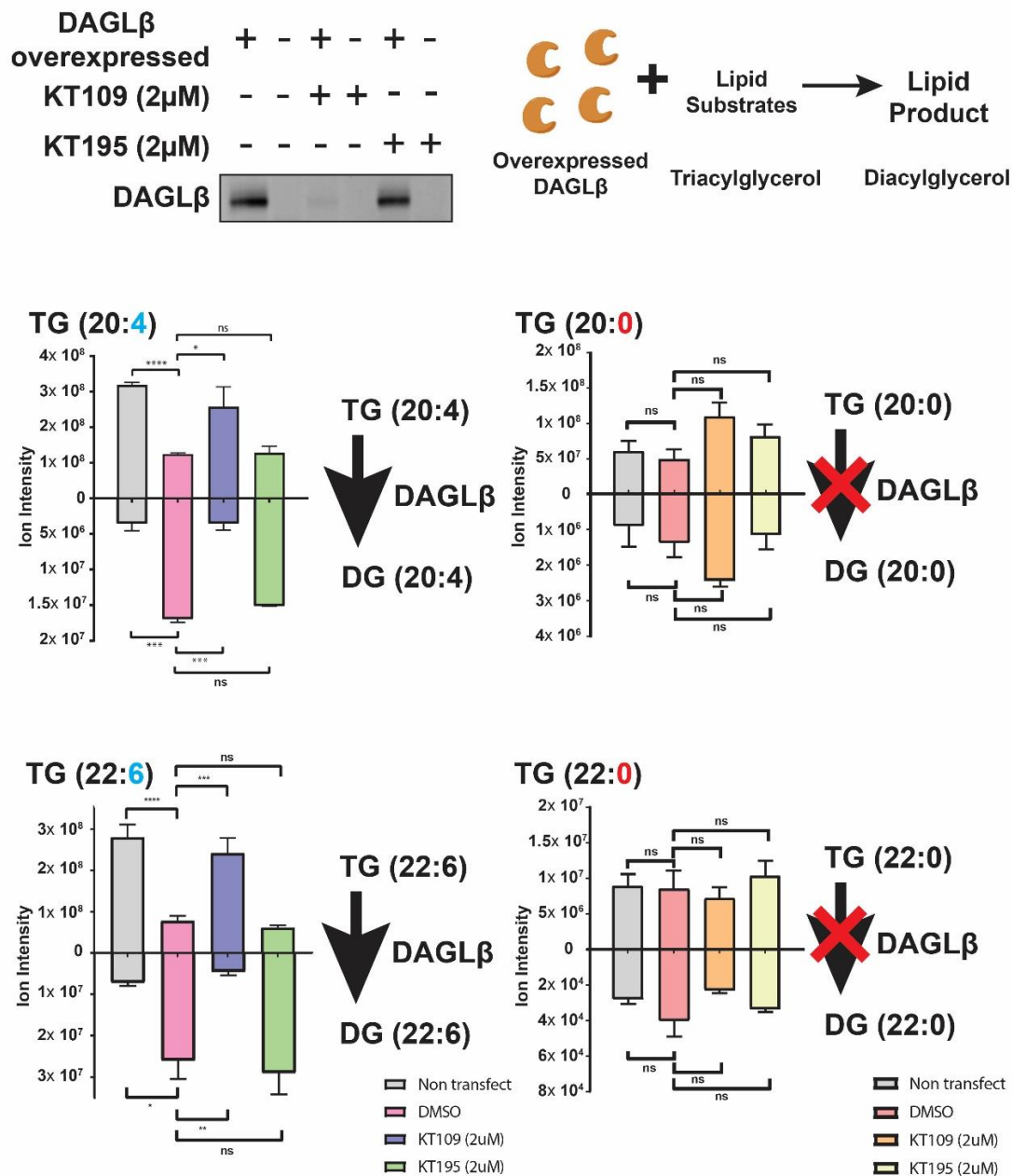


Figure 4.5 Biochemical substrate assay of DAGL β using triacylglycerols mouse DAGL β was overexpressed in HEK293T cells. The membrane fraction that contains enriched DAGL β activity was isolated for substrate assay against triacylglycerols. The DAGL β overexpression was confirmed using ABPP analysis using HT-01 probe. Furthermore, the DAGL β inhibitor KT109 and control inhibitor KT195 were tested against overexpressed DAGL β (A). The schematics of the substrate assay using overexpressed DAGL β proteome. The triacylglycerols were incubated with proteome and incubated for 4 hours at 25°C. Remaining substrates and the products were measured using mass spectrometer (B). Remaining TAGs that contain PUFA (20:4, and 22:6) were significantly decreased after being

incubated with DAGL β overexpressed proteome. DAGL β selective catalytic activity was further confirmed by the selective DAGL β inhibitor KT109 as well as control inhibitor KT195. The subsequent product formation of the corresponding diacylglycerols increased in DAGL β overexpressed proteome whereas it was inhibited when the DAGL β was inhibited by KT109. The control inhibitor KT195 showed no significant impact on DAGL β activity (C). TAGs with saturated fatty acids were tested against DAGL β overexpressed proteome. Saturated fatty acids that matches the number of carbons were tested (C20:0, and C22:0). The result showed no significant changes in the remaining substrate concentration nor the product concentrations.

4.4.5 ABPP discovery of FASN regulation by DAGL β using SILAC BMDMs We established a quantitative proteomics strategy that would be highly amenable to assessing functional changes in DAGL β -disrupted primary macrophages. We selected primary bone-marrow derived macrophages (BMDMs) for our studies because we reasoned that isotopic amino acids (i.e. SILAC method²¹) could be efficiently incorporated into macrophage proteomes during the rapid differentiation and proliferation of bone marrow stem cells. First, we confirmed that BMDMs differentiated under SILAC media conditions were phenotypically similar to standard media condition counterparts. For these studies, BMDMs were differentiated from bone marrow of mice using L929 supplemented media (SILAC or standard media) for 7 days following published procedures²² and as described in the Methods section. We used flow cytometry and established markers for BMDMs (F4/80 and CD11b) to compare macrophage content under standard and SILAC differentiation conditions. We observed comparable numbers of F4/80⁺CD11b⁺ macrophages between standard and SILAC media (both light and heavy) differentiations (**Figure 4.6.5**).

Next, we evaluated global changes in serine hydrolase activity between *Daglb*^{+/+} and *Daglb*^{-/-} macrophages using our newly established SILAC BMDM methodology. Serine hydrolases catalyze a wide array of metabolic and signaling functions and can provide further clues to DAGL β -regulated pathways. First, we confirmed that BMDMs expressed active DAGL β using our DAGL-tailored activity-based protein profiling (ABPP) probe, HT-01². We detected prominent HT-01 labeling of an ~70 kDa protein band that was present in proteomes from *Daglb*^{+/+}

BMDMs but absent from *Daglb*^{-/-} BMDMs (**Figure 4.1**). We also performed HT-01-based ABPP comparisons of *Dagla*^{+/+} and *Dagla*^{-/-} BMDM proteomes but could not detect active DAGL α (**Figure 4.1**). Thus, we focused the remainder of our macrophage studies on the DAGL β isoform. After confirming DAGL β expression and activity, we differentiated *Daglb*^{+/+} and *Daglb*^{-/-} BMDMs in light and heavy L929 supplemented SILAC media, respectively, followed by labeling proteomes with the serine hydrolase-directed probe FP-alkyne, click chemistry performed using biotin azide, avidin enrichment, on-bead trypsin digestion, and quantitative liquid chromatography-mass spectrometry (LC-MS) ABPP to measure changes in serine hydrolase activity in BMDM proteomes (**Figure 4.6 B**).

The activity profiles across the >50 detected serine hydrolases in BMDMs were largely unchanged (median ratio of ~1) between *Daglb*^{+/+} and *Daglb*^{-/-} proteomes with the exception of fatty acid synthase (FASN), which showed ~57% reduced activity (SILAC ratio or *SR* ~2.35, **Figure 4.6 C**). As expected, DAGL β peptides were absent in *Daglb*^{-/-} BMDM heavy proteomes, which resulted in a large SILAC ratio from light singleton peptides detected in *Daglb*^{+/+} proteomes (*SR* = 20, **Figure 4.6 C**). In agreement with our HT01-based ABPP studies, we could not detect DAGL α activity in our LC-MS studies (**Figure 4.6 C**). Our finding that key lipolytic activities (LIPA^{23, 24} and LPL^{25, 26}, *SR* ~1; **Figure 4.6 C**) were not altered from disruption of DAGL β provides additional support that lipid signaling effects were due to DAGL β and not compensatory activity from other lipases. The discovery that DAGL β inactivation selectivity modulates FASN activity was intriguing given FASN's key role in lipogenesis to synthesize fatty acids (FA), which

are used to synthesize diverse cellular lipids including phospholipids, triglycerides and cholesterol esters, or for the acylation of proteins²⁷⁻²⁹.

4.4.6 Chemical or genetic disruption of DAGL β activates AMP-activated protein kinase (AMPK) To further understand cross-talk between DAGL β and FASN pathways, we explored regulatory pathways upstream of FASN that are known to regulate macrophage inflammation^{30, 31}. Activation of AMP-activated protein kinase (AMPK) promotes FA oxidation and blockade of FA synthesis (i.e. lipogenesis) through phosphorylation and inactivation of acetyl-CoA carboxylase (ACC) and FASN downregulation³². We tested the effect of DAGL β inactivation on AMPK activation by monitoring phosphorylation of a critical regulatory threonine residue (T172) in the kinase domain³³. Blockade of DAGL β either through genetic or pharmacological means resulted in increased phospho-AMPK in basal and LPS-stimulated BMDMs (**Figure 4.6 D, E**).

Given that PKCs are capable of phosphorylating AMPK at S485/491, we explored the potential correlation between DAGL β -mediated blockade of PKC activity and AMPK activation via reduced S485/491 phosphorylation³⁴. LPS activation of BMDMs resulted in reduced phospho-AMPK, matching previous reports describing reduced AMPK dephosphorylation and inactivation with pro-inflammatory stimuli^{35, 36}. Concomitant with decreased phosphorylation of T172, we also observed enhanced phosphorylation of S485/491, which further supports AMPK inactivation upon LPS stimulation in BMDMs (**Figure 4.6.3**). Next, we evaluated AMPK activation state in DAGL β -inactivated BMDMs under LPS-activated states. Strikingly, the phosphorylation profile of AMPK was reversed

(decreased S485/491 and increased T172 phosphorylation) and supports DAGL β as a regulator of AMPK activation states in BMDM response to inflammatory stimuli (**Figure 4.6, 4.6.2**).

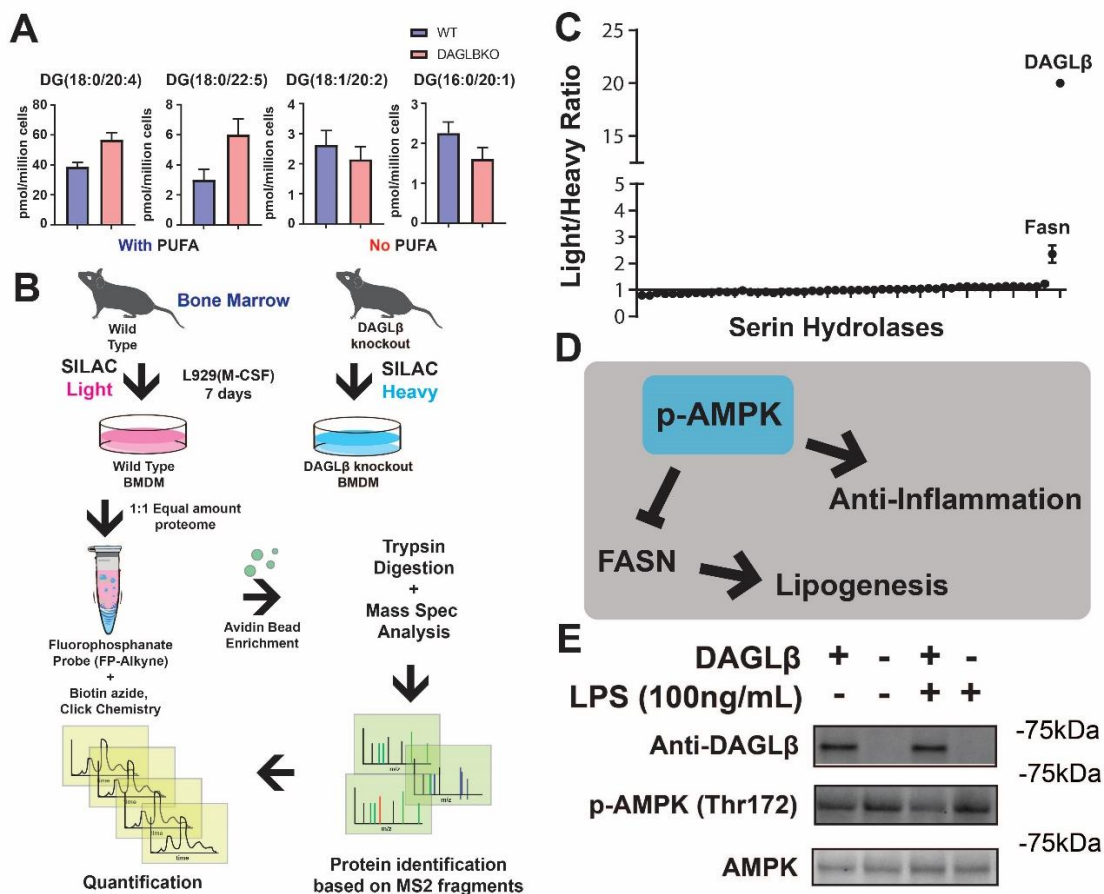


Figure 4.6 Quantitative chemoproteomic analysis of serine hydrolases in BMDMs BMDMs were differentiated from DAGL $\beta^{+/+}$ and DAGL $\beta^{-/-}$ mice. The bone marrow was cultured in the SILAC media. The bone marrow cells expand rapidly and incorporate SILAC media into proteins for SILAC analysis. Schematics of the ABPP proteomics sample prep is described. Proteomes were labeled with FP-alkyne and click chemistry with biotin-azide. Probe bound proteins were enriched in avidin beads and digested with trypsin. Digested peptides were analyzed using nanospray Q-Exactive Plus mass spectrometer. Data obtained from the analysis were analyzed using IP2 software for protein identification. Further quantification was performed in Skyline from data exported from IP2 (B). Light/Heavy peptide ratios were calculated for serine hydrolases found in BMDMs. The results show no activity detected for DAGL β in DAGL $\beta^{-/-}$ BMDMs. In addition, decrease in FASN activity was also shown in DAGL $\beta^{-/-}$ BMDM (C). The signaling pathways involving FASN regulation with anti-inflammatory effects are described. In addition, the activation of the AMPK pathway has been described to reduce FASN (D). The activation of the AMPK was tested in BMDMs. The result shows activation of AMPK in DAGL $\beta^{-/-}$ BMDMs (E). The diacylglycerols were analyzed from BMDMs generated from DAGL $\beta^{+/+}$ and DAGL $\beta^{-/-}$ mice. The results showed decreased DAG species with saturated/low-unsaturated FA whereas DAGs with PUFA FA showed increased in DAGL $\beta^{-/-}$ BMDMs as was reported previously.

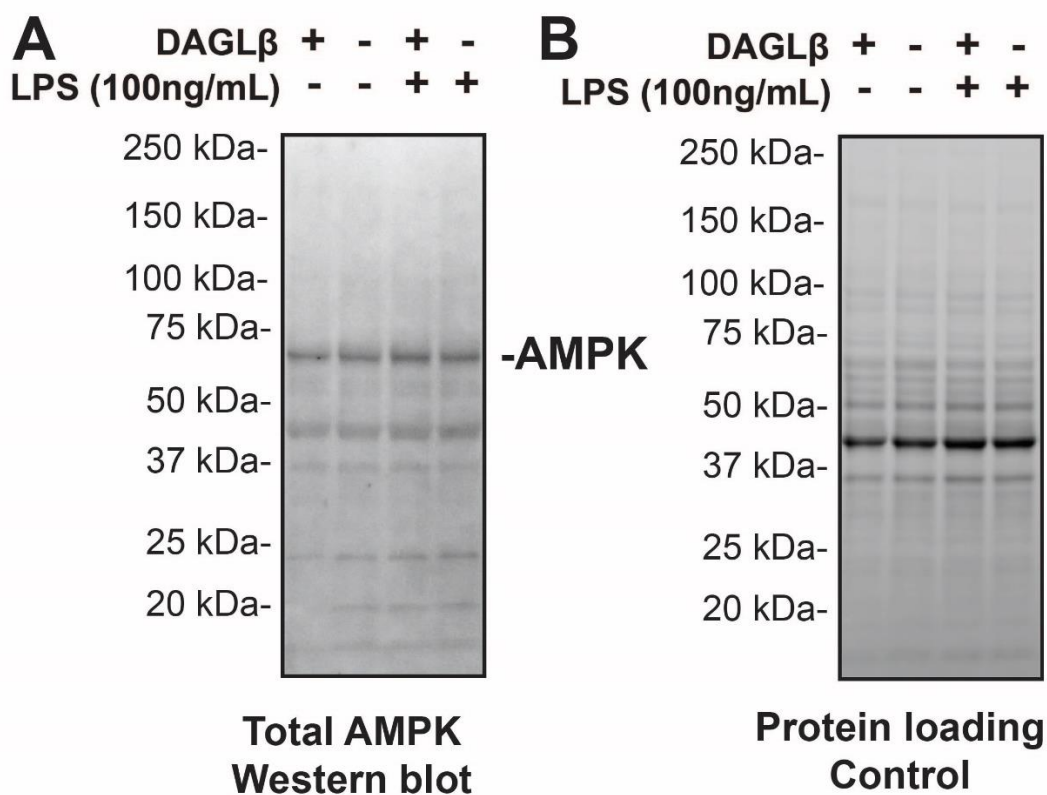


Figure 4.6.1 Western blot analysis of total AMPK levels in soluble fraction of BMDMs generated from DAGL β ^{+/+} and DAGL β ^{-/-} mice. BMDMs from DAGL β ^{+/+} and DAGL β ^{-/-} mice were treated with either vehicle or LPS (100ng/mL) for 1 hour at 37°C. cells were lysed and separated into soluble and membrane fractions using ultracentrifugation. The protein concentrations were normalized with BioRad DC assay. Soluble fraction Western blot analysis was performed with AMPK antibody (**A**). The protein loading control was analyzed using stain free gel (**B**).

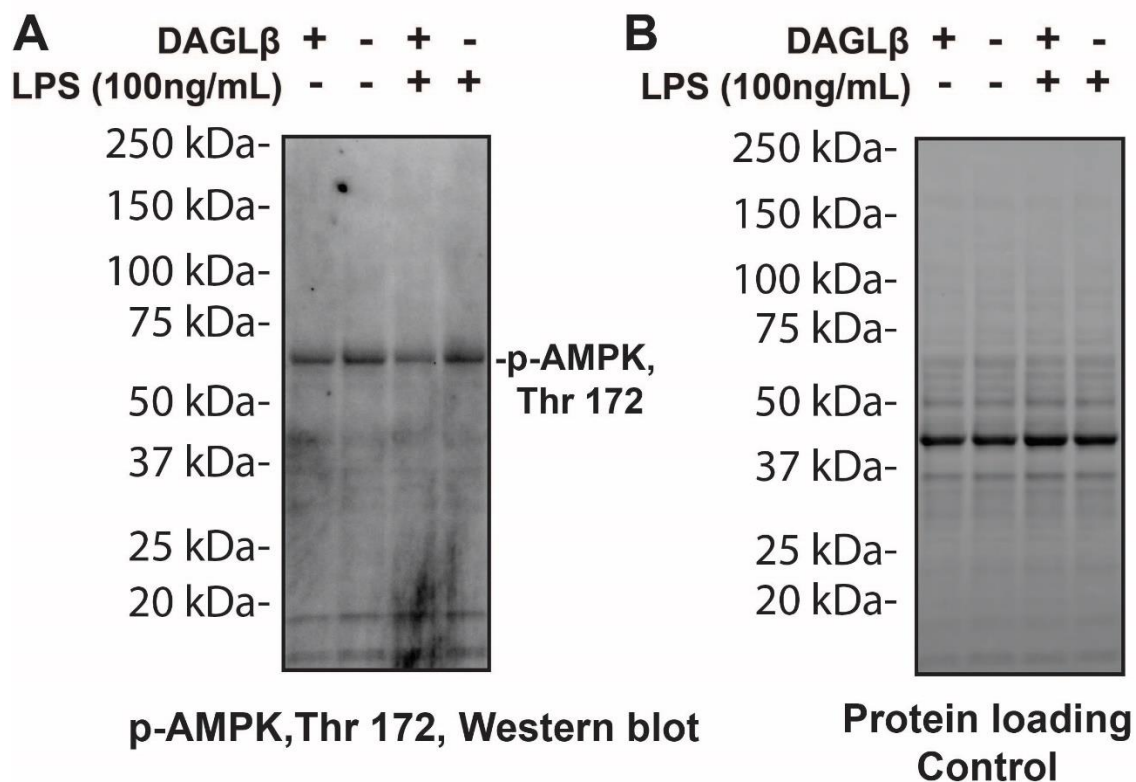


Figure 4.6.2 Western blot analysis of p-AMPK (Thr172) levels in soluble fraction of BMDMs generated from DAGL $\beta^{+/+}$ and DAGL $\beta^{-/-}$ mice. BMDMs from DAGL $\beta^{+/+}$ and DAGL $\beta^{-/-}$ mice were treated with either vehicle or LPS (100ng/mL) for 1 hour at 37°C. cells were lysed and separated into soluble and membrane fractions using ultracentrifugation. The protein concentrations were normalized with BioRad DC assay. Soluble fraction Western blot analysis was performed with p-AMPK Thr 172 antibody (**A**). The protein loading control was analyzed using stain free gel (**B**).

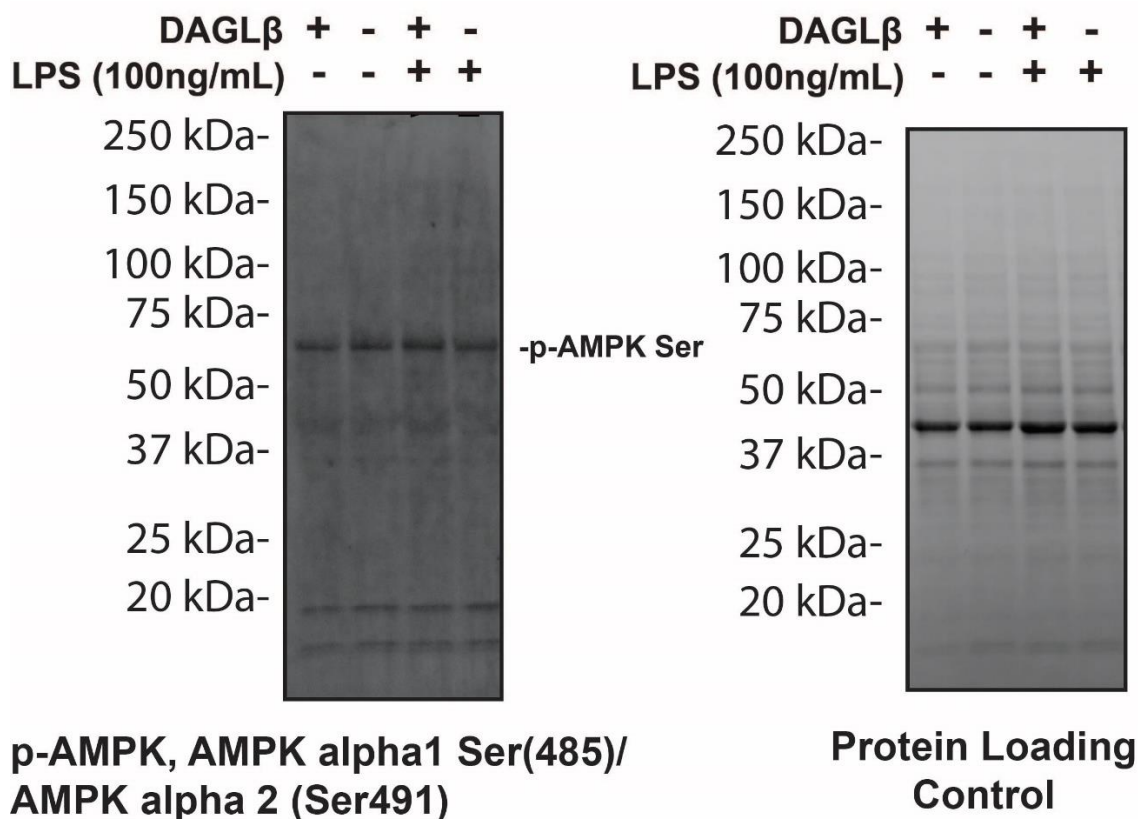


Figure 4.6.3 Western blot analysis of p-AMPK (Ser485/Ser491) levels in soluble fraction of BMDMs generated from DAGL $\beta^{+/+}$ and DAGL $\beta^{-/-}$ mice BMDMs from DAGL $\beta^{+/+}$ and DAGL $\beta^{-/-}$ mice were treated with either vehicle or LPS (100ng/mL) for 1 hour at 37°C. cells were lysed and separated into soluble and membrane fractions using ultracentrifugation. The protein concentrations were normalized with BioRad DC assay. Soluble fraction Western blot analysis was performed with p-AMPK alpha1 Ser 485/Ser491 antibody (**A**). The protein loading control was analyzed using stain free gel (**B**).

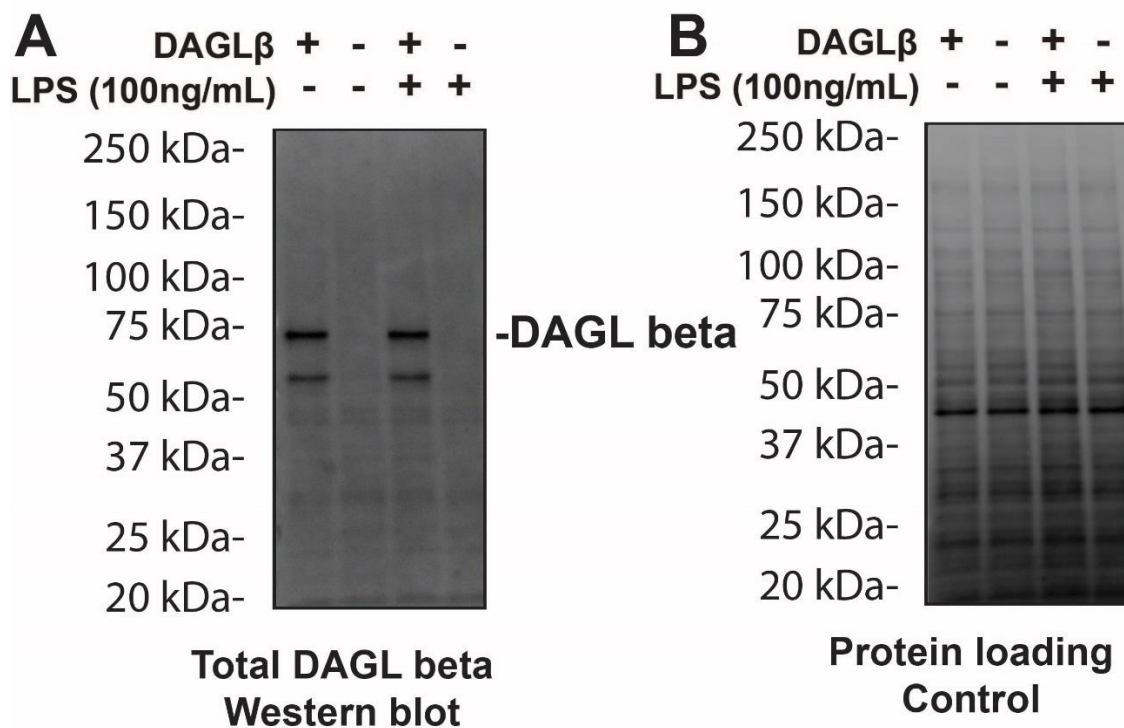


Figure 4.6.4 Western blot analysis of DAGL β levels in membrane fraction from BMDMs generated from DAGL $\beta^{+/+}$ and DAGL $\beta^{-/-}$ mice BMDMs from DAGL $\beta^{+/+}$ and DAGL $\beta^{-/-}$ mice were treated with either vehicle or LPS (100ng/mL) for 1 hour at 37°C. cells were lysed and separated into soluble and membrane fractions using ultracentrifugation. The protein concentrations were normalized with BioRad DC assay. Soluble fraction Western blot analysis was performed with DAGL β antibody (**A**). The protein loading control was analyzed using stain free gel (**B**).

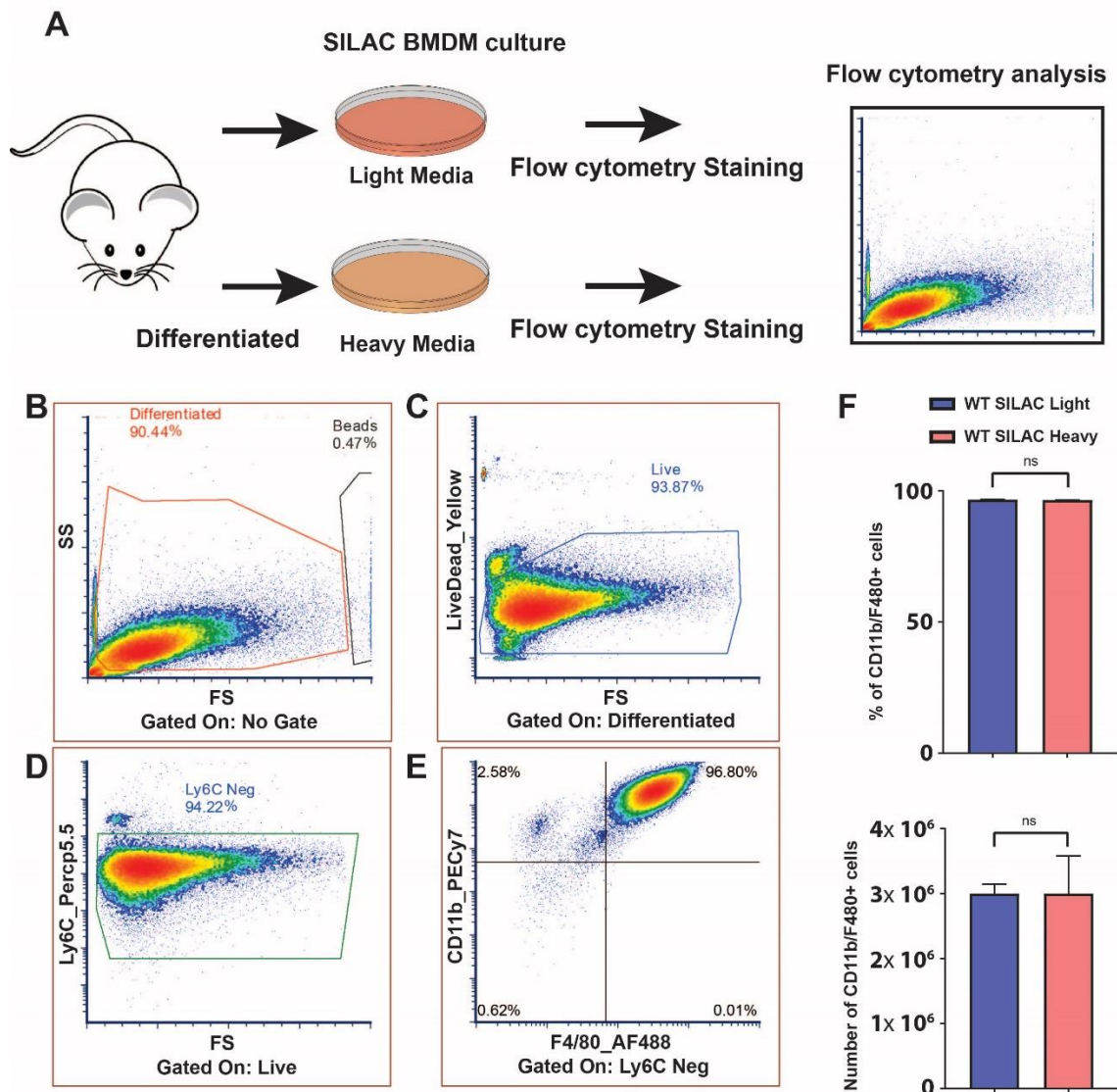


Figure 4.6.5 Flow cytometry analysis of the SILAC BMDM differentiation Bone marrow was harvested from a wild type mouse and cultured in SILAC media containing M-CSF for 7 days. Light media contained L-lysine and L-Arginine and the Heavy media contained Llysine ($^{13}\text{C}_6$, $^{15}\text{N}_2$), L-arginine ($^{13}\text{C}_6$, $^{15}\text{N}_4$). After the differentiation, cells were harvested and labeled with panels of antibodies including Ly6C, CD11b, and F4/80 (**A**). Gating strategy of the flow cytometry analysis is shown (**B**, **C**, **D**, **E**). The number of the BMDMs identified and counted using count beads were calculated as well as the percentage of the CD11b, F4/80 positive cells.

4.4.7 Chronic DAGL β blockade does not result in steatosis in mouse liver

One of the more common consequences of lipase inhibition is a lipid accumulation that results in steatosis. The development of steatosis has been documented in Hormone-sensitive lipase (HSL)³⁷, and Adipose Triglyceride Lipase (ATGL)³⁸. The development of steatosis is detrimental to the health of the mice as shown in the significantly reduced rate of survival. Therefore, development of the steatosis is considered one of the more significant side effects that results from the chronic lipase inhibition. To investigate the contribution of DAGL β inhibition to lipid accumulation in mice, we examined the lipid accumulation in the liver by genetic disruption at early and long-term disruption points (3 months and 10 months).

The *Daglb*^{+/+} and *Daglb*^{-/-} were placed on standard chow diet and sacrificed after desired timepoints. As a positive control, whole body *ATGL*^{-/-} mice (3 Mo), and wild type mice on HFD were used to demonstrate lipid accumulation in the liver (**Figure 4.7 C, F**). Livers of the mice were harvested at given timepoint and fixed with 10% formaldehyde in PBS. Livers were sectioned and stained with Haematoxylin and Eosin (H&E) staining. The H&E staining labels intracellular and extracellular proteins in the tissue. Areas where lipids accumulated within the tissue shows up in the stain by remaining clear compared to the cells.

The H&E staining results showed that the positive controls (*ATGL*^{-/-} and Wild type placed on HFD) showed clear lipid accumulation within the liver tissue as represented as circular area that remained clear (**Figure 4.7 C, F**). Interestingly, 3 months old *Daglb*^{-/-} showed no sign of steatosis compared to the *Daglb*^{+/+} counterpart (**Figure 4.7 A, B**). Therefore, we tested the liver of the 10 months old

Daglb^{-/-} and *Daglb*^{+/+}. As it was reported in previous literature, 10 months old wild type mice showed significant accumulation of lipids within the liver tissue. However, 10 months old *Daglb*^{-/-} mice showed little to no development of steatosis comparable to 3 months old wild type (**Figure 4.7 D, E**).

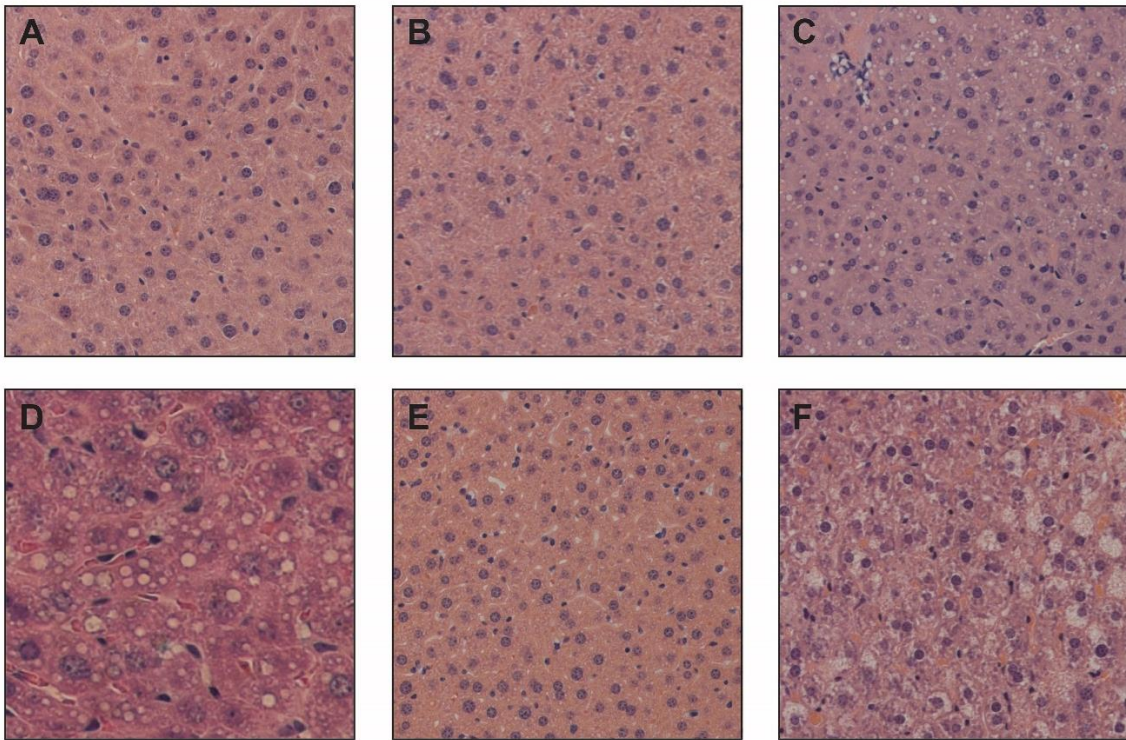


Figure 4.7 Hepatic steatosis and TG accumulation in DAGL β ^{+/+} and DAGL β ^{-/-} mice Mice were put on standard chow for 3 months (DAGL β ^{+/+} **A**, DAGL β ^{-/-} **D**), or for 10 months (DAGL β ^{+/+} **B**, DAGL β ^{-/-} **E**). 3 months old ATGL knockout (**C**) and mouse on high fat diet (HFD) (**F**) were used as a positive control. The liver samples were harvested from the mice and fixed in 10% formaldehyde solution. Following fixation step, tissues were stained with H&E staining. Steatosis and TG accumulation results in clear circular space after the H&E staining. The H&E staining showed no steatosis development in DAGL β ^{-/-} mice in both 3- and 10-months old mice.

4.5 DISCUSSION

DAGL β has emerged as a promising target for suppression of macrophage and microglia activation in animal models of pain and neuroinflammation³⁹⁻⁴¹. The broad anti-inflammatory activity of DAGL β inhibitors is mediated in part through blockade of prostaglandin and proinflammatory cytokine production². The pathways that mediate cross-talk between DAGL β lipid metabolism and cell signaling remain ill-defined and are needed to realize the translational potential of targeting DAGL β for inflammation. Here, we apply ABPP and metabolomics to discover a novel TAG lipase activity for DAGL β that upon disruption, lowers cellular DAG pools to attenuate PKC activity and activate AMPK via a key T472 phosphorylation site. Our findings identify AMPK as a kinase mediator of DAGL β that has broad implications for inflammation given that metformin, an AMPK activator, has shown anti-inflammatory activity in mice⁴² and humans^{43, 44}.

The ability to isotopically label primary macrophages by SILAC⁴⁵ provided a quantitative means for activity-based profiling of DAGL β -disrupted BMDMs. Functional insights into enzymatic changes led to discovery of a subtle but critical alteration in FASN activity that catalyzed efforts to explore key metabolic sensors like AMPK that potentially cross-talk with DAGL β (**Figure 4.6 E**). In a complementary set of experiments, we employed untargeted MS-metabolomics to discover a striking metabolic phenotype in DAGL β -inactivated macrophages (via both genetic and pharmacological means) that is characterized by accumulation of PUFA-esterified TAGs. While our data challenge previously reports that DAGL β is not a TAG lipase⁴⁶, our metabolomics (**Figure 4.2**) and biochemical findings

(**Figure 4.5**) illustrate the importance of unbiased global analyses to assign unique substrate specificities of enzymes in living systems. Our metabolomics findings were critical to explain how disruption of DAGL β , which should lead to DAG accumulation², results in reduced and not augmented PKC activity (**Figure 4.2**). Thus, our combined chemical proteomics and metabolomics strategy present two distinct, and likely interconnected, protein kinase pathways that are involved in macrophage signaling to explain the anti-inflammatory effects mediated by DAGL β .

These findings are especially significant in the light of the AMPK activator such as metformin or AICAR that show reduction in inflammatory responses. As for metformin's mechanism of action, inhibition of the mitochondrial function explains how it activates AMPK in relation to the basic function of the AMPK⁴⁷. The major role of AMPK is to serve as an energy sensor. AMPK detects AMP/ATP, and ADP/ATP ratios that indicate balances in the cellular energy homeostasis and get activated when the ATP levels are low⁴⁸. The activation of AMPK leads to generation of ATP by catabolic pathway as well as by shutting off cellular functions that utilize ATP. Therefore, the inhibition of the mitochondrial functions reduces the ATP synthesis in which activates AMPK to balance the ATP level within the cell. On the other hand, AICAR is an AMP mimetic which means that when the cells uptake AICAR, it functions as artificially "increased" level of AMP concentration⁴⁹. Once AICAR changes the ratio of ATP to AMP, AMPK is activated to increase the ATP production. The increased activity of AMPK leading to the anti-inflammatory functions have been reported in a number of biological systems including cases

where metformin treatment showed reduced circulating pro-inflammatory cytokines as well as reduced adipose tissue inflammation.

It is tempting to speculate a direct regulation of AMPK by DAGL β through PKC based on phosphorylation states of activating (T172) and inhibitory (S485/491) AMPK sites that appear to be modulated by DAGL β (**Figure 4.6.2**). Phosphorylation of S485/491 is reported to function as an off-switch for AMPK and several reports have demonstrated PKCs can phosphorylate this site³⁴. Future studies should focus on identification of the specific PKC isoform that phosphorylates S485/491 to inactivate AMPK in response to DAGL β activity. Given that previous studies established DAGL β as a key regulator of 2-AG and downstream proinflammatory lipid products (arachidonic acid (AA) and prostaglandins (PGE₂))^{2, 11, 50}, additional studies are warranted to understand how DAGL β activity is regulated under different macrophage activation states.

Our findings provide an alternative pathway for explaining how blockade of DAGL β results in AMPK activation, provides anti-inflammatory effects across multiple pain models including inflammatory pain^{1, 50}, neuropathic pain⁵⁰, and neuroinflammatory mouse models⁵⁰. Our findings are of translational relevance given that metformin (AMPK activator) has shown promising anti-inflammatory efficacy in humans^{43, 44}. The mechanism of action by DAGL β that our current understanding provides is limited to the arachidonic acid pathway. However, the therapeutic benefits that we observed from DAGL β inhibition cannot be explained by reduced arachidonic acid alone.

We describe DAGL β as a novel intracellular PUFA-specific TAG lipase in primary macrophages. Combined with previous annotation of its DAG lipase activity^{51, 52}, DAGL β is uniquely capable of sequential processing of TAG and DAG substrates to supply lipid precursors and signals for cell biology. Using our chemical approaches with Activity-Based Protein profiling (ABPP) tailored to DAGL activity, we demonstrated that PUFA-specific TAG lipase activity is conferred by DAGL β . Further analysis of the TAG population in the BMDMs showed insights into the DAG species that are generated by DAGL β using TAG as substrates. The majority of the TAGs in the BMDMs were made of fatty acids that contained saturated and/or non-PUFA unsaturated fatty acids. Populations with a PUFA were heavily skewed toward species with only one PUFA. As a result, the generated DAG species from TAG as substrates are DAGs with saturated and/or Non-PUFA fatty acids.

As a result, we were able to observe a selective decrease in DAG species that did not contain a PUFA (**Figure 4.6 A**). On the other hand, we also recapitulate a previously reported increase in DAG species such as DAG (18:0/20:4) (**Figure 4.6 A**). This increase in DAG (18:0/20:4) can be explained by the fact that there are other lipases in the environment still producing DAG even when DAGL β is inhibited. Therefore, DAG accumulation in BMDMs with DAGL β disruption likely derives from a source other than TAGs. In addition, we showed evidence demonstrating that DAGL β is able to process triarachidonyl glycerol to monoacylglycerol using the same assay. Along with previous evidence showing substrate processing of diacylglycerol that contains both saturated and

unsaturated fatty acids⁵¹, DAGL β is able to regulate diacylglycerols indiscriminately but confers selectivity only at triacylglycerol level.

An interesting observation from the PKC activation further supports that disruption of this enzyme is not going to lead to defective insulin signaling, insulin resistance, and the pathogenesis of type 2 diabetes from DAG accumulation (**Figure 4.2**). In addition to the PKC substrate activation, we decided to pursue whether DAGL β inhibition leads to steatosis in mice (**Figure 4.7**). Wild type mice and DAGL β knockout mice were placed on normal chow for the duration of the studies. After three and ten months on normal chow, liver tissues were harvested and analyzed using H&E staining. The accumulation of lipid shows as clear space as shown in positive control of lipid accumulation (3 months old ATGL knockout, wild type mouse placed on high fat diet (HFD)). The results showed that there was no visible lipid accumulation in 3-month-old DAGL β knockout mice compared to the wild type counterpart (**Figure 4.7 A, B**). For the 10-month-old wildtype mice, the liver tissues showed significant development of steatosis (**Figure 4.7 D**). This data recapitulated previous studies that showed steatosis in older mice³⁸. However, 10 months old DAGL β mice did not show increase in steatosis despite their age (**Figure 4.7 E**).

This finding was interesting given the fact that lipase inhibition has been shown to develop into inflammation/fatty liver diseases that often leads to hepatic fibrosis^{37, 38}. Such liver diseases are caused due to accumulation of bulk triacylglycerols showing enlarged lipid droplets in liver. Considering previous literature on lipase inhibition, chronic genetic disruption of DAGL β in mice has been

of one of the more puzzling aspect of studying this enzyme. DAGL β ^{-/-} mice did not have no obvious ill-effects observed other than beneficial phenotypes observed from a number of inflammatory models. *Our histology study showed no development of steatosis in liver (3 months, 10 months) demonstrating little changes to bulk level of triacylglycerol levels (**Figure 4.7 B, and E**). Our analysis on triacylglycerol intensity show that majority of the triacylglycerols were made of saturated/low unsaturated fatty acids. Unlike other lipid classes analyzed such as PC, PS, and PE, significantly small population of triacylglycerol species included PUFA species (**Figure 4.8 A**). We suspect that this observation may explain the lack of excessive accumulation of lipids due to small population of lipid species affected in the overall triacylglycerols. In addition, the impact of the DAG accumulation by inhibition of DAG lipase activity would also be leveraged by decrease in amount of diacylglycerol species generated from triacylglycerols by DAGL β (**Figure 4.6 A**).

In conclusion, we believe that discovery in defining enzyme selectivity of DAGL β addresses a number of important questions in understanding the impact and utility of targeting this enzyme. Previous works on DAGL β were able to identify DAGL β as a direct regulator of 2-AG, which requires sequential conversion by monoacylglycerol lipases to release arachidonic acid. This work suggests the alternative lipid signaling pathways that explains how neutral lipids are utilized as an important source of signaling molecules instead of simple fatty acid storing molecules.

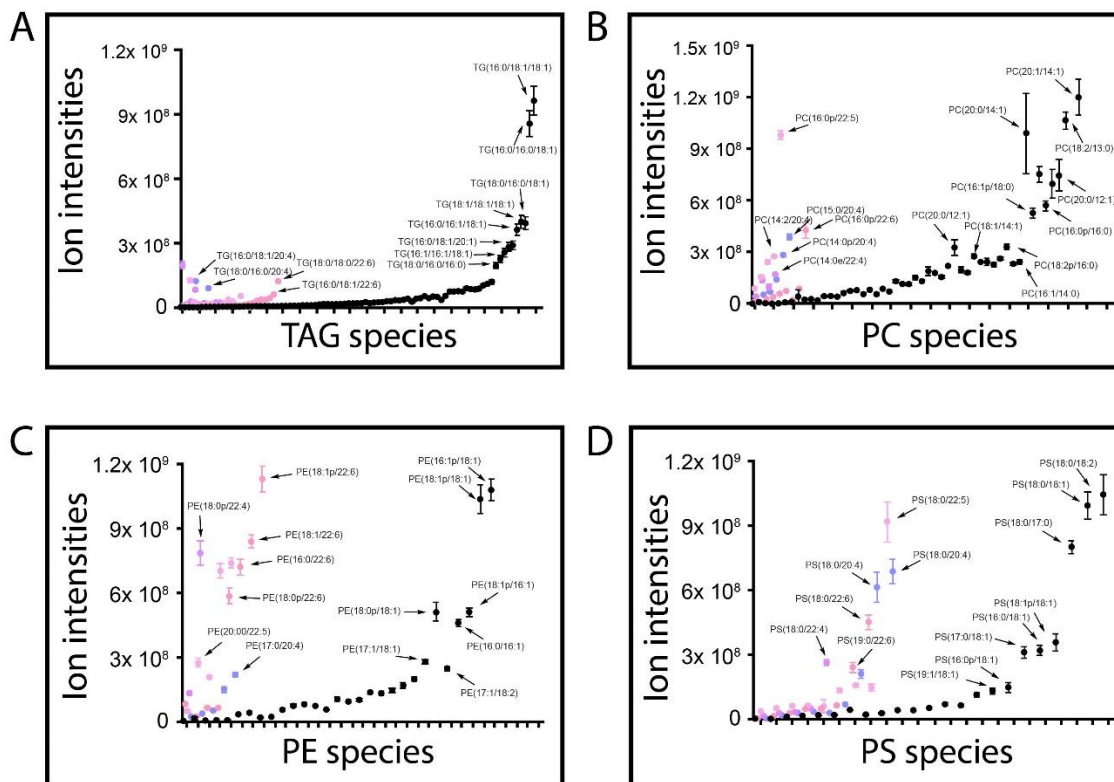


Figure 4.8 Untargeted lipidomics analysis of BMDM lipidomes BMDMs were extracted using folch method and analyzed using Q-Exactive Plus. Lipids were searched and aligned using LipidSearch™. The intensities of the lipid species corresponding to various lipid classes were analyzed including triacylglycerol (TAG, +NH₄ ion adduct, **A**), phosphatidylcholine (PC, +H ion adduct, **B**), Phosphatidylethanolamine (PE, +H ion adduct, **C**), and phosphatidylserine (PS, -H ion adduct, **D**). Each lipid species was colored-coded based on the fatty acids (PUFA FA were labeled (4 unsaturated or more) with color and saturated FA or FA with low unsaturation units (unsaturation units 3 or less)).

4.6 References

1. Shin, M., et al., *Liposomal Delivery of Diacylglycerol Lipase-Beta Inhibitors to Macrophages Dramatically Enhances Selectivity and Efficacy in Vivo*. *Molecular Pharmaceutics*, 2018. **15**(3): p. 721-728.
2. Hsu, K.-L., et al., *DAGL β inhibition perturbs a lipid network involved in macrophage inflammatory responses*. *Nat. Chem. Biol.*, 2012. **8**(12): p. 999-1007.
3. Wilkerson, J.L., et al., *Diacylglycerol lipase β inhibition reverses nociceptive behaviour in mouse models of inflammatory and neuropathic pain*. *Br. J. Pharmacol.*, 2016. **173**(10): p. 1678-1692.
4. Wongrakpanich, S., et al., *A Comprehensive Review of Non-Steroidal Anti-Inflammatory Drug Use in The Elderly*. *Aging and disease*, 2018. **9**(1): p. 143-150.
5. Chi, T.-Y., H.-M. Zhu, and M. Zhang, *Risk factors associated with nonsteroidal anti-inflammatory drugs (NSAIDs)-induced gastrointestinal bleeding resulting on people over 60 years old in Beijing*. *Medicine*, 2018. **97**(18): p. e0665-e0665.
6. Lalit, K., et al., *Advanced Drug Delivery Systems for Transdermal Delivery of Non-Steroidal Anti-Inflammatory Drugs: A Review*. *Current Drug Delivery*, 2018. **15**(8): p. 1087-1099.
7. Schäfers, M., et al., *Cyclooxygenase inhibition in nerve-injury- and TNF-induced hyperalgesia in the rat*. *Experimental Neurology*, 2004. **185**(1): p. 160-168.

8. Payne, R., *Limitations of NSAIDs for pain management: Toxicity or lack of efficacy?* The Journal of Pain, 2000. **1**(3): p. 14-18.
9. van Laar, M., et al., *Pain treatment in arthritis-related pain: beyond NSAIDs.* The open rheumatology journal, 2012. **6**: p. 320-330.
10. Hsu, K.-L., et al., *Discovery and Optimization of Piperidyl-1,2,3-Triazole Ureas as Potent, Selective, and in Vivo-Active Inhibitors of α/β -Hydrolase Domain Containing 6 (ABHD6).* J. Med. Chem., 2013. **56**(21): p. 8270-8279.
11. Hsu, K.-L., et al., *Development and Optimization of Piperidyl-1,2,3-Triazole Ureas as Selective Chemical Probes of Endocannabinoid Biosynthesis.* J. Med. Chem., 2013. **56**(21): p. 8257-8269.
12. Newton, A.C., *Protein Kinase C: Structure, Function, and Regulation.* Journal of Biological Chemistry, 1995. **270**(48): p. 28495-28498.
13. Obata, T., et al., *Peptide and Protein Library Screening Defines Optimal Substrate Motifs for AKT/PKB.* Journal of Biological Chemistry, 2000. **275**(46): p. 36108-36115.
14. Pearson, R.B. and B.E. Kemp, [3] *Protein kinase phosphorylation site sequences and consensus specificity motifs: Tabulations,* in *Methods in Enzymology.* 1991, Academic Press. p. 62-81.
15. Nishikawa, K., et al., *Determination of the Specific Substrate Sequence Motifs of Protein Kinase C Isozymes.* Journal of Biological Chemistry, 1997. **272**(2): p. 952-960.

16. Gajenthra Kumar, N., et al., *Untargeted lipidomic analysis to broadly characterize the effects of pathogenic and non-pathogenic staphylococci on mammalian lipids*. PLOS ONE, 2018. **13**(10): p. e0206606.
17. Chao, Y., et al., *Untargeted lipidomics based on UPLC-QTOF-MS/MS and structural characterization reveals dramatic compositional changes in serum and renal lipids in mice with glyoxylate-induced nephrolithiasis*. Journal of Chromatography B, 2018. **1095**: p. 258-266.
18. Forest, A., et al., *Comprehensive and Reproducible Untargeted Lipidomic Workflow Using LC-QTOF Validated for Human Plasma Analysis*. Journal of Proteome Research, 2018. **17**(11): p. 3657-3670.
19. Folch, J., M. Lees, and G.H.S. Stanley, *A SIMPLE METHOD FOR THE ISOLATION AND PURIFICATION OF TOTAL LIPIDES FROM ANIMAL TISSUES*. Journal of Biological Chemistry, 1957. **226**(1): p. 497-509.
20. Taguchi, R., M. Nishijima, and T. Shimizu, *Basic Analytical Systems for Lipidomics by Mass Spectrometry in Japan*, in *Methods in Enzymology*. 2007, Academic Press. p. 185-211.
21. Ong, S.-E., I. Kratchmarova, and M. Mann, *Properties of ¹³C-Substituted Arginine in Stable Isotope Labeling by Amino Acids in Cell Culture (SILAC)*. Journal of Proteome Research, 2003. **2**(2): p. 173-181.
22. Austin, P.E., E.A. McCulloch, and J.E. Till, *Characterization of the factor in L-cell conditioned medium capable of stimulating colony formation by mouse marrow cells in culture*. Journal of Cellular Physiology, 1971. **77**(2): p. 121-133.

23. Baratta, F., et al., *Reduced Lysosomal Acid Lipase Activity in Adult Patients With Non-alcoholic Fatty Liver Disease*. EBioMedicine, 2015. **2**(7): p. 750-754.
24. Pericleous, M., et al., *Wolman's disease and cholesteryl ester storage disorder: the phenotypic spectrum of lysosomal acid lipase deficiency*. The Lancet Gastroenterology & Hepatology, 2017. **2**(9): p. 670-679.
25. Perla, F.M., et al., *The Role of Lipid and Lipoprotein Metabolism in Non-Alcoholic Fatty Liver Disease*. Children (Basel, Switzerland), 2017. **4**(6): p. 46.
26. Jiang, Z.G., S.C. Robson, and Z. Yao, *Lipoprotein metabolism in nonalcoholic fatty liver disease*. Journal of biomedical research, 2013. **27**(1): p. 1-13.
27. Oliva, R.V. and G.L. Bakris, *Management of Hypertension in the Elderly Population*. The Journals of Gerontology: Series A, 2012. **67**(12): p. 1343-1351.
28. Jones, S.F. and J.R. Infante, *Molecular Pathways: Fatty Acid Synthase*. Clinical Cancer Research, 2015. **21**(24): p. 5434.
29. Qian, X., et al., *Regulation of fatty acid synthesis in immune cells*. Scandinavian Journal of Immunology, 2018. **88**(5): p. e12713.
30. Vasamsetti, S.B., et al., *Metformin Inhibits Monocyte-to-Macrophage Differentiation via AMPK-Mediated Inhibition of STAT3 Activation: Potential Role in Atherosclerosis*. Diabetes, 2015. **64**(6): p. 2028.

31. Sag, D., et al., *Adenosine 5'-monophosphate-activated protein kinase promotes macrophage polarization to an anti-inflammatory functional phenotype*. Journal of immunology (Baltimore, Md. : 1950), 2008. **181**(12): p. 8633-8641.
32. Luo, Z., M. Zang, and W. Guo, *AMPK as a metabolic tumor suppressor: control of metabolism and cell growth*. Future oncology (London, England), 2010. **6**(3): p. 457-470.
33. Stein, S.C., et al., *The regulation of AMP-activated protein kinase by phosphorylation*. Biochemical Journal, 2000. **345**(3): p. 437.
34. Salminen, A. and K. Kaarniranta, *AMP-activated protein kinase (AMPK) controls the aging process via an integrated signaling network*. Ageing Research Reviews, 2012. **11**(2): p. 230-241.
35. Fan, K., et al., *Lipopolysaccharide-Induced Dephosphorylation of AMPK-Activated Protein Kinase Potentiates Inflammatory Injury via Repression of ULK1-Dependent Autophagy*. Frontiers in immunology, 2018. **9**: p. 1464-1464.
36. Chen, C.-C., et al., *Amelioration of LPS-Induced Inflammation Response in Microglia by AMPK Activation*. BioMed Research International, 2014. **2014**: p. 9.
37. Reid, B.N., et al., *Hepatic Overexpression of Hormone-sensitive Lipase and Adipose Triglyceride Lipase Promotes Fatty Acid Oxidation, Stimulates Direct Release of Free Fatty Acids, and Ameliorates Steatosis*. Journal of Biological Chemistry, 2008. **283**(19): p. 13087-13099.

38. Wu, J.W., et al., *Deficiency of liver adipose triglyceride lipase in mice causes progressive hepatic steatosis*. Hepatology, 2011. **54**(1): p. 122-132.
39. Gao, Y., et al., *Loss of retrograde endocannabinoid signaling and reduced adult neurogenesis in diacylglycerol lipase knock-out mice*. J Neurosci, 2010. **30**(6): p. 2017-24.
40. Tanimura, A., et al., *The endocannabinoid 2-arachidonoylglycerol produced by diacylglycerol lipase alpha mediates retrograde suppression of synaptic transmission*. Neuron, 2010. **65**(3): p. 320.
41. Ogasawara, D., et al., *Rapid and profound rewiring of brain lipid signaling networks by acute diacylglycerol lipase inhibition*. Proc Natl Acad Sci U S A, 2016. **113**(1): p. 26-33.
42. Di Fusco, D., et al., *Metformin inhibits inflammatory signals in the gut by controlling AMPK and p38 MAP kinase activation*. Clinical Science, 2018. **132**(11): p. 1155.
43. Yue, W., et al., *Repurposing of Metformin and Aspirin by Targeting AMPK-mTOR and Inflammation for Pancreatic Cancer Prevention and Treatment*. Cancer Prevention Research, 2014. **7**(4): p. 388.
44. Gejjalagere Honnappa, C. and U. Mazhuvancherry Kesavan, *A concise review on advances in development of small molecule anti-inflammatory therapeutics emphasising AMPK: An emerging target*. International Journal of Immunopathology and Pharmacology, 2016. **29**(4): p. 562-571.
45. Weintz, G., et al., *The phosphoproteome of toll-like receptor-activated macrophages*. Molecular Systems Biology, 2010. **6**(1): p. 371.

46. Bisogno, T., et al., *Cloning of the first sn1-DAG lipases points to the spatial and temporal regulation of endocannabinoid signaling in the brain*. J. Cell Biol., 2003. **163**(3): p. 463-468.
47. Zhou, G., et al., *Role of AMP-activated protein kinase in mechanism of metformin action*. The Journal of clinical investigation, 2001. **108**(8): p. 1167-1174.
48. Gowans, Graeme J. and D.G. Hardie, *AMPK: a cellular energy sensor primarily regulated by AMP*. Biochemical Society Transactions, 2014. **42**(1): p. 71.
49. Kim, J., et al., *AMPK activators: mechanisms of action and physiological activities*. Experimental & Molecular Medicine, 2016. **48**: p. e224.
50. Wilkerson, J.L., et al., *Diacylglycerol lipase β inhibition reverses nociceptive behaviour in mouse models of inflammatory and neuropathic pain*. Br J Pharmacol, 2016. **173**(10): p. 1678-92.
51. Bisogno, T., et al., *Cloning of the first sn1-DAG lipases points to the spatial and temporal regulation of endocannabinoid signaling in the brain*. J. Cell Biol., 2003. **163**(3): p. 463.
52. Hsu, K.L., et al., *DAGLbeta inhibition perturbs a lipid network involved in macrophage inflammatory responses*. Nat. Chem. Biol., 2012. **8**(12): p. 999.

Chapter 5: Conclusions and future directions

5.1 Summary

The research described in this thesis investigated the function of DAGL β , which is an enzyme annotated to cleave diacylglycerols in an *sn*-1 specific manner. We discovered that inflammation can be attenuated by DAGL β disruption. We show that DAGL β activity is highly enriched in bone marrow-derived macrophages (BMDMs). Our work demonstrates that DAGL β activity is selectively enriched in phagocytes, such as macrophages, and that liposomal small molecule delivery can target macrophages to improve selectivity and efficacy *in vivo*.

We also discovered that DAGL β activity is enriched in bone marrow-derived dendritic cells (BMDCs). BMDCs function in both adaptive and innate immunity and thus presents a model system to evaluate how DAGL β disruption impacts regulation of the immune system. We showed that disruption of DAGL β blocked inflammatory cytokine and lipid (2-AG and arachidonic acid) responses to LPS stimulation of BMDCs. Interestingly, we demonstrated that DAGL β disruption had no impact on BMDC's capacity to prime CD8+Tcells.

Lastly, by measuring changes in PKC activity, we demonstrated that DAGL β inhibition does not lead to hyperactivation of PKC-mediated signaling. In addition, we discovered a novel metabolic activity of DAGL β for hydrolyzing TAGs containing PUFA. Based on the population of TAGs found in BMDMs, we show that DAGL β targets a select population of TAGs. Our findings expand the scope of

metabolic and signaling functions mediated by DAGL β and pave the way for future studies to investigate these pathways further.

5.2 Conclusions and significance

In light of the opioid crisis, new strategies for management of pain are needed. The current options for pain treatment include NSAIDs, SSRIs, corticosteroids, and opioids. A key challenge of current treatment options is chronic treatment results in side-effects and/or addiction.

As one of the most widely used drugs for treating inflammation, NSAIDs are efficacious for inflammation because they inhibit cyclooxygenases (COX) that are responsible for arachidonic acid metabolism that leads to prostaglandin biosynthesis. However, chronic treatment with NSAIDs results in gastrointestinal and cardiovascular side-effects. DAGL β inhibitors have emerged as a viable alternative for modulating inflammation by targeting alternative sources of arachidonic acid in macrophages and dendritic cells.

DAGL β inhibitors are efficacious in preclinical neuropathic pain models including chronic constriction injury (CCI) and chemotherapy-induced peripheral neuropathy. In contrast, NSAIDs are not efficacious in neuropathic pain models suggesting potentially different modes of action. Our work utilized unbiased metabolomics to discover novel lipid substrates for DAGL β in primary macrophages. Our results show accumulation of TAGs that contained PUFAs (poly-unsaturated fatty acids). Performing subsequent substrate assays with TAGs

with varying unsaturation units and chain length showed that DAGL β cleaves TAGs with specificity for PUFAs.

Our findings position DAGL β as a novel TAG lipase in BMDMs that will likely perform different functions compared with other TAG lipases including ATGL. ATGL is known to process triacylglycerol to generate diacylglycerols that contain fatty acids at *sn*-1,3 position which suggests that this enzyme cleaves TAGs at the *sn*-2 position. However, once ATGL is activated by a co-activator called CGI-58, it switched its selectivity toward the *sn*-1 position of the fatty acid. Here, effective substrate processing by ATGL has been demonstrated against saturated fatty acid/mono-saturated fatty acid containing glycerolipids.

We also explored the function of DAGL β in the context of its potential impact on both innate and adaptive immunity. The cannabinoid receptors are differentially regulated by the expression patterns depending on the tissue types. For instance, CB1 receptors are expressed in the central nervous system whereas CB2 receptors are expressed in cells with hematopoietic origin. Therefore, understanding how inhibition of DAGL β , which is responsible for bulk production of endocannabinoid 2-AG, impact innate and adaptive immunity was an important question for us to answer.

The lipid analysis of the BMDCs for 2-AG and arachidonic acid showed a reduction in DAGL β disrupted BMDCs whereas DAGL β ^{+/+} and DAGL α ^{-/-} showed no change. In addition, innate immune function was investigated by observing reduced pro-inflammatory cytokine in DAGL β ^{-/-} BMDCs. Finally, adaptive immune function was tested by analyzing the BMDC function of priming CD8⁺ T cells. To

our surprise, DAGL β -/- BMDCs showed no differences in their T-cell priming function.

The significance of this finding is that innate and adaptive immune functions by DAGL β in dendritic cells are regulated independently. As it has been shown that cannabinoid signaling is important in DC functions, reduction in 2-AG could result in adaptive immune functions carried out by DCs. However, the result showed that DAGL β -/- nor DAGL α -/- BMDCs showed differences in T-cell priming capacity.

Lastly, we demonstrated the selective targeting of such immune cells by taking advantage of their phagocytic function. Phagocytes efficiently take up particles through active-phagocytosis. In fact, phagocytes often pose a significant challenge in drug delivery via liposomes due to their ability to take up particles in their environment. With that in mind, we developed a liposomal delivery system where DAGL β inhibitors are encapsulated within the liposome. In addition, we tested the encapsulated inhibitors in the inflammatory pain model for efficacy. The results showed that we were able to achieve more than a hundred-fold reduction in total compound injected into mice compared to its free-compound to get the same anti-nociceptive effects.

5.3 Limitations and Future direction

Our work explored chemical biology and mass spectrometry to investigate cellular and physiological functions of DAGL β . The following sections describe the limitation of the current studies and future studies for further advancing this project.

Liposomal KT109 delivery study utilized liposomes to show development of the selective delivery method for phagocytes. In this study, liposomes were not decorated with additional functionalities. Though the particle size increase by liposome encapsulation resulted in remarkable improvement in selectivity and efficacy, there are possibilities of modifications including antibody decorations for targeting a specific subset of macrophages or other phagocytes. In addition, the current formulation of the liposome is not amenable for orally bioavailability.

To address these concerns, I propose the following. First, macrophages exist in a number of different forms depending on the tissue location or presence of external stimuli. The markers that target macrophages specifically (CD11b and F4/80) could hone in the liposome delivery for increased selectivity of the liposome. The increased selectivity in liposomes could provide benefits including fewer off-targets and improved efficacies.

Additionally, the composition of the lipids that make up the liposomes could be formulated to make liposomes bioavailable. Previous work on liposomal delivery has shown that insulin could be encapsulated in the liposome and delivered orally to achieve reduced glucose levels. Thus, the formulation of the liposome could be adjusted to deliver liposomal KT109.

For the dendritic cell studies with the CD8+T-cell priming experiment, our focus was to determine the endpoint study of demonstrating whether DAGL β disruption results in CD8+ T-cell priming events. The signaling pathways that make up the immunological responses involve the regulation of complex protein machinery. In addition, there are many different cell types that could impact the result of the immune studies involving lipid signaling pathways.

Thus, there could be additional future studies that could elucidate the impact of DAGL β disruption in the immunological system. For instance, the presence of DAGL β activities in subsets of T cell populations has not been demonstrated. If DAGL β activity is present in T cells or other relevant cell types involved in the development of the adaptive immunity, selective or systematic disruption of the DAGL β in each population to observe changes in resulting immune function would be necessary for future studies.

Lastly, the focus of our biochemical studies regarding DAGL β substrate specificity and the discovery of novel signaling pathways was to elucidate relevant novel activities that are outside what is known in the literature. Through the untargeted-lipidomics and subsequent substrate assays, we were able to identify novel activities for DAGL β and its potential connection to lipid and protein signaling pathways.

The positional selectivity (*sn*-1 or *sn*-2) of DAGL β has been investigated in previous studies. As we investigate further how DAGL β processes its substrates, positional specificity of the enzyme at the TAG level will be important. It has been shown that DAGL β processes diacylglycerol at *sn*-1 specific manner. In our

substrate assay, we were able to observe that triacylglycerol that contains three PUFA were able to process from TAG to MAG (monoacylglycerol). This phenomenon leads to question such as does DAGL β generate more than one type of DAG species? From the current studies, it is possible that the observation of diacylglycerol and monoacylglycerol species are coming from DAGL β activity at sn-1 or sn-3 position in which case could subsequently processed to generate sn-2 glycerolipid. However, it is also possible that DAGL β generates 1,3 DAG species in which we currently do not have enough data to support if the remaining DAG species are present as an intermediate waiting to be processed by DAGL β or if those 1,3 DAG remain in the reaction because DAGL β isn't able to process.

To address this question, future studies could investigate DAGL β in two experiments to test the specificity of the enzyme. First, isolated 1,3- , 1,2- or 2,3-DAGs could be tested against DAGL β . This experiment will show direct evidence of the substrate specificity of DAGL β at TAG level. In addition, TAGs could be incubated with DAGL β and the reaction mixture could be analyzed using chiral column that could identify the presence of each DAG species.